Schweizerische Eidgenossenschaft
Confédération suisse
Confederazione Svizzera
Confederaziun svizra

Federal Department of the
Environment, Transport, Energy and Communications DETEC

Swiss Federal Office of Energy SFOE
Dam Safety Section

Diagnosis of alkali-aggregate reaction in dams

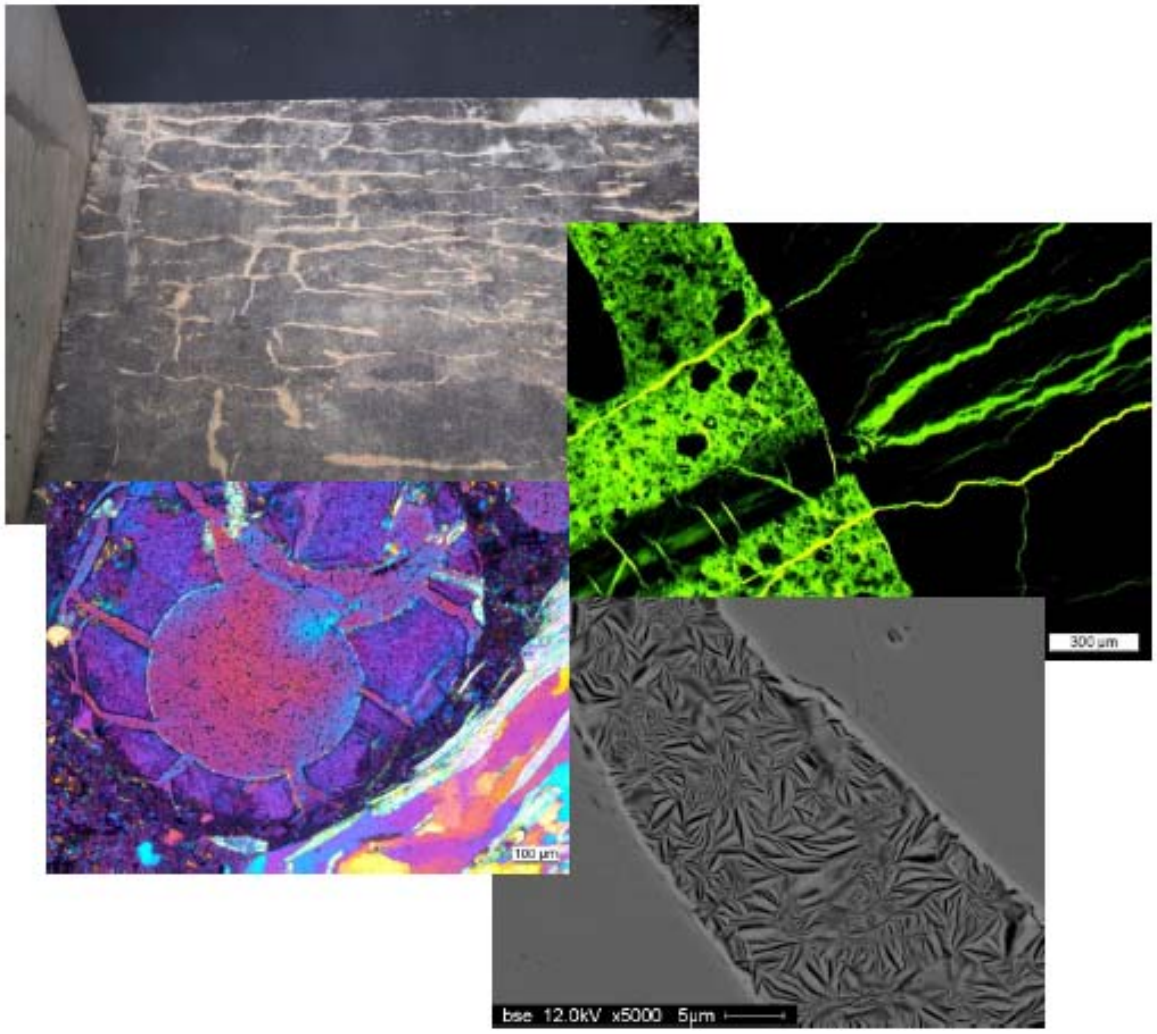

December 2013

Andreas Leemann and Michele Griffa
Empa — Swiss Federal Laboratories for Materials Science and Technology
Laboratory for Concrete / Construction Chemistry
Überlandstrasse 129
CH-8600 Dübendorf
Switzerland

Impressum

BFE-Projekt:
Auftrag 8100000598
Vertrag SI/500863-01

Datum:
Dezember 2013

Auftraggeber:
Bundesamt für Energie, Sektion Aufsicht Talsperren, 3003 Bern

Auftragnehmer und Verfasser:
Dr. Andreas Leemann und Dr. Michele Griffa, Empa, Abteilung Beton / Bauchemie, Überlandstrasse 129, CH-8600 Dübendorf

Begleitung:
Dr. Johannes Maier, Sektion Aufsicht Talsperren, Bundesamt für Energie, CH-3003 Bern

Diese Studie wurde im Rahmen der dem Bundesamt für Energie BFE zugewiesenen Aufgaben als Aufsichtsbehörde für die Sicherheit der Talsperren erstellt. Für den Inhalt sind allein die Studienverfasser verantwortlich.

TABLE OF CONTENTS

1. Introduction

1.1 General information

In the alkali-aggregate reaction (AAR) minerals present in aggregates react with the alkaline pore solution of the concrete (pH 13.0–13.5). The term AAR includes the reaction with silica, silicates and carbonates. In this report AAR relates to the reaction with silica and silicates. The reaction with carbonates is denoted specifically as alkali-carbonate reaction (ACR). As the AAR product takes up water, stress is generated that can lead to expansion and cracking of concrete. Typically, such cracks are formed years or even decades after the affected structures were built. Any type of concrete structures can be affected, provided three prerequisites are present: (1) sufficient alkalinity of the pore solution, (2) reactive minerals in the aggregates and (3) a sufficient moisture level. AAR is one of the most important deterioration mechanisms in concrete, leading to substantial damages of structures worldwide [e.g. Bérubé et al., 2000a; Tang & Deng, 2004; Broekmans, 2008; Thomas & Kwilosz, 2012].

AAR has to be dealt with on the level of prevention, diagnosis, prognosis and repair.

- Nowadays it is well known that **AAR in new structures can be prevented** by adding mineral admixtures like blast furnace slag, fly ash, microsilica, lithium salts or combinations of them [e.g. Kawamura & Takemoto, 1988; Bérubé & Duchesne, 1993; Thomas et al., 1999; Lane & Ozyildirim, 1999; Duchesne & Bérubé, 2001; Collins et al., 2004]. However, meaningful test methods to assess the potential reactivity of a specific jobsite concrete with its particular combination of aggregates, cement and mineral additions are still being evaluated and discussed [e.g. Thomas et al., 2006; Leemann & Merz, 2013; Lindgard et al., 2013a; Lindgard et al., 2013b].
- The **diagnosis of AAR in structures** showing deformations or the development of cracks can include several steps:
  - In a first on-site inspection, signs indicating that AAR is present in a concrete structure are analyzed and recorded. In a following in-depth investigation, the presence of AAR has to be confirmed using different types of microscopy. A diagnosis can become difficult, as AAR often occurs in combination with other mechanisms leading to concrete deterioration (e.g. chloride induced rebar corrosion, freeze-thaw damage, delayed ettringite formation etc.). Additionally, it can be challenging to diagnose AAR at a very early stage of the reaction, when an initial expansion is present but the AAR-specific signs are only in part or weakly developed.
  - Once the occurrence of AAR is established, its extent in various parts of the structure has to be analyzed. Additionally, the mechanical properties of the concrete and their possible degradation due to AAR have to be studied.
  - As a first step in **prognosis**, a determination of the residual expansion potential can be used to assess how much the concrete in a given structure will expand in the future.
- Modeling can provide information about the behavior of a structure. As such it can help with the identification of critical parts of a structure, with the **prognosis** of its behavior and with the definition of a stage when measures have to be taken.
- Depending on the affected structure or structural component, there are various approaches to **repair or rehabilitation**. However, these measures can be expensive and often lead only to temporary improvements of the situation.

1.2 Diagnosis

If the monitoring of a dam shows irreversible deformations that are neither caused by thermal effects nor by changes in the water level, questions about possible causes arise - with AAR being one of them. There are several excellent documents dealing with the diagnosis of AAR in various types of structures [e.g. Fournier et al., 2010; Godard et al., 2013]. They outline in detail the different steps required. This report focuses on the diagnosis of AAR in concrete dams on the material level. Dams are special in regard to AAR as already relatively small expansions (which would be of no or little concern for other structures) may lead to substantial problems. Consequently, the challenge in dams is often to diagnose AAR at a very early stage or when it is only weakly developed. In that case, AAR-typical features are less obvious.

In the following, the typical appearance of AAR is presented, in order to facilitate its identification and diagnosis in dams. Microscopy is emphasized as the major tool, as it makes possible to reliably identify even weakly developed AAR. Recommendations about experimental approach, sample selection and preparation are given where it seems essential for diagnosing AAR. However, the document is not intended as a general guide for concrete petrography (see insterad [St. John, et al., 1998]) and the application of various experimental techniques.

The content of this state-of-the-art-report is mainly based on the experience of Empa with AAR in Switzerland. Consequently, it is typical for AAR with relatively slow-reacting quartz as the main reactive phase.

2. Studies identifying AAR in dams

AAR occurs in concrete dams worldwide [Charlwood, 2013]. In the international literature, several cases of AAR in dams are described. In the following, some examples of the methods used to identify AAR are presented.

Among the first cases of AAR in India were a gravity dam and a power house built in the early sixties [Mullick, 1988]. Cracking of the concrete and displacements of up to 3 centimeters led to misalignments of machinery and difficulties to operate the installed equipment, like gates. AAR was identified on concrete cores visually and with scanning electron microscopy (SEM) combined with energy dispersive X-ray spectroscopy (EDX). Furthermore, the AAR product was characterized with X-Ray diffraction (XRD) and Infrared (IR) spectroscopy. Cores from the dam that were stored in KOH solution showed a further reaction potential [Mullick et al., 1987].

In an Australian dam, the occurrence of AAR was confirmed visually and with SEM [Cole et al., 1981]. XRD was additionally used. In a second Australian dam, the AAR product was investigated using XRD, IR spectroscopy and SEM in combination with EDX [Shayan, 1988].

In a study including five North American dams, AAR was identified visually and using optical microscopy on polished sections [Stark & De Puy, 1987]. Cores with diameters of 7.5 and 10.0 cm were immersed both in water and in a 1 M NaOH solution to determine the residual expansion potential. Differences in length change larger than 0.020 % between the cores stored in water and the ones stored in the 1 M NaOH solution were judged as significant.

The presence of AAR in three Portuguese dams was verified using SEM with EDX [Fernandes et al., 2004; 2007; 2008]. In addition, the uranyl acetate test, the residual expansion test, the soluble alkali content, creep tests, compression tests and a petrographic examination were conducted.

The first case identifying AAR in Switzerland reported in the literature is the Illsee dam [Regamy & Hammerschlag, 1995]. Here, a microstructural study was carried out with optical microscopy on thin sections.

In all these cases, AAR was identified visually and by microscopy. In the majority of cases, SEM was used. This may be representative only when optical microscopy on polished sections, thin sections or a combination of both is used. However, AAR had already progressed to a quite obvious level in these cases, thereby facilitating the diagnosis. On the contrary, in several Swiss dams significant deformations are measured but no obvious signs of AAR are observed visually. Therefore, in some of the following descriptions we point out methods to diagnose AAR that may be employed already at an initial state of the reaction.

3. Methods for AAR identification

3.1 Introduction

Concrete is a local or regional product. Therefore, it is usually known if the local aggregates are potentially susceptible to AAR. However, dams are often built in remote areas. As a local source has to be used for the aggregate production, it is likely that new quarries have to be established. Such quarries lack a track record in regard to AAR. Therefore, no conclusions about the potential reactivity can be drawn in such cases. Anyhow, the sources for aggregates and cement should be determined.

Diagnosing AAR includes several steps, starting with the inspection of the structure. Based on the inspection and the available data, coring sites are defined and the samples taken are analyzed with different methods, starting with a visual assessment and finally extending the range to sub-micrometer level observation.

3.2 Visual inspection

3.2.1 On-Site

Visual signs of a significantly developed AAR in Swiss dams occur as cracks. Pop-outs at the concrete surface that are observed in other countries generally lack in Switzerland as they are usually caused by very fast and strongly reacting aggregates as chert (nearly absent in Switzerland). Pop-outs in Swiss concrete are instead typically a result of freeze-thaw damage. It has always to be kept in mind that any concrete structure exhibits a certain degree of cracking and that different mechanisms can cause cracking (restrained shrinkage, freeze-thaw, etc.).

The crack pattern observed on the surface in concrete affected by AAR without major restraining forces usually corresponds to the pattern caused by shrinkage, commonly referred to as "map-cracking" (Figure 3.1). The relative volume changes due to shrinkage and AAR correspond. In shrinkage, the surface of the concrete witnesses a negative volume change due to drying compared to the inner part of the concrete with higher moisture content. In AAR the inner part of the concrete expands more than the outer one due to the more favorable conditions for the reaction (higher moisture content, less alkali leaching) resulting in the same relative volume change as in shrinkage. As a result, shrinkage cracks are initially reactivated by AAR. With the ongoing reaction, existing cracks are widened and different crack patterns can develop, depending on the restraining stresses present and their orientation.

When a structural component is restrained in one direction parallel to the investigated surface, AAR-induced cracks tend to show a preferred orientation parallel to the compressive stress (Figures 3.2 and 3.3). The expansion occurs in the direction of the lowest degree of restraint.

An important characteristic of cracks caused by AAR are the deposits formed along the cracks. In general, there are two different types of deposits: one as a result of AAR, the other due to portlandite leaching.

First, the alkalis are leached from the concrete. However, they occur only in relatively small amounts and form only water-soluble salts. As a result, they do not lead to permanent deposits along the crack rims at concrete surfaces exposed to rain. The deposits caused by AAR typically cause a dark rim along the crack edges (Figures 3.3-3.5). The pore solution of concrete with AAR shows an increased level of silicon [Leemann et al., 2008]. When the concrete surface is exposed to cyclic wetting and drying as it is in areas exposed to rain, silicon-rich pore solution reaches the concrete surface, where amorphous silica and minor amounts of calcium are precipitated. In areas that are not exposed to cyclic wetting and drying, these deposits do not form (Figure 3.5). The second mechanism leading to the formation of deposits along the cracks is caused by moisture or water penetrating the concrete in larger amounts and transporting dissolved ions to the surface. This mechanism has a higher transport capacity than the cyclic wetting and drying by rain. As such, not only silicon-rich solution is transported to the surface, but the cement paste is leached. Consequently, portlandite precipitates at the surface of the concrete and carbonates due to the reaction with CO_2. The color of these deposits depends on their composition. When they are entirely formed of calcite, they can be white or at least bright colored. With increasing silicon content, they become darker. However, the darkening can be caused by biological activity and by the inclusion of organic material as well.

When a dam is inspected looking for signs of AAR, not only the dam itself but additional structures or structural components built within the same project and likely with aggregates from the same source as used for the dam should be included. In general, it is easier to closely inspect the surfaces of such additional structures due to better accessibility. Additionally, they are often built using a concrete with a higher cement content than the one used for the dam. This increases the likelihood for clear signs of AAR.

Figure 3.1: Cracks at the outlet of an overflow.

Figure 3.2: Cracks at the inlet of an overflow with preferred orientation parallel to the restraining compressive stress.

Figure 3.3: Dark-rimmed cracks showing a preferred orientation parallel to the compressive stress at the entrance of a tunnel.

Figure 3.4: Cracks in a supporting wall lined with darkish deposits.

Figure 3.5: Supporting wall at the entrance of a gallery. Cracks lines with darkish deposits in the area exposed to rain and without deposits in the sheltered area.

3.2.2 Cores

After the visual inspection of a dam, coring sites are defined. The choice is strongly influenced and limited by accessibility, usually more than in other structures. Survey data about the deformation of the dam may indicate where expansion is relatively large or small, respectively. Samples from both types of areas have to be taken. Special attention should be given to areas where an expansion is critical for the integrity of the structure or where concentrations of stresses are likely to occur. The number of cores to be taken depends on the type and complexity of the dam under investigation and on the level of detail and representativeness

required. Before a core is taken, its orientation (up/down) should be clearly marked on the surface of the concrete included in the core. This step allows identifying the orientation of cracks. This is important when a preferred orientation of cracks is present, as it can be compared with the assumed stress field.

After the cores are taken, they should be immediately sealed in plastic bags to prevent any moisture loss and carbonation. This will be of major importance when the residual expansion potential will be determined (see paragraph 5). In the laboratory the cores are to be photographed and described, best in a room with a relative humidity of 90% or higher.

The visual inspection of the cores can reveal different indications for AAR. Cracks in cores are usually not as easy to recognize as on the concrete surface. This especially applies, if there is only minor cracking (as it is often the case in dams). When a core is taken directly into a crack visible at the concrete surface, the crack path can usually be followed for a certain length within the concrete (Figure 3.6). When the core is cut along its length axis for further sample preparation, cracks are easier to recognize. Of course cracks are not only caused by AAR, but may have a different origin. However, there are additional signs for AAR in cores other than cracks that can be recognized by eye.

On the surface of a freshly taken or cut core, aggregates with a dark rim indicate the presence of AAR (Figure 3.6). These dark rims are caused by the AAR products that preferably fill the porosity (pores and microcracks) at the edge of aggregates. However, the dark rims can also be caused by weathering of the aggregates before they were used in concrete. Therefore, they are no definite signs for AAR. When a core is allowed to dry for several hours or days, whitish deposits can form at the interface between aggregate and cement paste or still within the aggregates (Figure 3.7). These deposits typically consist of Na_2CO_3. Part of the sodium in the AAR product is only bound as hydrated ions and can therefore be transported with the evaporating water to the surface exposed to drying. Due to the reaction with CO_2, Na_2CO_3 is formed. Such an exudation of sodium can be even observed in impregnated samples used for microscopy [Jakobsen et al., 1992]. These exudations are a clear sign for AAR.

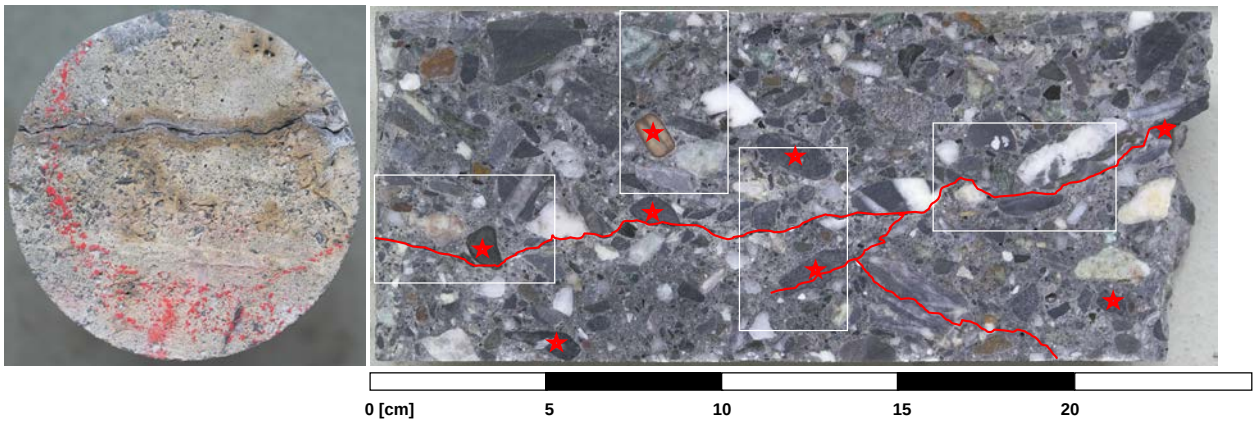

Figure 3.6: Core with a diameter of 100 mm cut along its length axis. The visually recognizable cracks are marked in red. Aggregates with a dark rim are pointed out with a red star. The white rectangles indicate the position of areas intended for the preparation of thin sections. Core from the entrance area of an underpass.

The most obvious and definite sign for the presence of AAR observable in cores are often the white deposits in voids (Figure 3.8). As the pore solution of concrete with AAR is enriched in silicon, silicon-rich precipitates can form in voids of the cement paste. Often, pores directly beside strongly reacted aggregates show these deposits as a result of the local increase in the silicon concentration of the pore

solution. They start to form along the edge of the voids and may fill them entirely. The composition of these deposits can vary (see paragraph 3.4.2), but silicon is always a major component.

Figure 3.7: Core with a diameter of 100 mm broken perpendicular to its length axis after drying due to exposure to air. Close to edge of the aggregates a whitish product is formed. Concrete from a bridge. Photo taken by R. Gall.

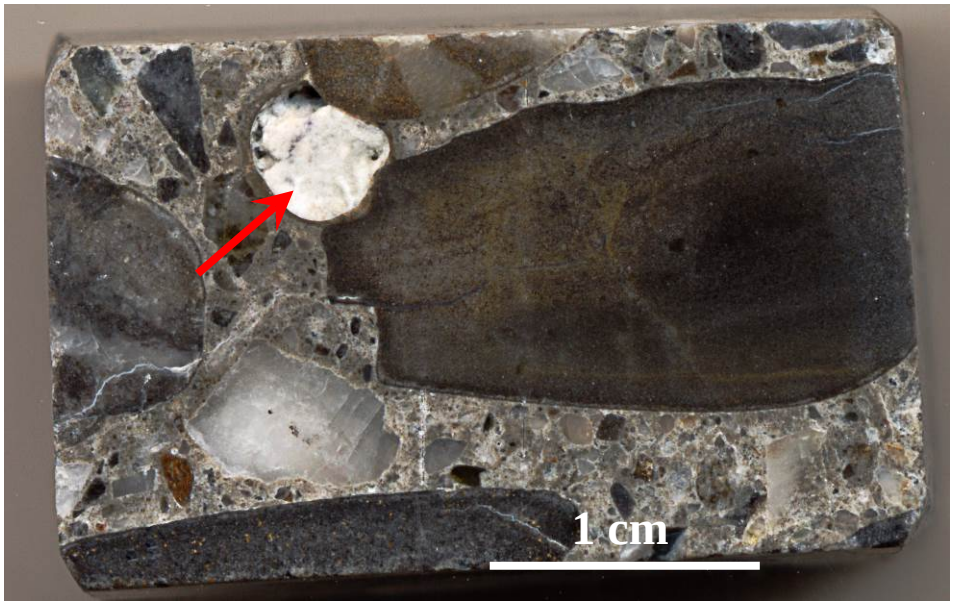

Figure 3.8: Deposit of white, silicon-rich product in a void of the cement paste. Concrete from a bridge. Image made with a flatbed scanner.

There is the possibility to treat the cores with uranyl acetate, which is mainly absorbed by the AAR products and replaces the alkalis and calcium [Natesaiyer & Hover, 1989; AASHTO, 2004]. After the treatment, the AAR products are luminescent under ultra violet light and are easily recognizable. Due to the radioactivity and the toxicity of the uranyl acetate this method cannot be recommended without reservations.

3.3 Optical microscopy

3.3.1 Introduction

3.3.1.1 General information

Thin sections studied with a polarized light microscope are the most effective way to investigate concrete for diagnosing AAR or other degradation mechanisms [e.g. St. John et al., 1998]. On one hand, thin sections are relatively easy to produce. On the other hand, the microscope allows a detailed study of the microstructure, with a resolution of a few micrometers. Using the different filters and apertures of a polarized light microscope, minerals can be identified based on their texture and optical properties in the transmitted light mode. Here thin sections can be studied in single polarized light, with crossed polarizers and with crossed polarizers with inserted gypsum plate. The use of fluorescent dyes in the epoxy resin expands the possibilities of the microscope, as it allows to qualitatively assessing the porosity of the concrete. Porous areas contain a high amount of epoxy and with it of dye. Therefore, they display a high fluorescence in contrast to dense parts of the concrete. Aggregates for example appear dark, voids and cracks bright and the cement paste falls in between. There even have been successful attempts to determine the water-to-cement-ratio (w/c) of concrete based on the luminescence of the cement paste [Jakobsen et al., 1999]. However, usually only a rough estimation is possible, as the luminescence is dependent on the thickness of the thin section (which may vary to a certain degree from place to place) and on the grain size distribution of the aggregates, in particular the amount of fines in the sand.

3.3.1.2 Sample selection

After the visual inspection of the cores, samples for the investigation with the microscopes are selected. Samples at different concrete depths should be taken. It is recommended to prepare the samples in such a way that the investigated surface of the samples varies in relation to the length axis of the core. As an example, they can be oriented parallel, perpendicular or at an angle of 45 ° in relation to the length axis of the core (see paragraph 4.3, Table 4.1). If cracks in the structure show a preferred orientation, this type of sample selection and preparation ensures representativeness.

Two different approaches can be used for sample selection. If the goal is only to identify AAR, areas showing AAR-related features (cracks, pores filled with products, aggregates with dark rims) should be selected. This will enable to confirm the presence of AAR using microscopy. However, if the goal is not only to identify AAR but to provide information about its extent in various parts of a structure, the samples have to cover all representative parts of the structure.

The position of the selected samples in relation to the core depth and the core location has to be documented, before continuing with sample preparation.

3.3.1.3 Sample preparation

The concrete is cut to a sample size suitable for thin sections. It is recommended to carefully grind the surface used for the investigation while applying only a small force to press the sample on the polishing disc. Artifacts from cutting can be removed using this approach and the surface is already relatively smooth (Figure 3.9). Immediately after grinding, the sample should be cleaned with compressed air and the drying procedure has to be started to minimize any chemical reactions.

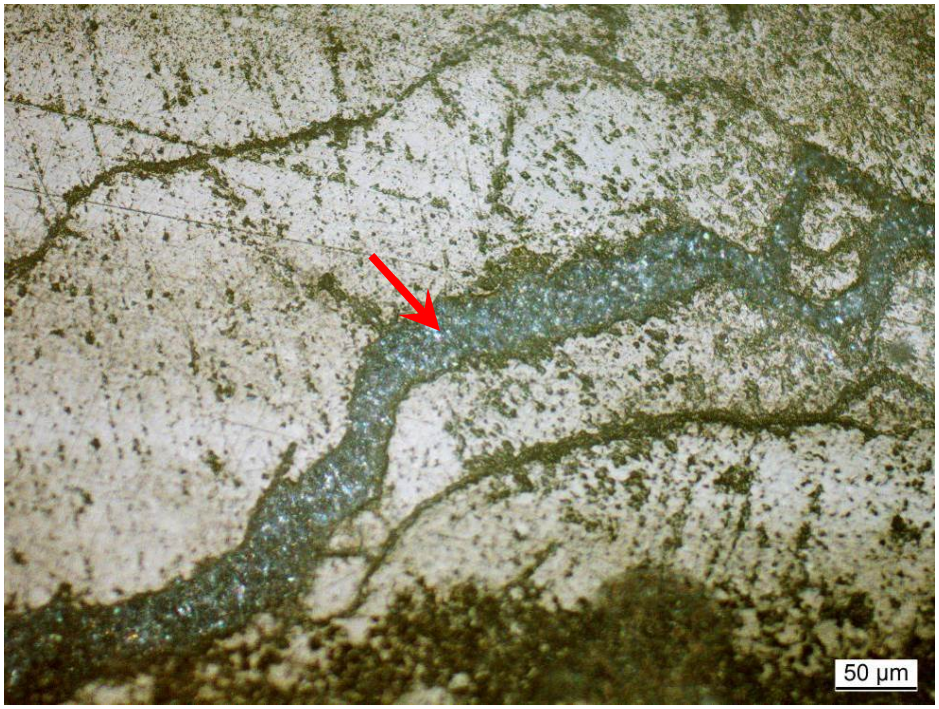

Figure 3.9: Crack within an aggregate filled with AAR product (arrow) in a freshly cut and ground concrete before drying and impregnation. Note the small domains reflecting the light of the microscope.

The precut samples are dried in an oven (e.g. at 50 °C for three days) and impregnated with epoxy resin that contains a dye displaying fluorescence under ultraviolet light. It is recommended to remove 1.5-2.0 mm from the cut surface of the sample after impregnation by polishing, to avoid artifacts caused by cutting and grinding. The polished surface is glued to a glass carrier. A cut is made leaving only a thin slice of concrete on the glass carrier. This slice is polished to a thickness of 20-30 µm (Figure 3.10). The remaining piece of impregnated concrete can later be used to prepare polished sections for the investigation with the SEM.

It is advantageous to have large **thin sections**, as features like cracks can be followed over the length of several centimeters. Typical thin sections cover an area of approximately 35 × 50 mm^2, but thin sections up to a size of 90 × 50 mm^2 can be produced. In St. John et al. [1998], further information about the microscopy on thin sections prepared from concrete are given.

Figure 3.10: Thin section and corresponding impregnated concrete sample (area of concrete on thin section: 50 × 90 mm^2).

The observations made on a thin section are best noted on a data sheet containing a sketch or an image of the thin section that can for example be obtained using a flatbed scanner (see Figure 4.2). Locating important observations on the image facilitates data acquisition.

It has to be pointed out that considerable experience (several years) is advantageous when thin sections are studied and the features present are interpreted using the polarized light microscope (Figure 3.11). A very valuable way to expand the expertise of any person doing thin section analysis, whether she/he is experienced or not, is the analysis of **polished thin sections** without cover glass using both the polarized light microscope and SEM/EDX. With this approach, features of the microstructure that are interpreted from the observations with the optical microscope in a certain way can afterwards be further analyzed with SEM/EDX. Consequently, the original interpretation is either confirmed or not. The knowledge gained from this approach is valuable for further thin section analysis, even when it is not combined with SEM/EDX afterwards. Furthermore, the combination of the two methods helps to partly overcome the main disadvantage of the polarized light microscope: the lack of chemical analysis. The main disadvantage of polished thin sections is their size. Due to technical reasons, they can be only produced in relatively small size (e.g. 23 × 35 mm^2).

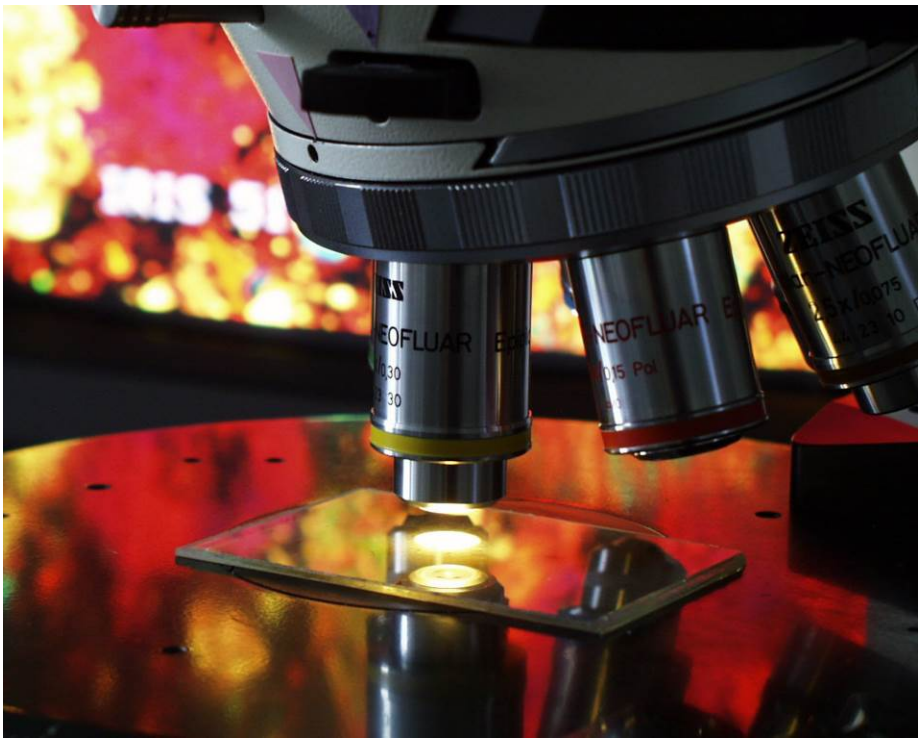

Figure 3.11: Polarized light microscope using crossed polarizers with inserted gypsum plate (see screen behind the microscope) to study thin sections.

3.3.2 Diagnosing AAR

3.3.2.1 Crack patterns

In general, it is easier to study cracks in the fluorescent light mode. When the cracks are empty and consequently filled with epoxy, their fluorescence is very high and they can easily be recognized. When they are filled with AAR products, their fluorescence is still considerably higher than the one of the aggregate. Therefore, they are still easy to recognize within aggregates. When cracks in the paste are filled with reaction product, they are usually recognizable as their fluorescence usually differs from the one of the paste (Figures 3.12 and 3.13). Cracks, and the patterns they form, can be used as indications for AAR,

as discussed below. Furthermore, they can be used to identify reacted aggregates. In the transmitted light mode it is easier to recognize cracks in single polarized light (e.g. Figure 3.19).

Due to the water uptake of the AAR product within the aggregate, stress is generated. When the stress reaches an aggregate-specific threshold, the aggregate cracks and the crack progresses into the cement paste. The crack in the cement paste may reach only a length of a few millimeters before is not detectable anymore. On the other hand, cracks may run through the entire thin section, crossing several aggregates. The reason for this feature is that other aggregates than the initially cracked one may have already built up an internal stress without cracking. As the stress field of several aggregates can overlap, the first crack propagates into the direction of the tensile stress. This type of domino effect can lead to rows of cracked aggregates linked by the same crack (Figure 3.12). These feature is a clear sign for AAR, but it usually only occurs when AAR is well progressed.

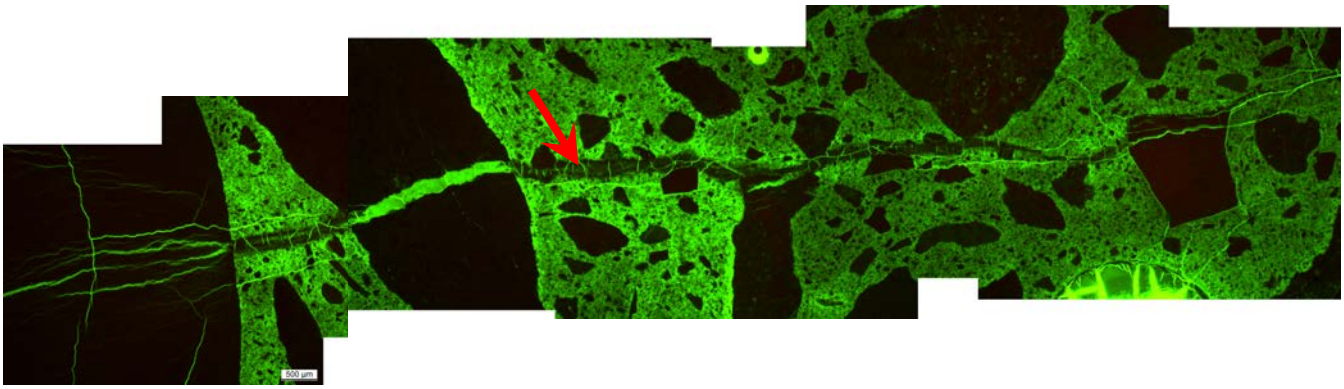

Figure 3.12: Crack (arrow) filled with AAR products running through several aggregates and the cement paste. Note that the crack is filled with AAR products that have a high fluorescence within the aggregate but a lower one in the cement paste. Fluorescent light mode. Concrete from a bridge.

Often cracks in the paste are mainly related to single aggregates in the investigated area of the concrete defined by the size of the thin section. Figure 3.13 shows such a crack. There is an additional crack at the lower edge of the aggregate that is not indicative for AAR as it travels along the interface between aggregate and cement paste. Such cracks can be caused as well by other mechanisms like shrinkage. The simultaneous occurrence of cracks generated by different mechanisms makes the analysis more difficult. Sometimes it is not possible to decide from the evidence at hand, if a crack was generated by AAR or has another origin. Therefore, a thin section should always be studied entirely to get an overview of the microstructural features present, before any type of in-depth study and analysis is done. Several thin sections are needed for an assessment of any degradation mechanism.

For the diagnosis of AAR, it is important to find crack patterns as shown in Figures 3.12 or 3.14. Microcracks or cracks in aggregates per se are not an indication for AAR, as they may have originated before the aggregate was used in concrete. Especially magmatic or metamorphic rocks often display microcracks that are not related the AAR (Figures 3.15 and 3.16). This applies as well to any artificially-crushed rock material. Occasional cracks in aggregates are without any relation to damaging mechanism and occur in any concrete.

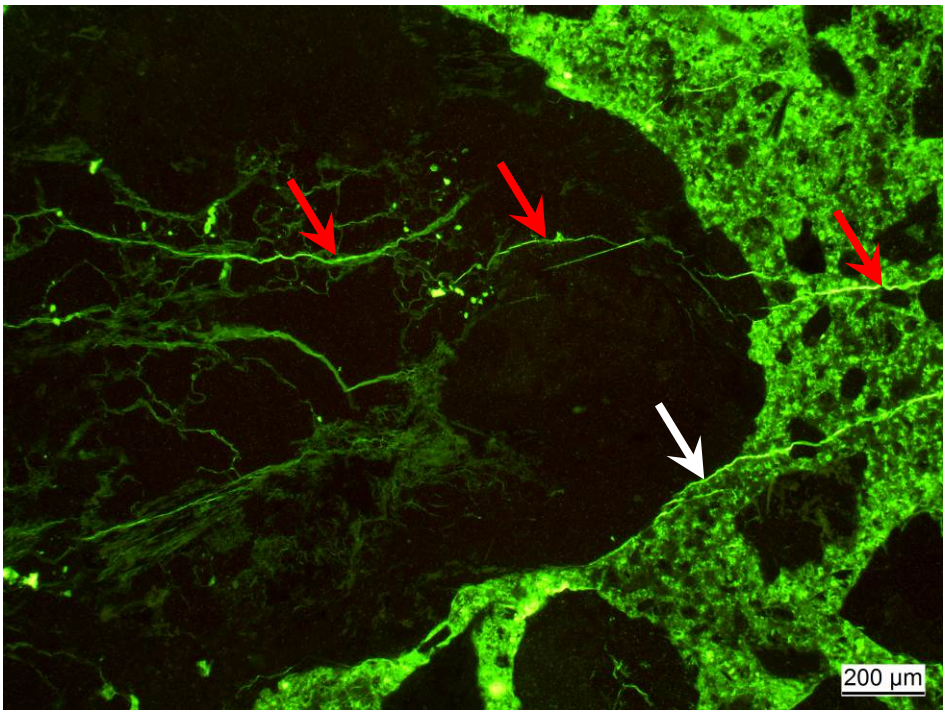

Figure 3.13: Aggregate with microcracks (red arrows). One cracks is running from the aggregate into the paste, another one travels along the interface between aggregate and paste before running into the paste as well (white arrow). Fluorescent light mode. Concrete from a dam.

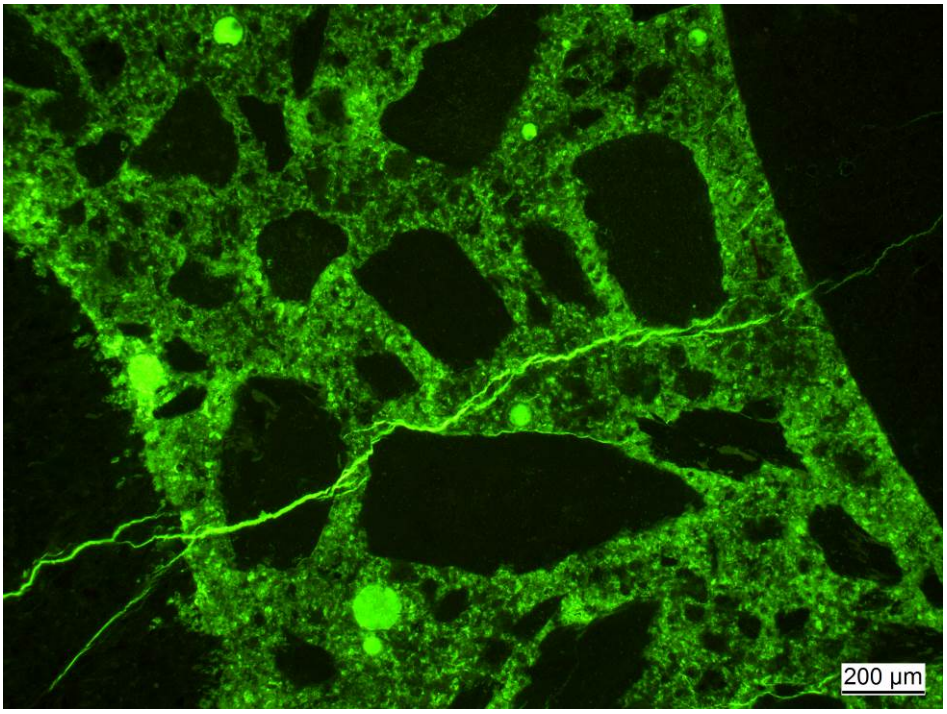

Figure 3.14: Crack running from one large aggregate to another, cutting through a small one in between. Fluorescent light mode. Concrete from a dam.

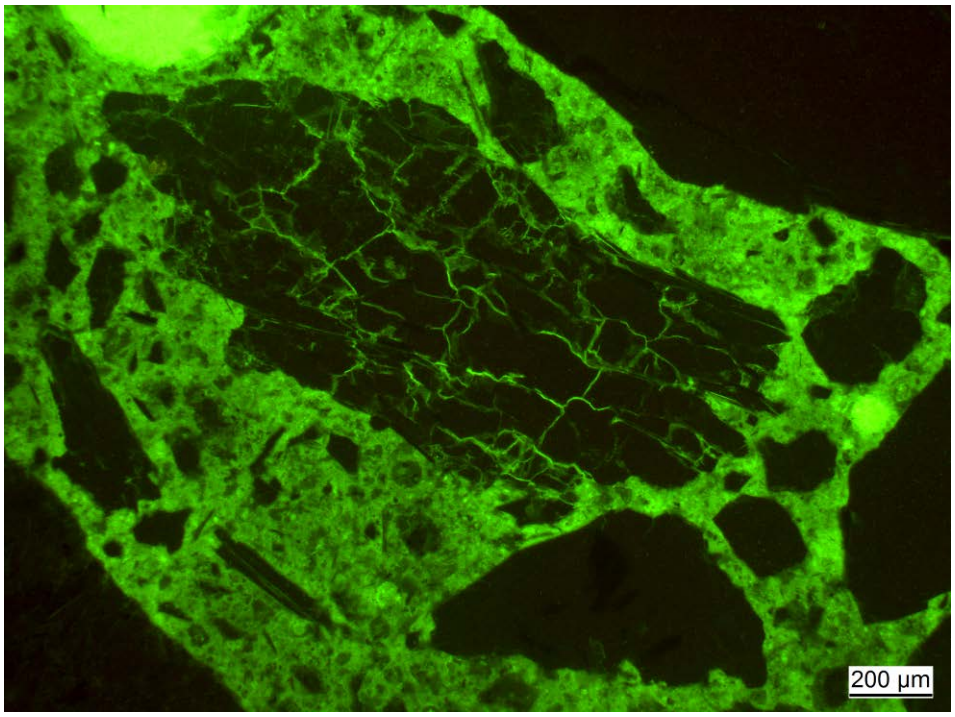

Figure 3.15: Aggregate with internal microcracks. Fluorescent light mode. Concrete from a dam.

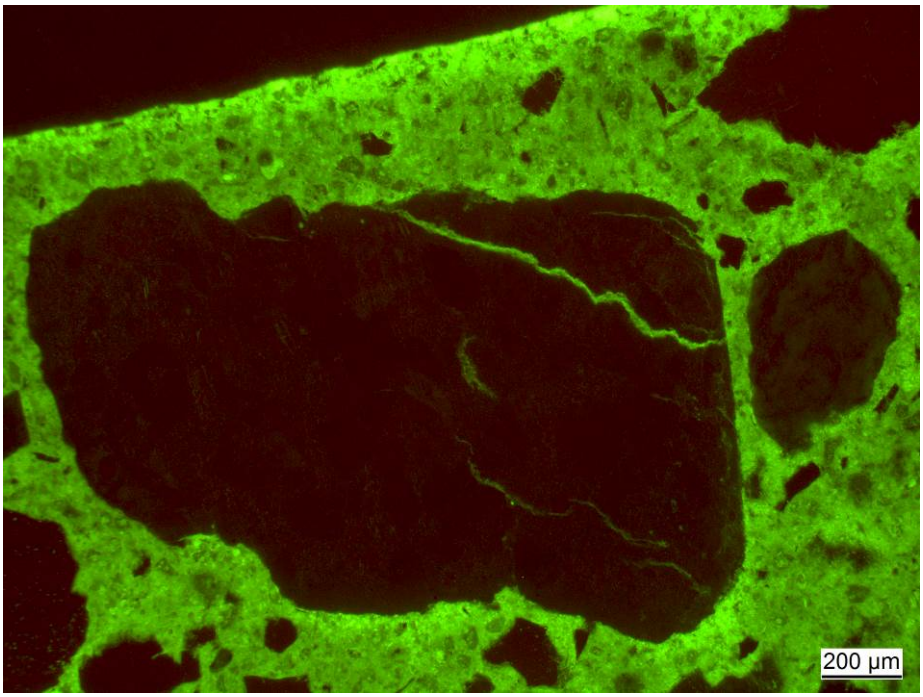

Figure 3.16: Aggregate with internal crack. Fluorescent light mode. Concrete from a dam.

However, there are certainly aggregates displaying microcracks caused by AAR without showing a crack or cracks running into the paste, as the plane of the crack may not intersect with the plane of the thin section. Or there may be a crack travelling along the interface of one aggregate indicating no AAR: But it might be caused by AAR in another aggregate. Therefore, the amount of reacted aggregates is generally

underestimated. Part of such aggregates can still be recognized as reacted, if the cracks contain AAR products (see following paragraph).

In dams at an initial stage of AAR, the same crack patterns as described above can be observed. However, cracks running a length of several centimeters and cutting through several aggregates are significantly less frequent than in a concrete with well-developed AAR. Additionally, cracks width is lower.

Of course, cracks in a concrete can be caused by other processes than AAR. Most common are shrinkage cracks (either by drying of the concrete in the structure or later during sample preparation), cracks caused by mechanical loading in the structure, cracks caused by the coring procedure or in the lab by cutting. Therefore, cracks cannot be used as only feature to diagnose AAR. The products formed by AAR play an important part in the diagnosis as discussed in the following paragraph.

3.3.2.2 AAR products

AAR products can be found within aggregates and in the cement paste. Their occurrence is a definite sign for AAR. AAR products can be best recognized in the transmitted light mode, preferably with crossed polarizers and gypsum plate inserted.

AAR products in aggregates are present mainly in cracks caused by AAR. Less frequently, they can be observed in voids present in the aggregates. However, the amount of the AAR products present is no indication for the severity of concrete deterioration, which has to be assessed separately based on the extent of cracking.

In some agggregates the cracks are empty except at the edge of the aggregate, where they form a kind of plug (Figure 3.17). In other cases, the reaction products do not completely fill the cracks (Figure 3.18). In such situations, it is important to closely inspect the sample, to make sure rock fragments generated by crack formation are not mistakenly interpreted as AAR product. If the rock fragments consist of carbonates they can easily be distinguished from the AAR product due to their color under crossed polarizers. In the case of silicate rock fragments, the AAR products display features that make them recognizable in most of the cases (see discussion on the characteristics of the AAR product below). In other cases, the AAR products completely fills the cracks in the aggregates (Figure 3.19).

In dams where AAR is at an early stage, cracks completely filled with AAR product are not very frequent. More frequent are cracks that are empty or show the first AAR products in the cracks (Figure 3.18). In such cases, the additional use of SEM/EDX is recommended.

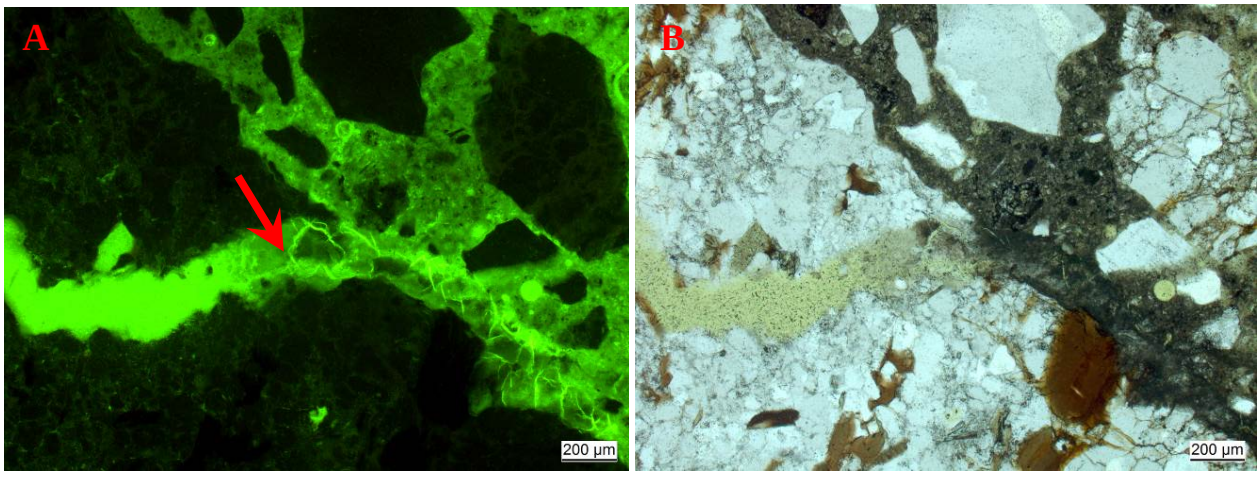

Figure 3.17: AAR products forming a plug at the edge of the an aggregate (arrow) and filling the crack running into the paste. Fluorescent light mode (A) and polarized light (B). Concrete from a dam.

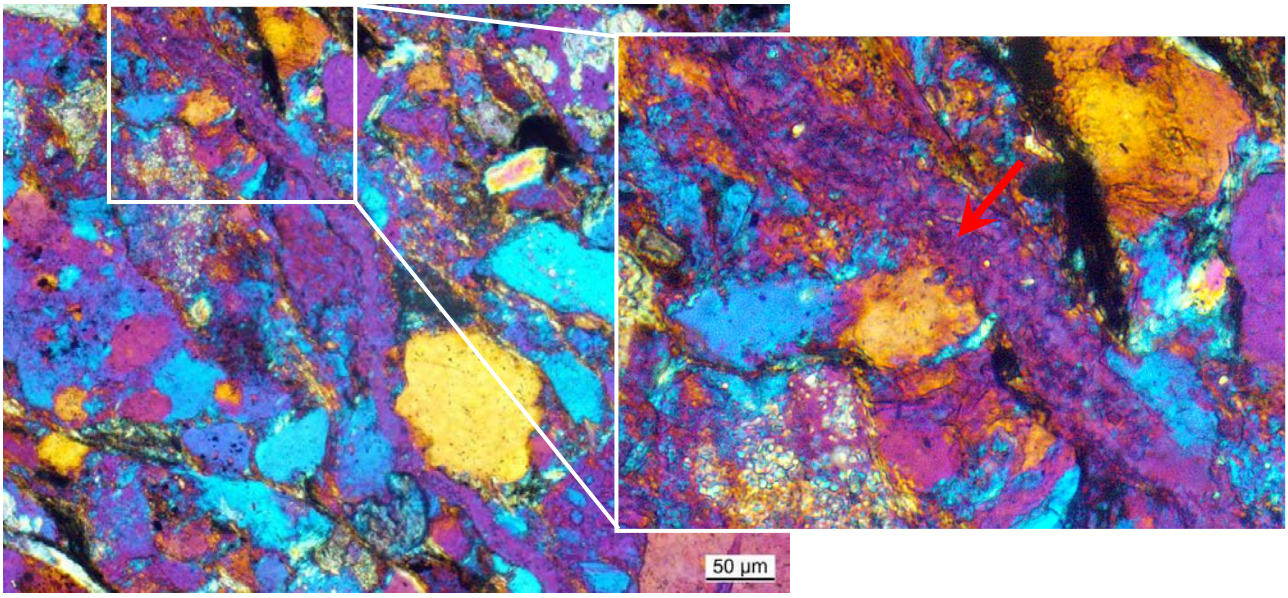

Figure 3.18: Crack partly filled with AAR product and rock fragments (arrow). Crossed polarizers and gypsum plate. Concrete from a dam.

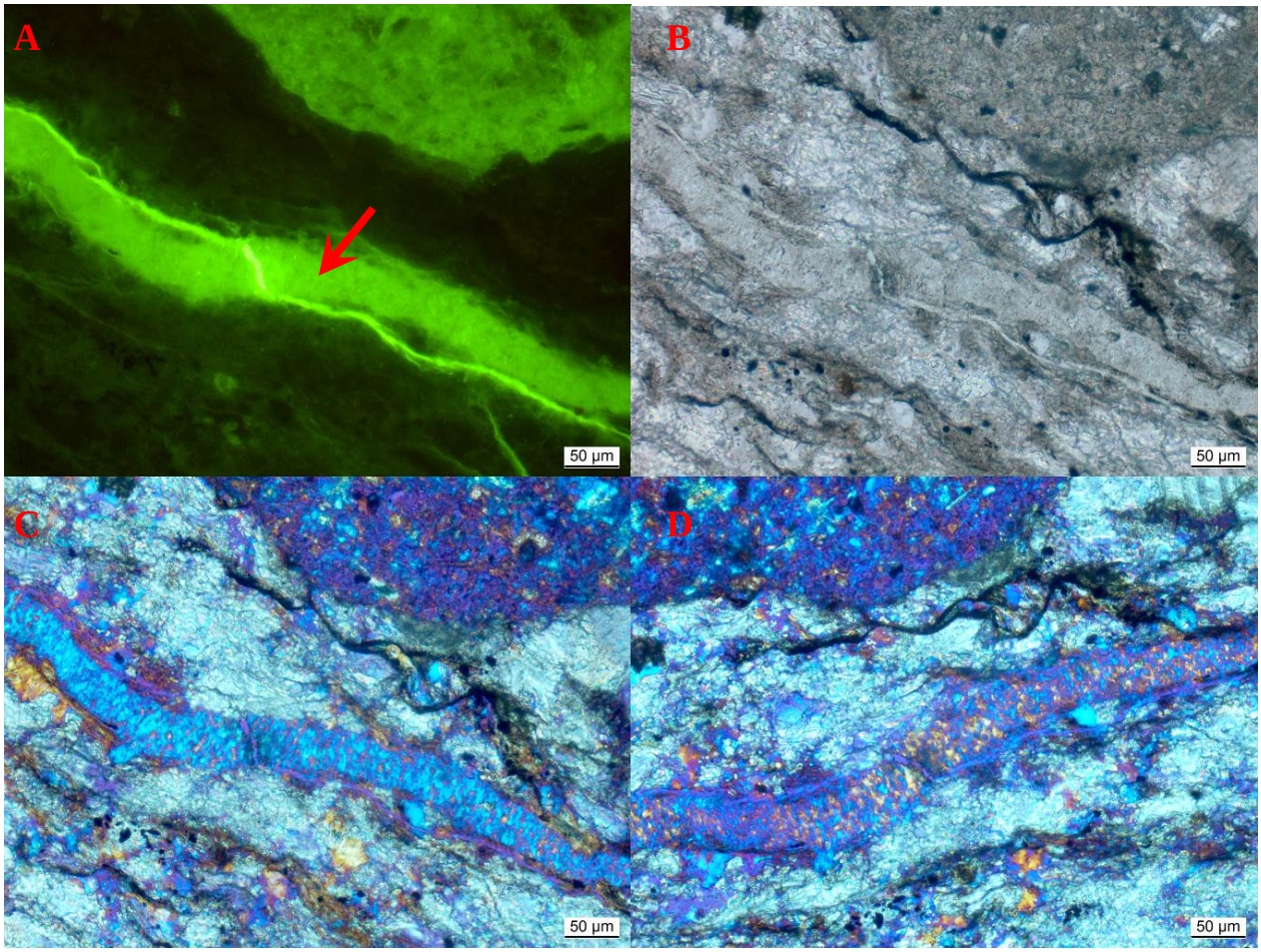

Figure 3.19: Identical location in a thin section imaged with different light modes showing AAR products (arrow) completely filling a crack (A: fluorescent light, B: polarized light, C: with crossed polarizers and gypsum plate), D: same as C but turned by about 45 °. The small empty crack running parallel to the crack filled with AAR product is an artifact of sample preparation. Concrete from a dam.

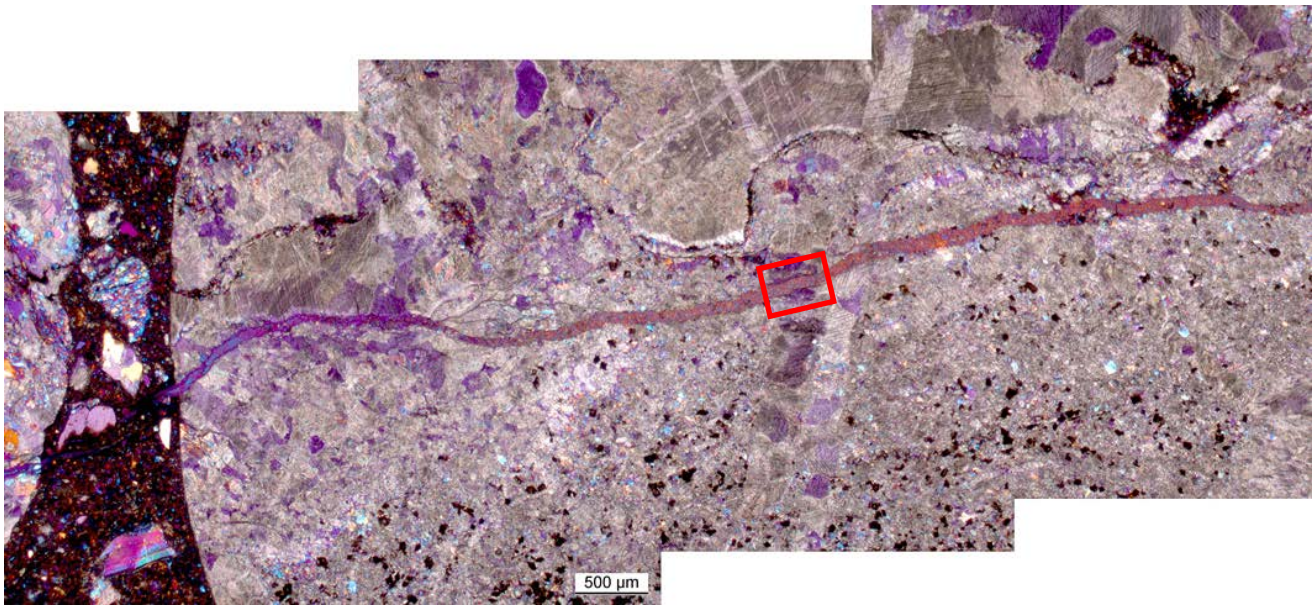

Figure 3.20: Crack running through an aggregate. The red rectangle indicates the location of the following image. Note that the AAR product in the crack is refractive but then changes to amorphous as the crack approaches the left edge of the aggregate. The bluish color very close to the edge of the aggregate is caused by epoxy filling the partly empty crack. Crossed polarizers with gypsum plate. Concrete from a bridge.

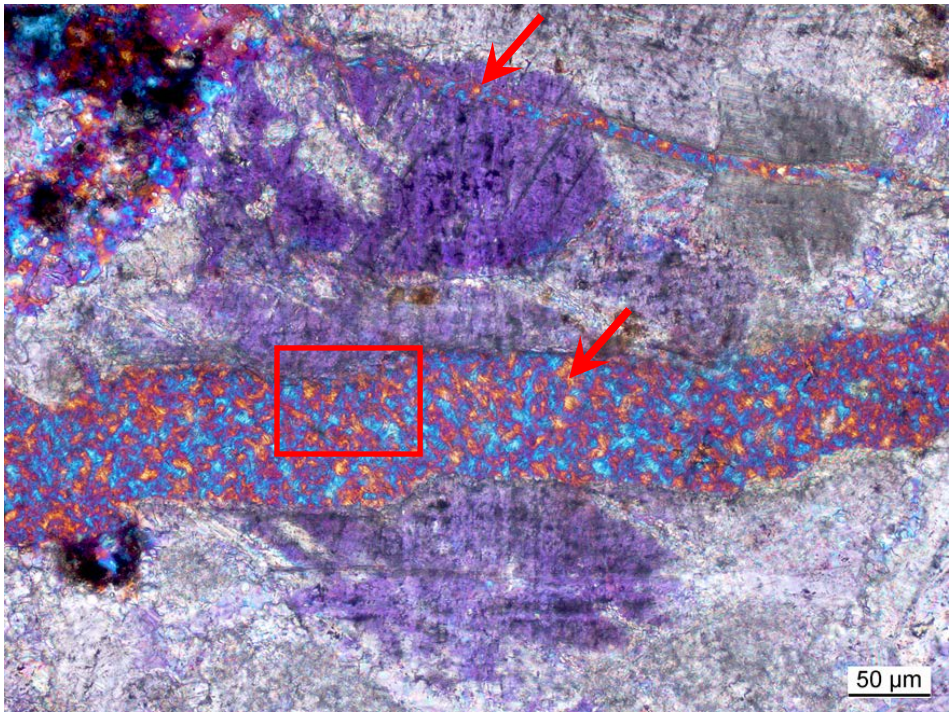

Figure 3.21: Crystalline AAR product filling cracks (red arrows). The image represents the area marked in Figure 3.20. The red rectangle indicates the location of the SEM image shown in Figure 3.30. Crossed polarizers with gypsum plate.

The AAR product within aggregates usually has the same characteristics. It is refractive (showing that it is a crystalline material) and displays small domains with the same crystal orientation (Figures 3.20 and 3.21). The size of these domains ranges from about 1 to about 10 µm. As the size of these domains is usually of the same size in a specific aggregate, the AAR product can be distinguished from silicate rock fragments (having similar optical properties as the AAR product but different grain size) in the crack. However, sometimes the resolution limits given by the thickness of the thin section, the optical quality of the lens, its magnification and the wavelength of light do not permit to distinguish between AAR products and silicate rock fragments. If the crack width decreases below 20 µm, it is difficult to recognize the AAR product with any confidence (Figure 3.22). However, observation by SEM can solve such problems.

At the edge of the aggregate, the AAR product changes its characteristics: it is amorphous and can consequently be described as a gel (Figure 3.23). This change goes together with a change in chemical composition as shown in paragraph 3.4.2.

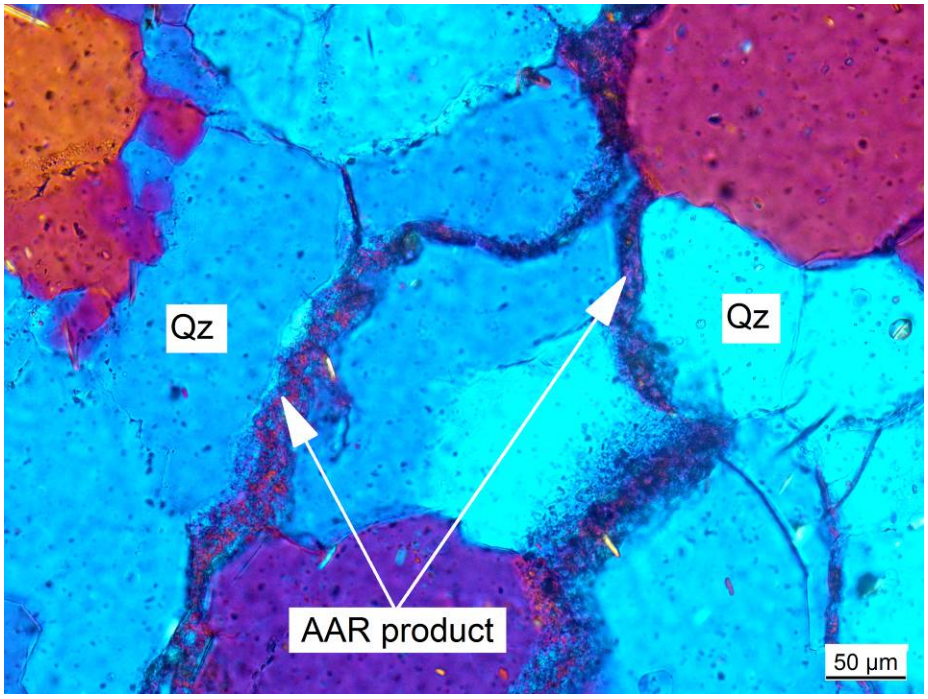

Figure 3.22: AAR product in cracks cutting through a gneiss aggregate (Qz = quartz). The typical texture of the AAR product can be recognized in the sections of the crack with larger width but not in the narrower ones. Crossed polarizers with gypsum plate. Concrete from a dam.

AAR products in the cement paste occur in cracks caused by AAR, as an "impregnation" of the cement paste directly around reacted aggregates but mostly in direct vicinity where a crack from the aggregates meets the paste and in voids.

Cracks in the paste, originating in cracked aggregates, can be empty, partly or completely filled with AAR product.

In the cracks of the cement paste, the AAR product is amorphous. Sometimes it is of lower porosity than the crystalline product, resulting in a lower luminescence (Figure 3.12). In some cases, several bands running parallel to the crack edges can be observed in the amorphous AAR product.

The AAR product found in air voids of the cement paste is of variable morphology. It can be amorphous or crystalline (Figures 3.24-26), but in the majority of the cases it is amorphous. Some times ettringite needles

are present in the air voids together with the AAR product. This applies in particular to concrete with high moisture content as it is the case in dams (see paragraph 3.6).

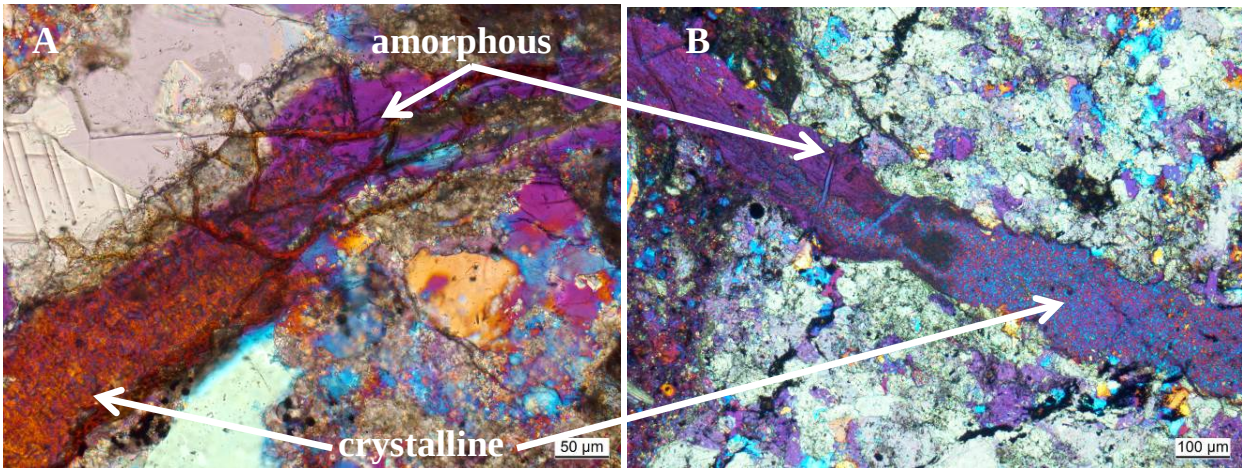

Figure 3.23: Two examples showing the transition from crystzalline to amorphous AAR product at the edge of an aggregate. The same area of the polished thin section (Figure 3.23A) is shown again in Figure 3.33. Crossed polarizers with gypsum plate. Concrete samples from a bridge.

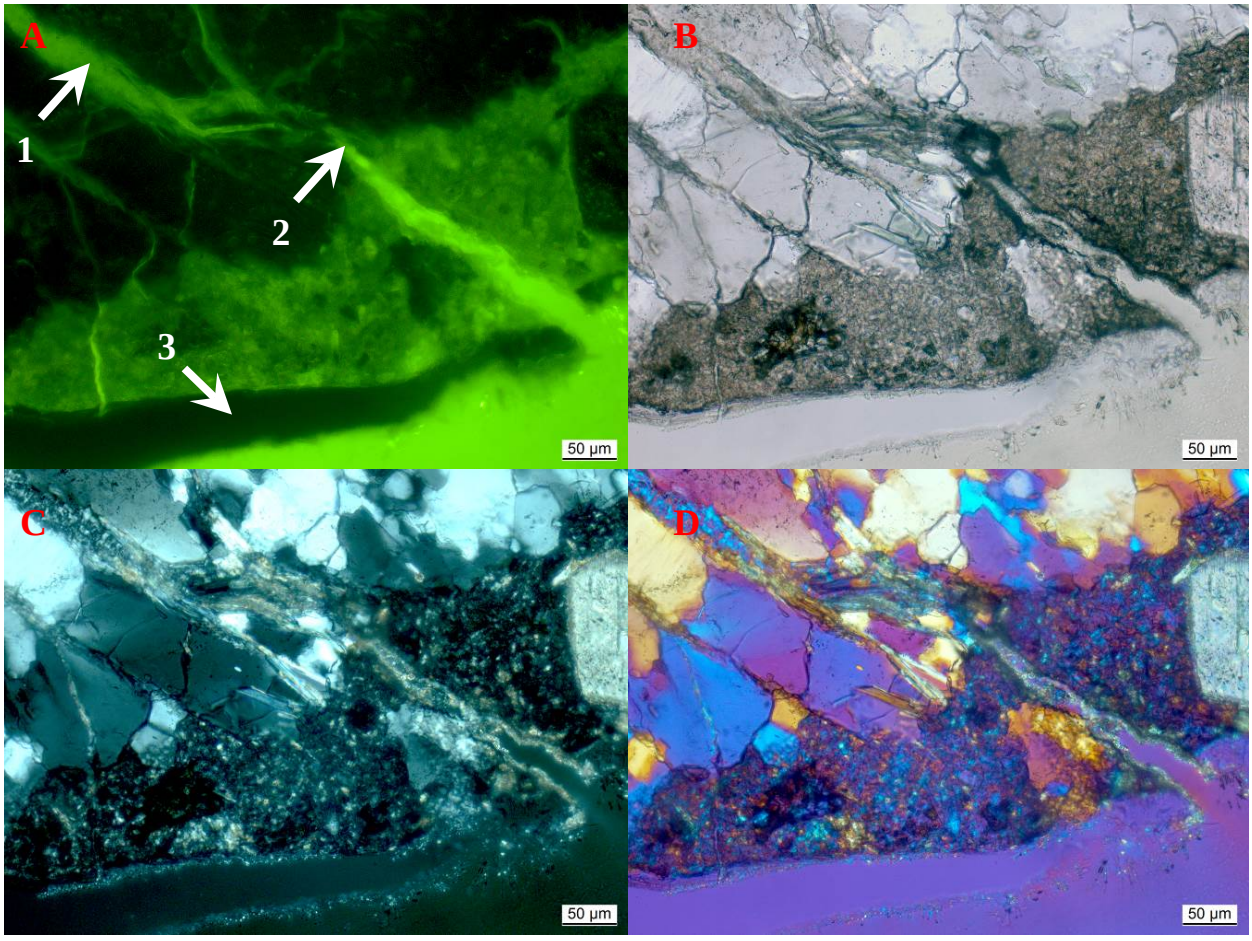

Figure 3.24: Identical location in a thin section using different light modes (A: fluorescent light, B: polarized light, C: with crossed polarizers, D: with crossed polarizers and gypsum plate). A crack filled with crystalline AAR product (1) runs from the aggregate into the paste, where it is partly filled with amorphous and with some carbonated AAR products (2). The crack ends in a void that shows a rim of amorphous AAR product (3). Concrete from a dam.

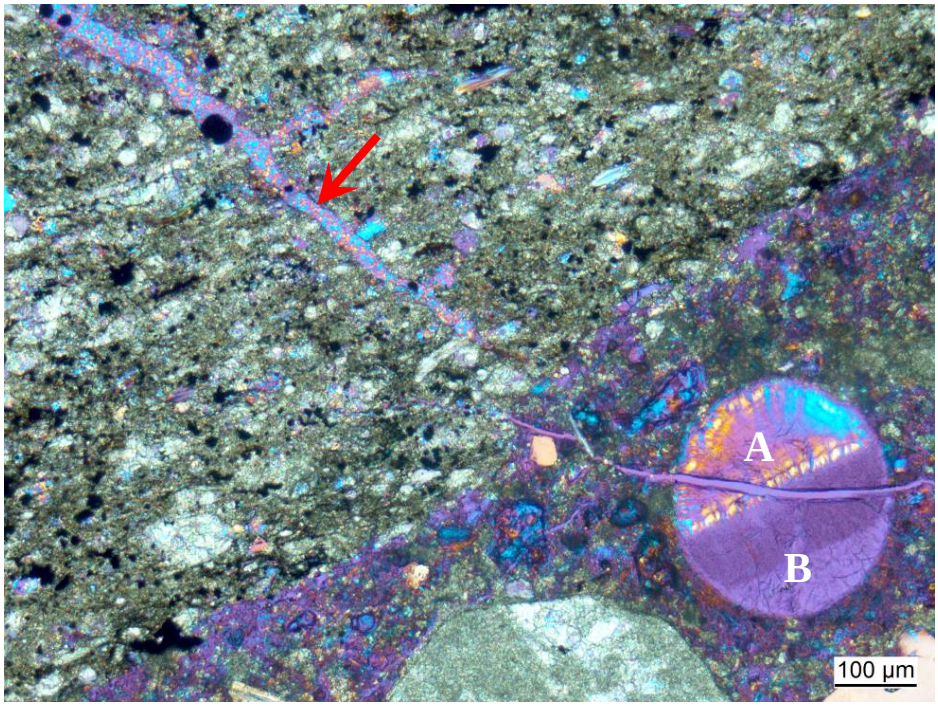

Figure 3.25: Crack filled with crystalline AAR product (arrow) and air void filled with partly crystalline (A) and partly amorphous (B) AAR product. Crossed polarizers with gypsum plate. Concrete from a dam.

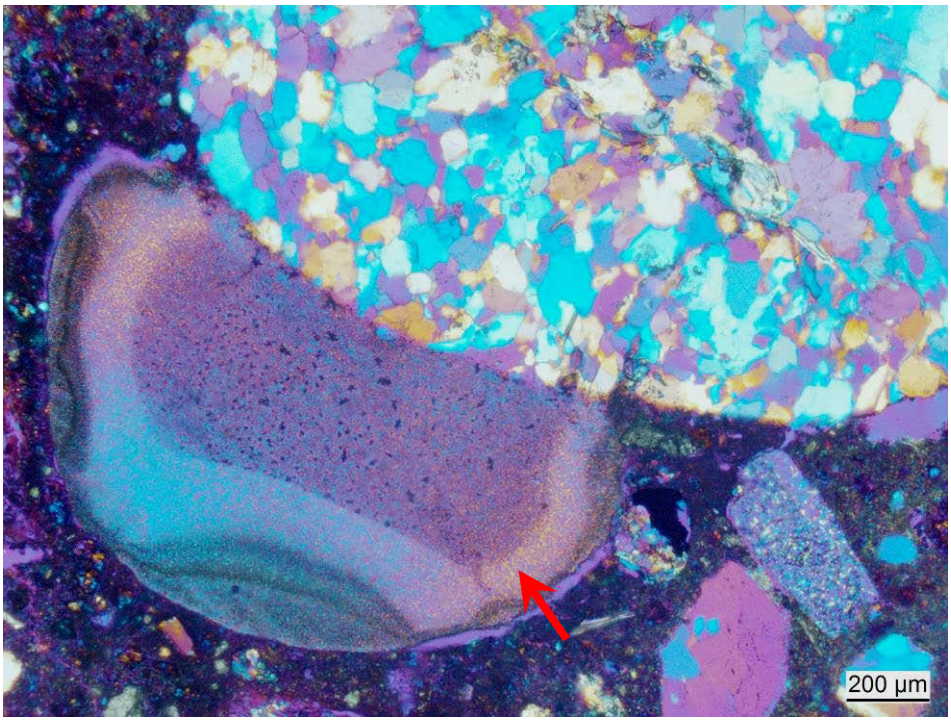

Figure 3.26: Air void filled with crystalline AAR product (white arrow). Crossed polarizers with gypsum plate. Concrete from a bridge.

A remark has to be made about the structure of the AAR product. Based on the optical properties of the AAR product, it has been pointed out above that the AAR product within the slow reacting Swiss aggregates is crystalline. Furthermore, it has been confirmed in several studies by XRD that the AAR

product within aggregates can be a crystalline phase [Cole et al., 1981; Cole & Lancucki, 1983; Marfil & Maiza, 2001; Peterson et al., 2006; Katayama, 2012]. In spite of this, the AAR product is generally referred to as "gel". In some studies, partly acknowledging the evidence at hand, the AAR product is described as "crystalline gel" or "textured gel". In a few publications it is claimed that drying of the sample turns the gel into a crystalline product [e.g. Davies & Oberholster, 1988]. However, this does not apply for any of the numerous concrete samples studied during the last 15 years at Empa. As it can be seen in Figure 3.9, the crystalline nature of the AAR product can already be observed in the undried concrete as domains with the same optical orientation, which reflect the light from the microscope as discussed in Leemann & Lura [2013]. Additionally, measurements of undried samples with micro-XRD at two different synchrotrons have shown that the AAR product can be a crystalline material (unpublished data). The occurrence of amorphous AAR products as a first phase within aggregates seems to be related to fast-reacting aggregates and samples exposed to accelerated testing conditions [Katayama, 2012; Leemann & Lura, 2013]. The transformation from a crystalline AAR product to a secondary amorphous product by taking up calcium from the cement paste is described in paragraph 3.4.

3.4 SEM combined with EDX

3.4.1 Introduction

The most widespread tool to characterize the microstructure and the local chemical composition of cement-based materials is the scanning electron microscope (SEM) in combination with energy dispersive X-ray spectroscopy (EDX). However, it has to be pointed out that the data about chemical composition obtained are only semi-quantitative. The accuracy of the results depends on the specific microscope and adjustments used. In the majority of the cases, the data obtainable with SEM/EDX are sufficient for the investigation of cement-based materials. If quantitative data are needed, they can be obtained with an electron probe micro analyzer (EPMA) equipped with wavelength-dispersive X-ray spectroscopy (WDS). However, as the acceleration voltage of the electron beam in the EPMA is usually higher than in the SEM, the interaction volume is larger and the spatial resolution is consequently lower. A summary of electron microscopy applied to cement-based materials can be found in Richardson [2002]. Further information about the application of SEM on concrete is given for example in Richardson [2002], Kjellsen et al. [2003] and Scrivener [2004].

It is preferable to study the composition of AAR products with SEM/EDX on impregnated and polished samples. Breaking concrete samples, drying, coating them and analyzing the broken surfaces afterwards should be avoided even if this approach is used in some studies dealing with cement and concrete. The reason is that solved ions are transported to the drying surface, often overprinting or at least distorting the chemistry of the original surface. Additionally, the surface roughness further affects the results, allowing only for a qualitative analysis. Even on the surface of thin sections or polished sections, exudations from the AAR product can sometimes be observed a couple of months after sample preparation. These exudations usually consist of sodium as the main component. The sodium originates in the AAR product, which contains sodium not only as chemically bound but also as hydrated ions (see paragraph 3.4.2). With some residual moisture of not-impregnated areas of the AAR product, the sodium is transported to the polished surface. There it forms droplets [Jakobsen et al., 1992] or, after the reaction with CO_2, needles of Na_2CO_3 (Figure 3.27). However, unlike on broken surfaces, such mineral formations are easily recognizable as artifacts on polished sections.

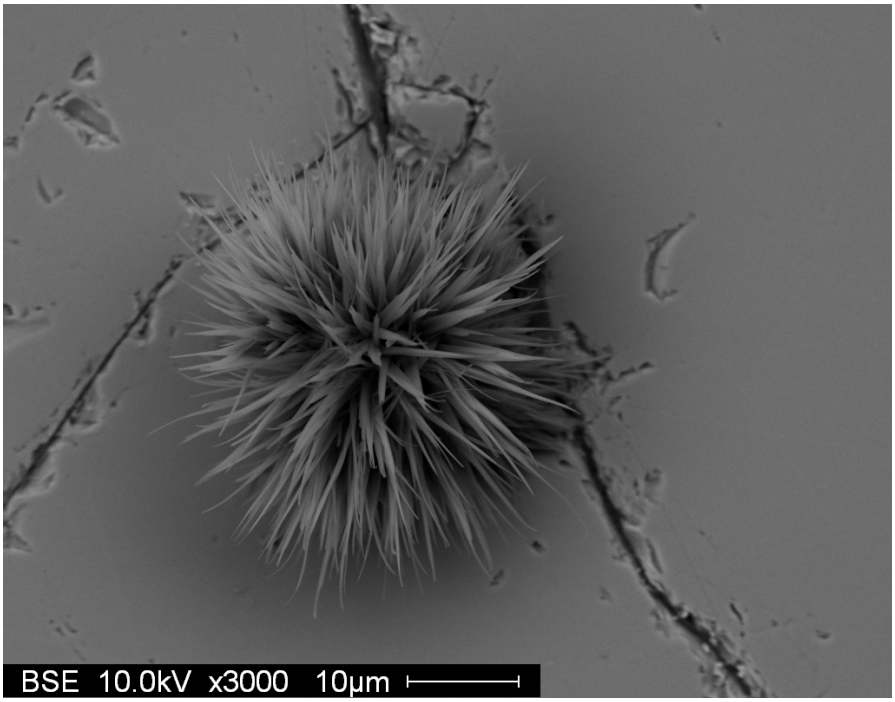

Figure 3.27: Formation of Na_2CO_3 on the surface of a polished section in an aggregate with AAR. Concrete from a bridge.

Samples for SEM/EDX are selected, dried and impregnated in the same way as the ones for thin sections (see paragraph 3.3.1). After removing 1-2 mm by polishing to avoid artifacts introduced by cutting and grinding the sample before impregnation, the surface to-be-investigated is polished. It is recommended to make an image of the sample before carbon-coating, because it can be used as a map, facilitating orientation during the investigation with SEM. Such an image can be obtained by different means, but an image with sufficiently high resolution is very easy to obtain using a flatbed-scanner (Figure 3.28). The last step is the carbon coating to make the sample conductive.

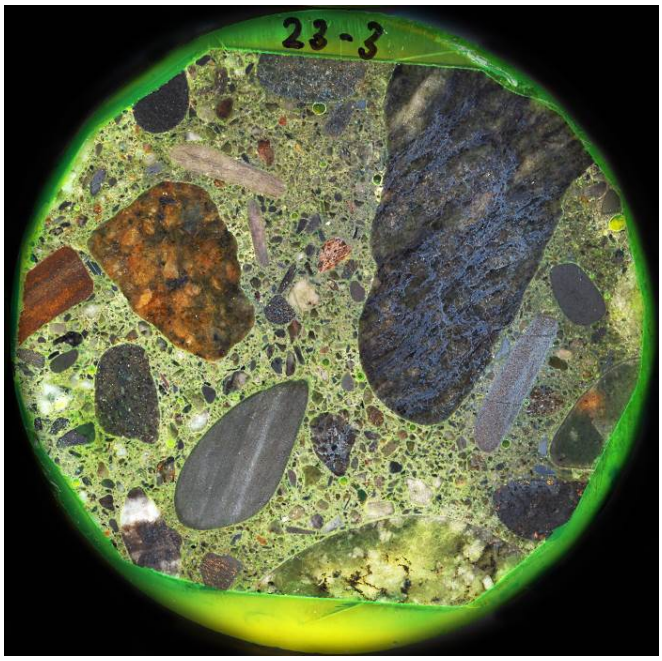

Figure 3.28: Impregnated and polished concrete sample coated with carbon for SEM investigation (diameter of sample: 50 mm). Image obtained using a flatbed-scanner. Concrete from a dam.

The crack patterns in AAR-affected concrete are obviously independent of the microscopic method applied. As the crack patterns typical for AAR have already been discussed in the previous paragraph covering thin sections, the following paragraph directly focuses on the characteristics of the AAR product. In addition, the higher resolution used in SEM makes it unpractical for mapping crack patterns.

3.4.2 Characteristics of the reactions products

3.4.2.1 Advanced stage of AAR

The crystalline AAR product within aggregates shows microcracks caused by drying that indicate a sheet-like morphology of the mineral forming domains with the same orientation (Figures 3.29 and 3.30). The morphology that can be present in air voids (Figure 3.31) indicates that domains showing the same orientation both in the polarized light microscope and the SEM are indeed stacks of single crystals. This agrees as well with the rosette-type morphology of the crystalline AAR product formed in voids, as reported in many papers [e.g. Shayan & Quick, 1989; De Ceukelaire, 1991; Katayama, 2012] and shown in Figure 3.31. The composition of the crystalline AAR product varies relatively little [Katayama, 2012; Leemann & Merz, 2013]. This applies both to different areas of a large structure like a dam (Table 3.1) and to other types of structures.

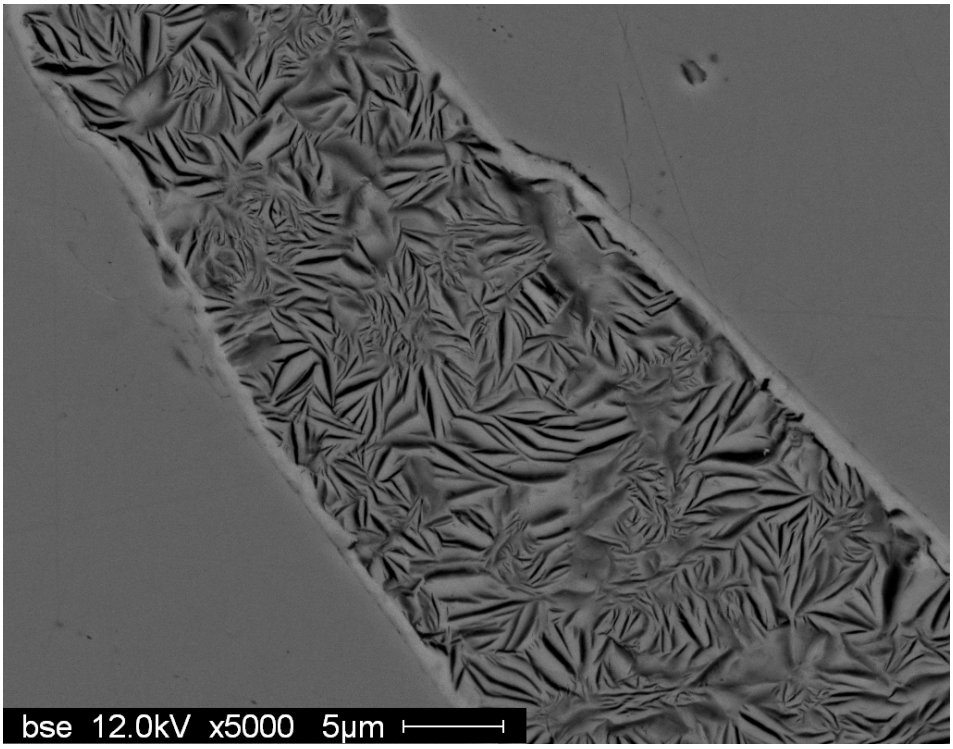

Figure 3.29: Crack in a gneiss aggregate filled with reaction product. Concrete from a dam.

Table 3.1: Chemical composition of the AAR product in three different sections of a dam. 160 points analyzed.

Element	O	Na	Mg	Al	Si	S	K	Ca	Fe	Ca/Si	(Na+K)/Si
	[Mol-%]									[-]	
BL11-2	40.5	1.9	0.3	0.9	36.5	0.3	8.4	10.4	0.7	0.28	0.28
BL16-2	40.5	1.5	0.4	2.5	36.0	0.3	8.2	9.7	0.7	0.27	0.27
BL23-6	43.3	2.0	0.3	0.8	34.9	0.4	7.6	9.7	0.6	0.28	0.28

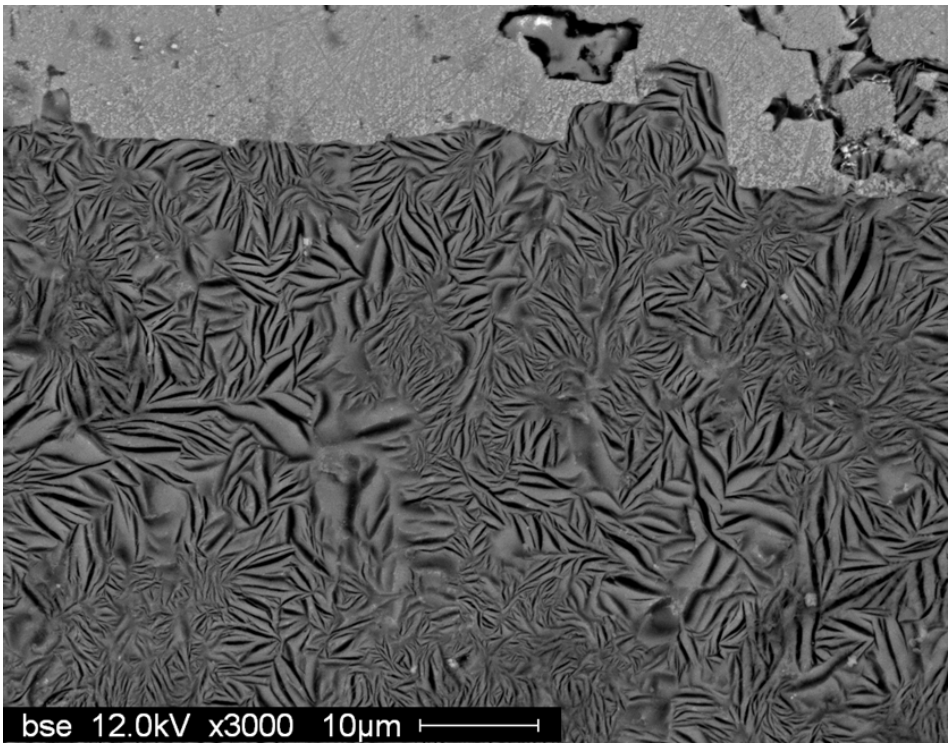

Figure 3.30: This image corresponds to the area marked with a red rectangle in Figure 3.21. Concrete from a bridge.

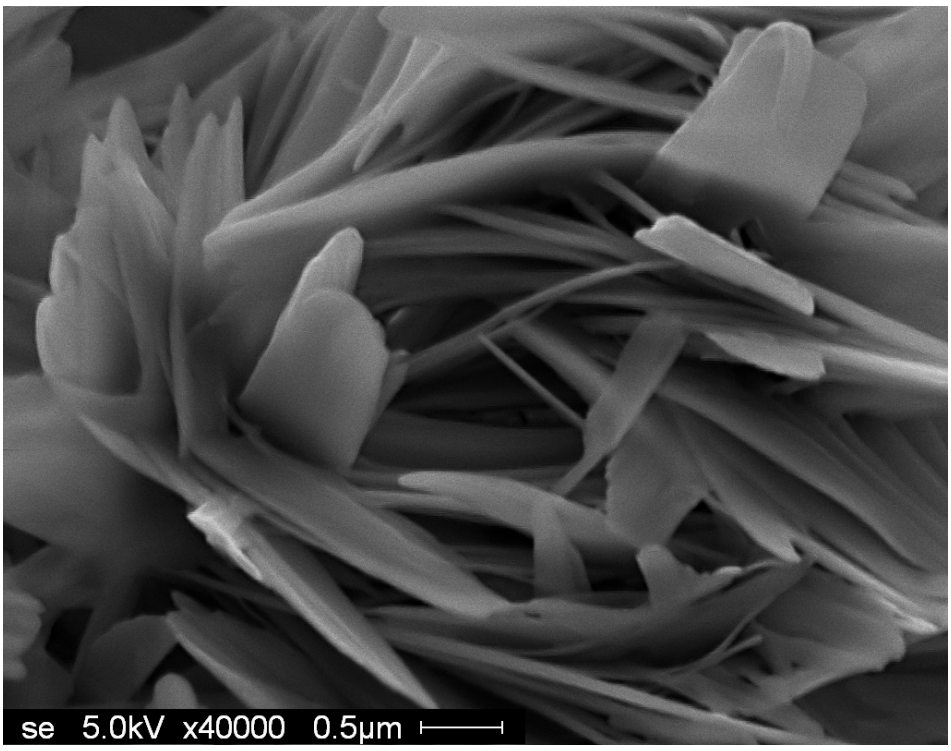

Figure 3.31: Morphology of crystalline AAR product in an air void. Concrete from a bridge.

The amorphous AAR product at the edge of aggregates does not display the multitude of small shrinkage cracks typical for the crystalline AAR product, but appears instead to be homogenous. Sometimes, bands

running parallel to the crack edge are present. This applies in particular for the AAR product filling cracks in the cement paste.

The change from crystalline to amorphous goes together with a change in composition. The calcium content of the AAR product increases and the alkali content decreases (Table 3.2). This change in composition has been reported in several studies [e.g. Knudson & Thaulow, 1975; Thaulow et al., 1996; Thomas, 2001; Leemann & Lothenbach, 2008; Katayama, 2012; Leemann & Merz, 2013]. The Ca/Si-ratio of about 0.22-0.30, typical for the crystalline AAR product, can increase to values above 1.0 [Katayama, 2012]. An example in concrete from a dam is shown in Figure 3.32. The decrease in alkali content going together with the change from crystalline to amorphous can be seen as well in the elemental mapping shown in Figure 3.33.

The range in composition of the AAR product present in large pores and voids of the cement paste shows the same range as the one filling cracks. The crystalline AAR product present in air voids (Figurer 3.31) has the same composition as the crystalline product within aggregates, whereas the amorphous product has higher calcium and lower alkali content.

Table 3.2: Composition of the reaction product in four different aggregates ([1] = crystalline AAR product, [2] = amorphous AAR product at the edge of aggregates). Data from Leemann & Lura, 2013.

elements in mol-%	aggregate				
	G2-8[1]	G5a[1]	G4-1[1]	G5a[2]	G4-1[2]
O	42.8 ± 3.5	46.5 ± 3.0	47.3 ± 2.0	45.2 ± 1.4	45.6 ± 1.6
Na	2.0 ± 0.6	2.1 ± 0.4	2.2 ± 0.5	3.7 ± 0.5	3.4 ± 0.5
Mg	0.4 ± 0.2	0.4 ± 0.3	0.5 ± 0.3	0.4 ± 0.2	0.4 ± 0.2
Al	0.7 ± 0.2	0.8 ± 0.2	1.0 ± 0.4	0.6 ± 0.1	0.6 ± 0.2
Si	35.6 ± 2.0	33.9 ± 3.2	34.4 ± 1.7	32.1 ± 1.0	32.2 ± 1.2
S	0.3 ± 0.2	0.4 ± 0.3	0.5 ± 0.3	0.5 ± 0.2	0.6 ± 0.2
K	8.0 ± 0.8	7.0 ± 0.8	5.0 ± 1.4	4.8 ± 0.4	4.4 ± 0.6
Ca	9.6 ± 0.9	8.6 ± 0.5	8.7 ± 0.8	12.1 ± 1.0	11.8 ± 1.8
Fe	0.7 ± 0.3	0.3 ± 0.5	0.5 ± 1.0	0.6 ± 0.2	0.2 ± 0.3
Ca/Si	*0.27 ± 0.02*	*0.26 ± 0.03*	*0.25 ± 0.03*	*0.38 ± 0.03*	*0.37 ± 0.06*
(Na+K)/Si	*0.28 ± 0.03*	*0.27 ± 0.05*	*0.21 ± 0.03*	*0.27 ± 0.03*	*0.24 ± 0.03*
points	*106*	*29*	*33*	*29*	*28*

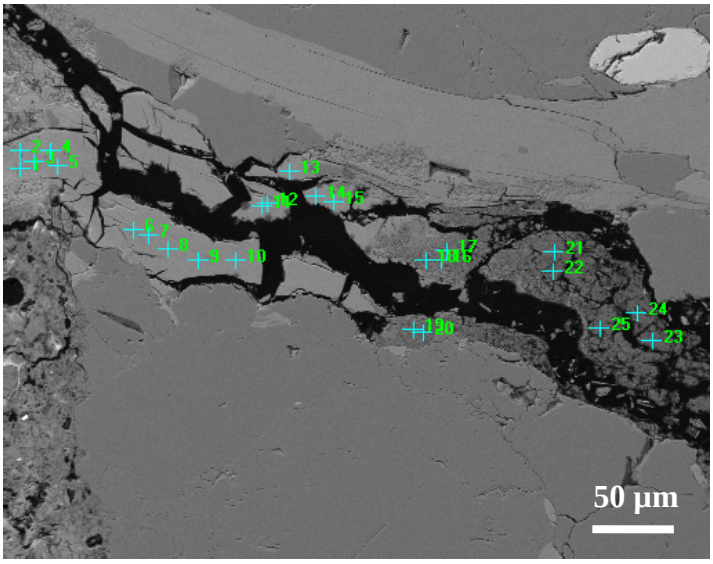

Figure 3.32: Reaction product at the edge of an aggregate changing from crystalline (points 16-25) to amorphous (points 1-15) Location of the points shown in Table 3.3.

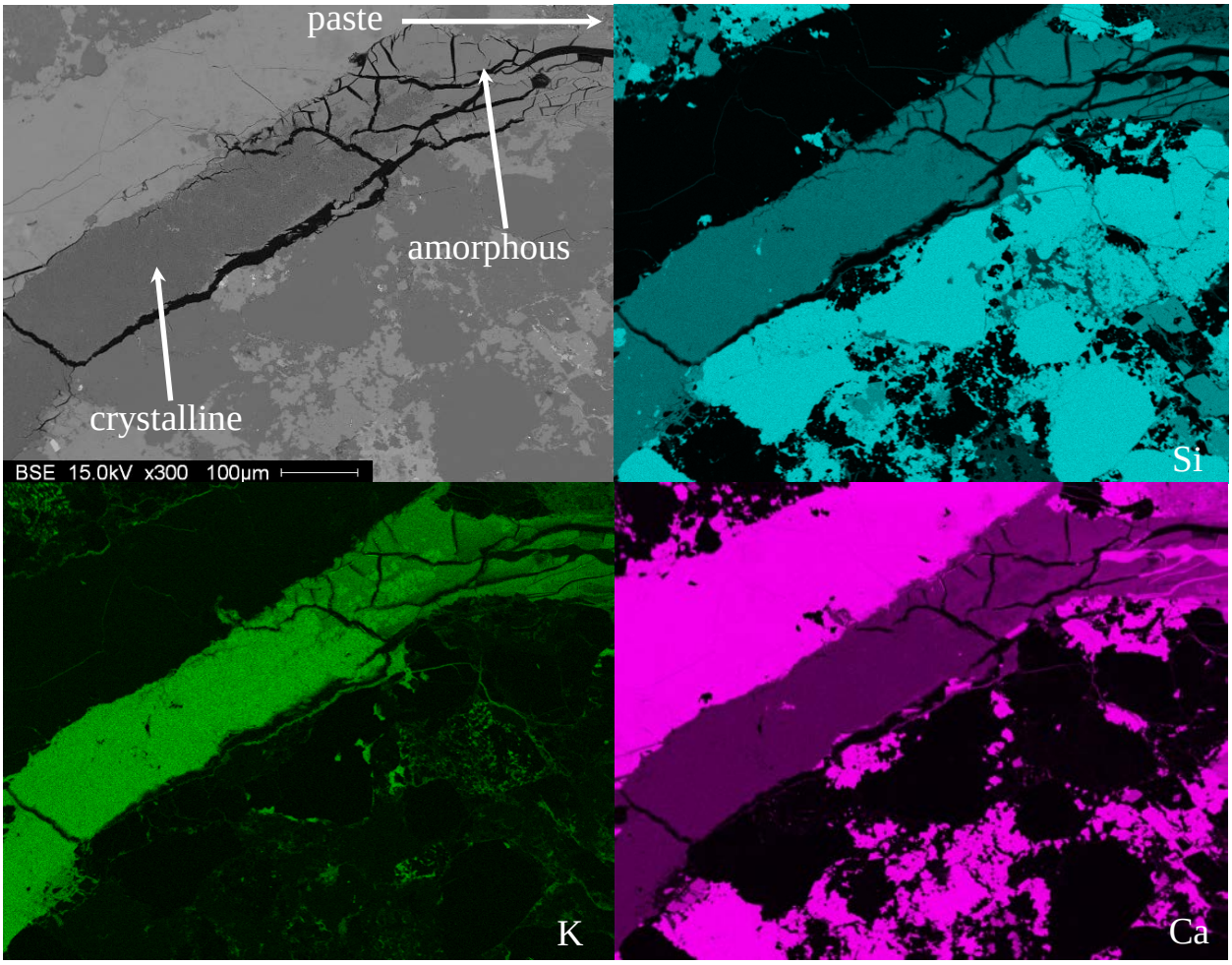

Figure 3.33: Crack filled with crystalline and amorphous AAR product at the interface to the cement paste and matching element mapping. Note that potassium signal in the amorphous AAR product is weaker than in the crystalline, indicating a lower concentration. The opposite applies to calcium. Figure 3.23A shows the same location from this polished thin section, but is made with the polarized light microscope.

Table 3.3: Composition of the AAR product shown in Figure 3.33. Points 1-5 show the composition of the AAR product filling the cracks in the paste, points 6-15 the one of the amorphous AAR product within the aggregate and points 16-25 the one of the crystalline product.

Points	O	Na	Mg	Al	Si	S	K	Ca	Fe	Ca/Si	(Na+K)/Si
	[mol-%]									[-]	
1-5	45.0	0.6	0.3	0.8	29.7	0.2	2.9	19.6	0.8	0.68	0.11
6-15	43.3	1.6	0.2	0.5	35.1	0.3	6.8	11.5	0.8	0.33	0.24
16-25	42.5	1.4	0.3	0.7	36.1	0.3	8.0	10.0	0.7	0.28	0.26

3.4.2.2 Initial stage of AAR

Because cracks in aggregates are often empty or only partly filled at an initial stage of AAR, it is important to distinguish AAR products from rock fragments. With SEM it is easy to make this distinction. Usually it can already be made based on size and backscattering contrast (Figure 3.34). If in doubt, EDX can be used for verification.

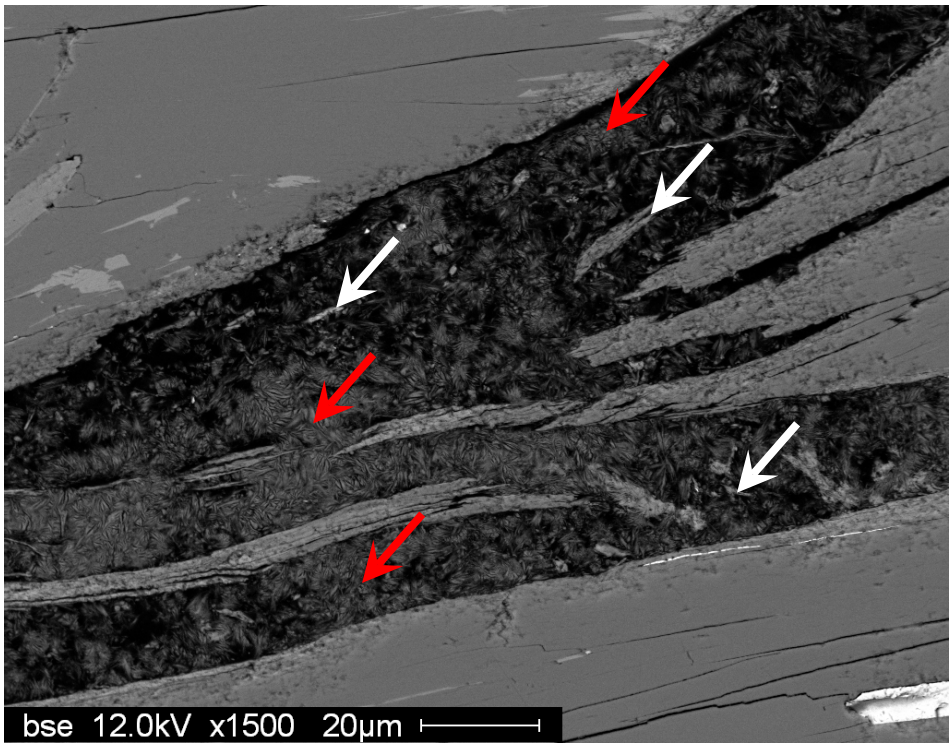

Figure 3.34: Crack within gneiss aggregate containing rock fragments (white arrows) and AAR product (red arrows). The particles with higher back-scattering contrast are rock fragments, the fine-grained material with lower backscattering contrast is AAR product. Concrete from a dam.

If AAR is at an initial state or develops only weakly, the typical crack pattern can be present but the microcracks are empty. In such cases, it is important that one is aware how AAR develops in relatively slow-reacting aggregate with quartz as reactive mineral. The pore solution of the concrete diffuses into these usually low-porosity aggregates (typical porosity: 1-2 %). AAR starts at the mineral boundaries of the quartz. When the critical stress level is exceeded, the aggregate cracks. Usually, one to a few main cracks form. But apart from these major cracks, reacted aggregates typically develop microcracks (crack width ranges from nm to µm) along the quartz grain boundaries (Figures 3.35 and 3.36). Here the stress

leading to the cracking of the aggregate was generated. Microcracking along the boundaries of quartz minerals caused during the initial cracking is relatively easy to detect in silicates but it is less pronounced in carbonates containing quartz.

It is challenging to prove the presence of AAR products at the boundaries of the quartz minerals after the initial cracking, due to the resolution limits of the EDX. With a diameter of 0.5 to 3 µm, depending on the microscope and the settings used, the interaction volume of the electron beam is considerably larger than the expected volume of the reaction product. However, if EDX line scans are placed across the boundary of two adjacent quartz grains (Figure 3.37), the presence of AAR product can often be shown. Beside the two dominating elements silicon and oxygen, calcium and alkali (potassium and/or sodium depending on the composition of the cement used) are the only other elements above the noise level (Figure 3.38). As these two elements are the main components of the AAR product, it presence can be shown this way. When AAR proceeds, first small cracks are filled with AAR product, before the larger cracks start to fill. Most often, the filling of larger cracks starts from the edge of the aggregates, as shown previously.

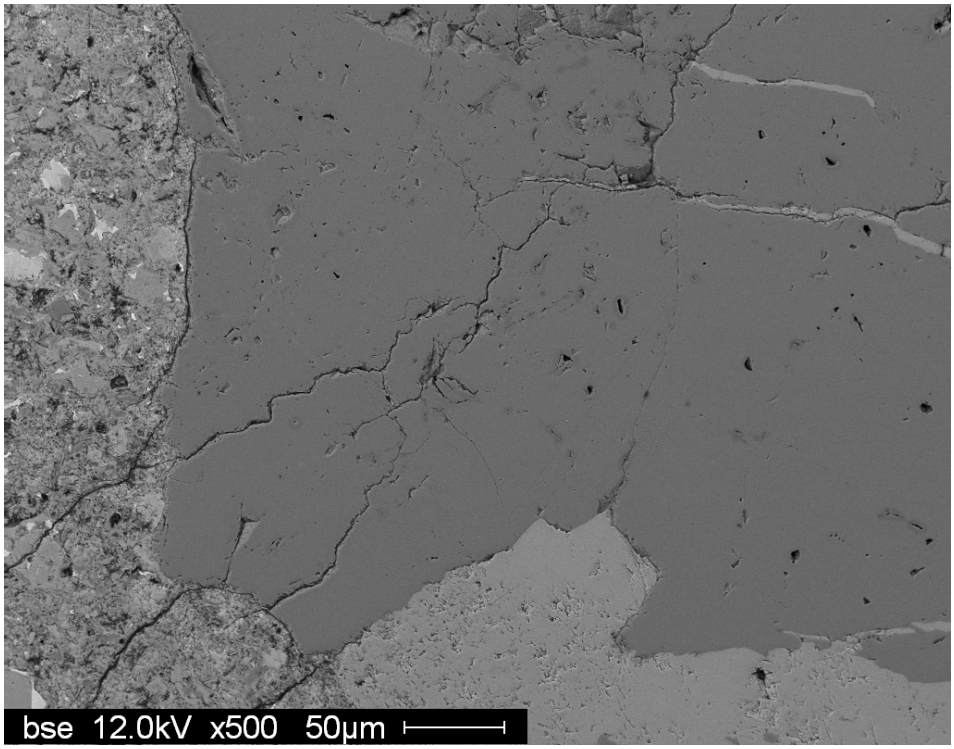

Figure 3.35: Gneiss aggregate displaying a typical AAR crack pattern without AAR products observable in the cracks. Concrete from a dam.

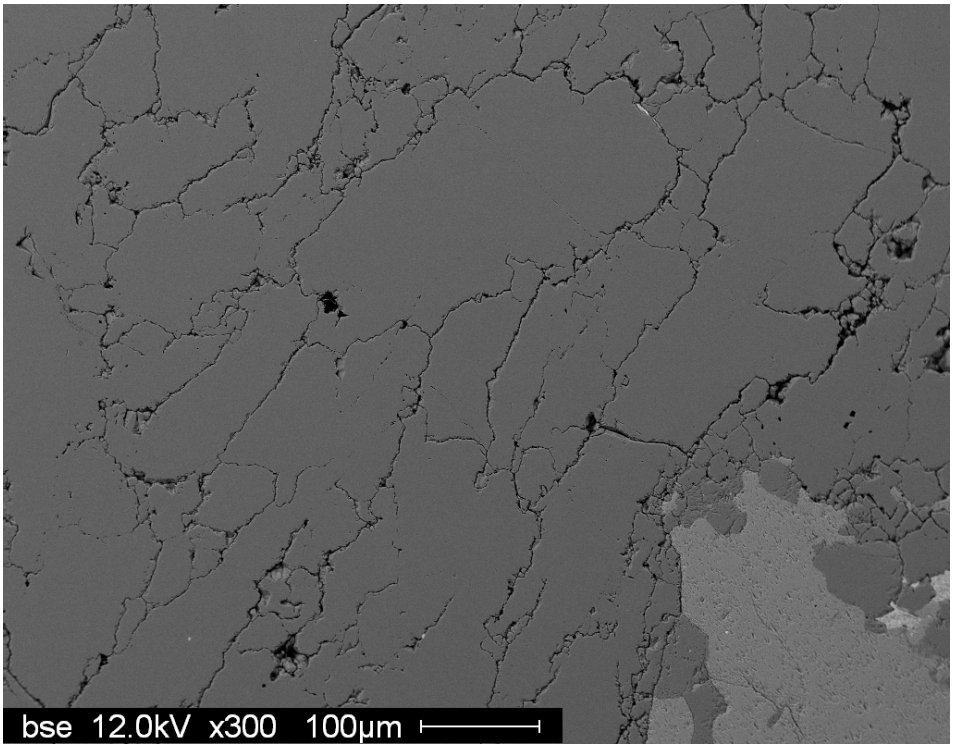

Figure 3.36: Gneiss aggregate with quartz minerals cracked along their boundaries. Concrete from a dam.

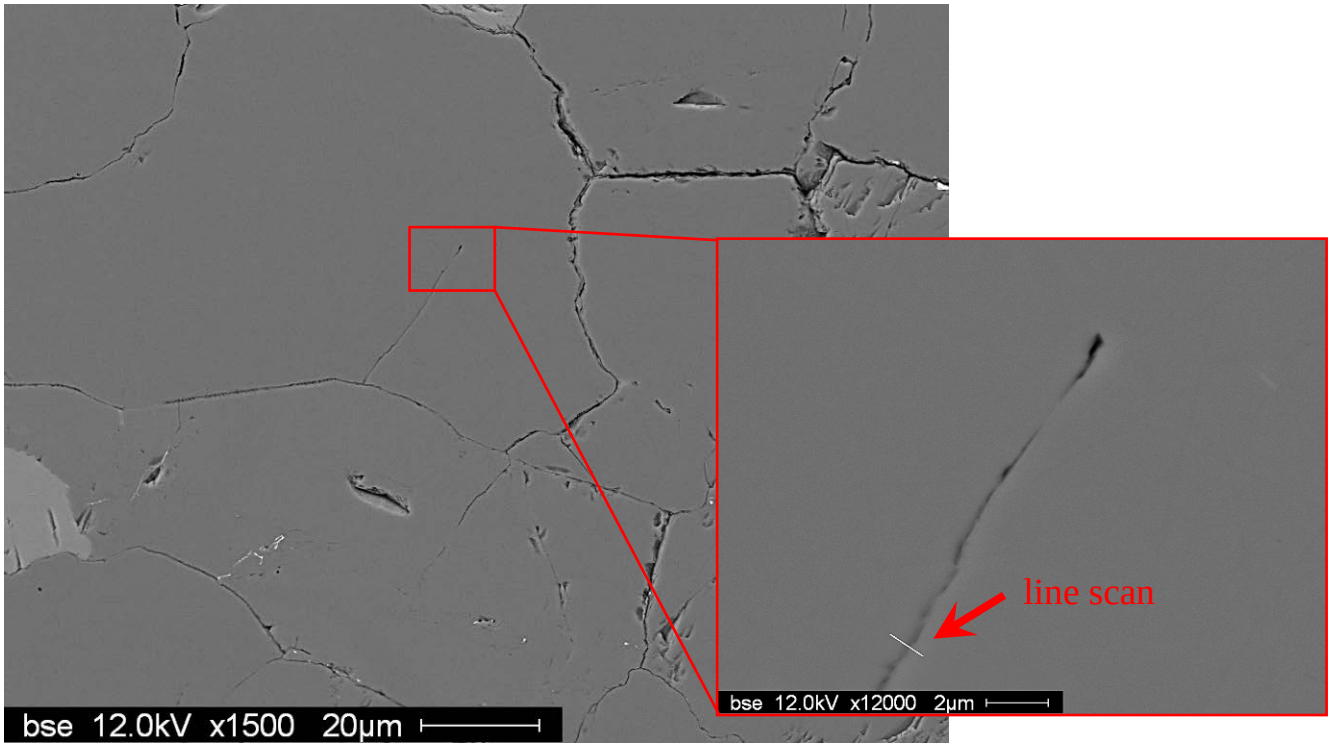

Figure 3.37: Location of an EDX line scan between two quartz grains in gneiss aggregate. The red rectangle in the larger image indicates the location of the smaller image, on which the EDX line scan shown in Figure 3.38 was taken. Concrete from a dam.

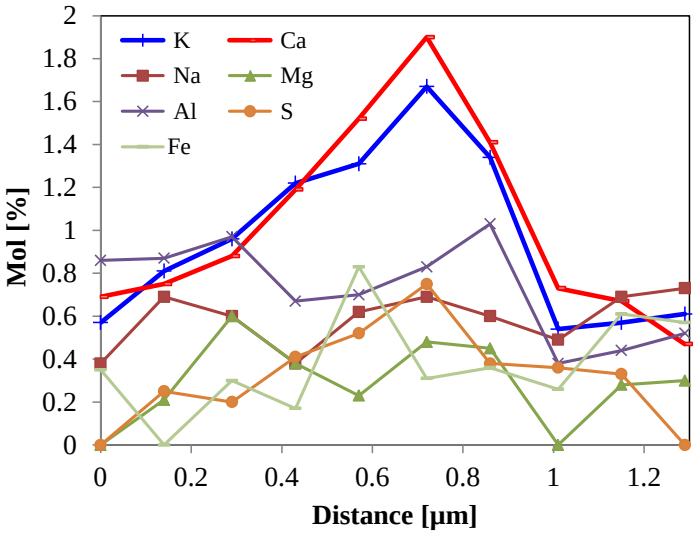

Figure 3.38: Elemental composition across the boundary of two quartz grains. Silicon and oxygen not visible (contents above 2 mol-%) due to scale chosen on y-axis.

3.5 Some remarks about alkali-carbonate reaction

The debate whether ACR can cause expansion or not goes on since decades. In the alkali-carbonate reaction, the alkali hydroxides present in the pore solution of the concrete react with dolomite ($MgCO_3$), leading to the formation of insoluble brucite (Figure 3.39) and soluble alkali carbonate. The alkali carbonate dissolves and reacts with the less soluble $Ca(OH)_2$, leading to the formation of alkali hydroxides and secondary $CaCO_3$. Therefore, a typical rim of calcite forms in the cement paste around reacting dolomites (Figure 3.40). In essence, the reaction seems to be a dedolomitisation. There is a strong indication that the expansion is caused by very fine-grained SiO_2 particles present in the aggregates and not the alkali-carbonate reaction itself [Katayama, 2010; Katayama, 2012]

In Switzerland, no case of concrete damage due to ACR has been reported so far. However, sings of ACR can be observed in many cases when dolomite is present in the aggregates.

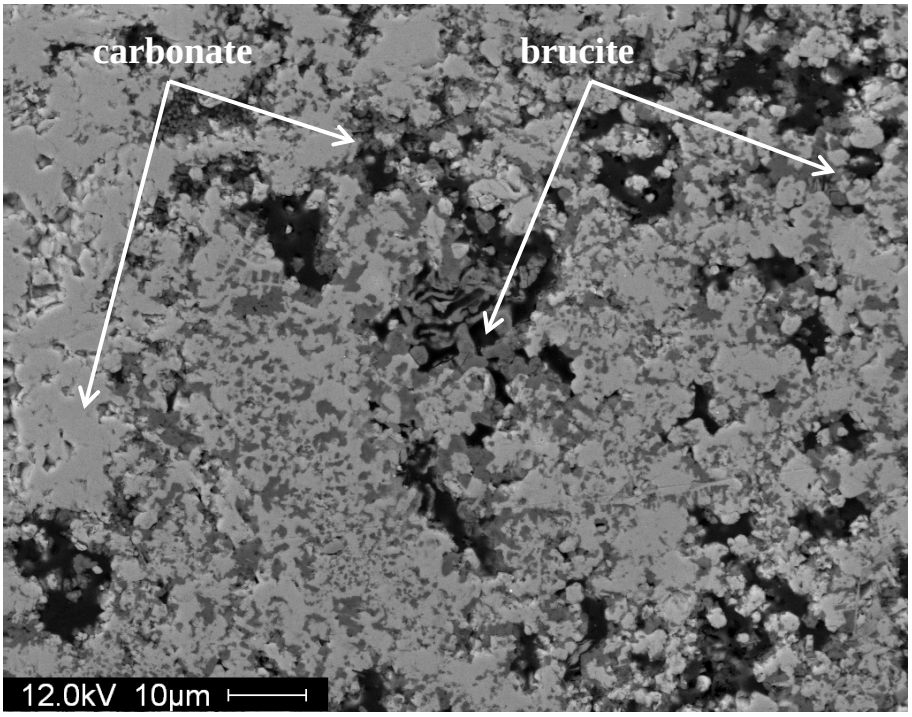

Figure 3.39: Alkali-carbonate reaction in a carbonate. The light-grey minerals are calcite ($CaCO_3$) and dolomite ($MgCO_3$), the dark-grey phase is brucite ($Mg(OH)_2$) and the black phase is porosity. Concrete from a dam.

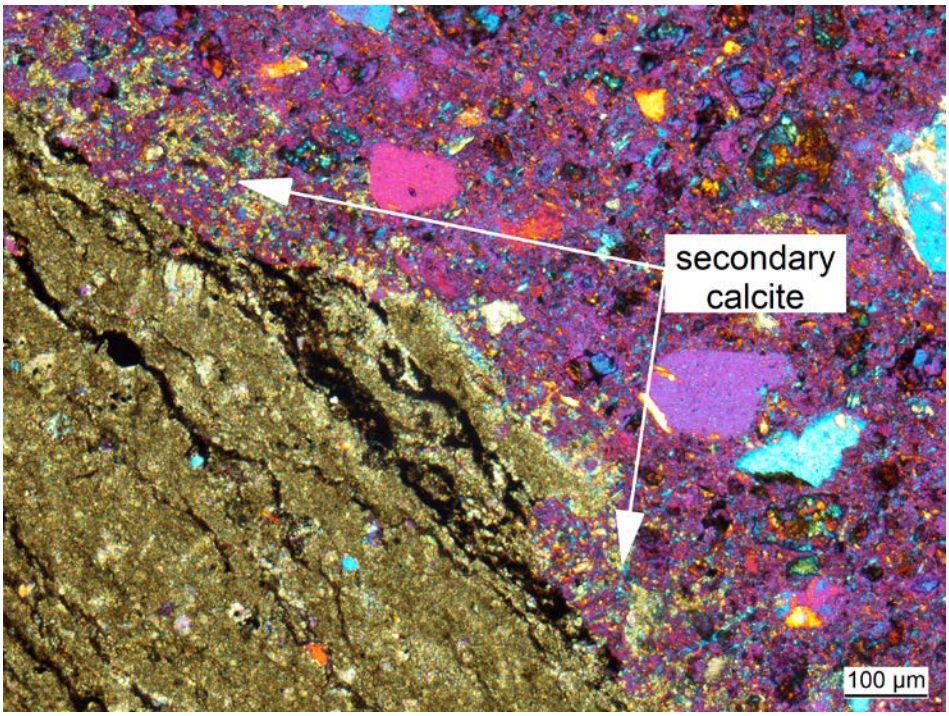

Figure 3.40: Carbonation of the cement paste (brown domains in cement paste displaying the same color as the carbonate aggregate) close to an aggregate containing dolomite. Concrete from a dam.

3.6 Some remarks about ettringite formation and iron sulfide oxidation

Secondary ettringite formation in air voids (Figure 3.41) is typical for concrete with high moisture content, as it is the case in dams, wastewater treatment plants, swimming pools etc. In these environments it is no

sign of internal or external sulfate attack. EDX point analysis of the cement paste in a dam concrete with frequent formation of ettringite in the air voids and the cement paste of a tunnel concrete damaged by external sulfate attack makes clear the difference when plotted in a S/Ca-Al/Ca-diagram (Figure 3.42). The points in the Al/Ca-range of the calcium-silicate-hydrate (CSH) show a clear shift towards a higher S/Ca-ratio, with some points moving in the direction of ettringite in the tunnel concrete. Both trends are not present in the dam concrete, which has a considerable lower sulfur content in the cement paste (1.1 mol-%) compared to the tunnel concrete (5.3 mol-%).

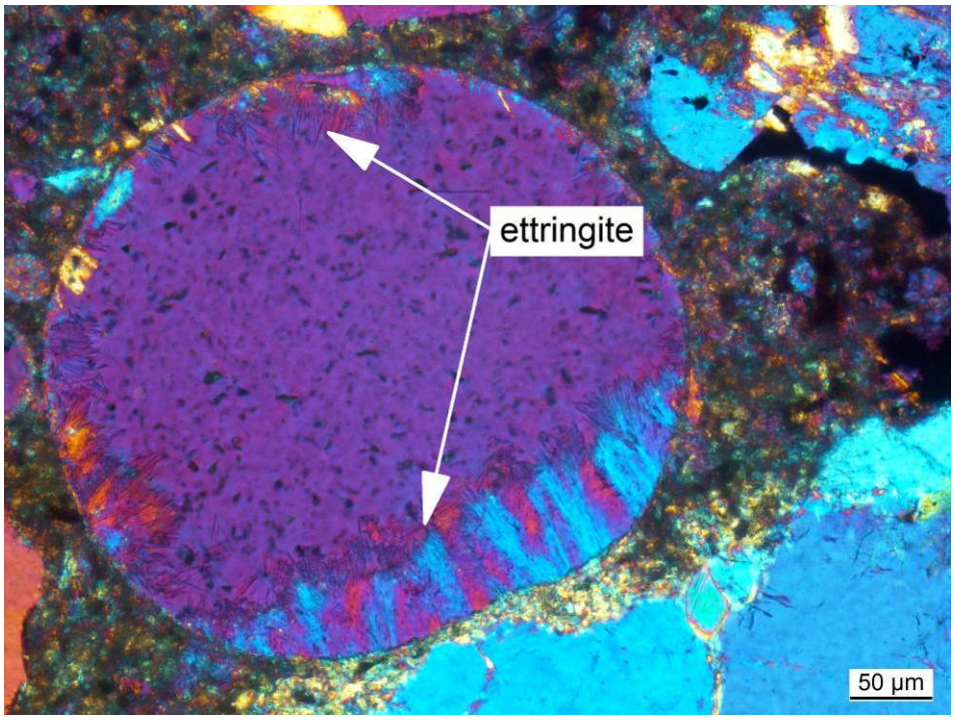

Figure 3.41: Formation of ettringite needles in air void. Concrete from a dam.

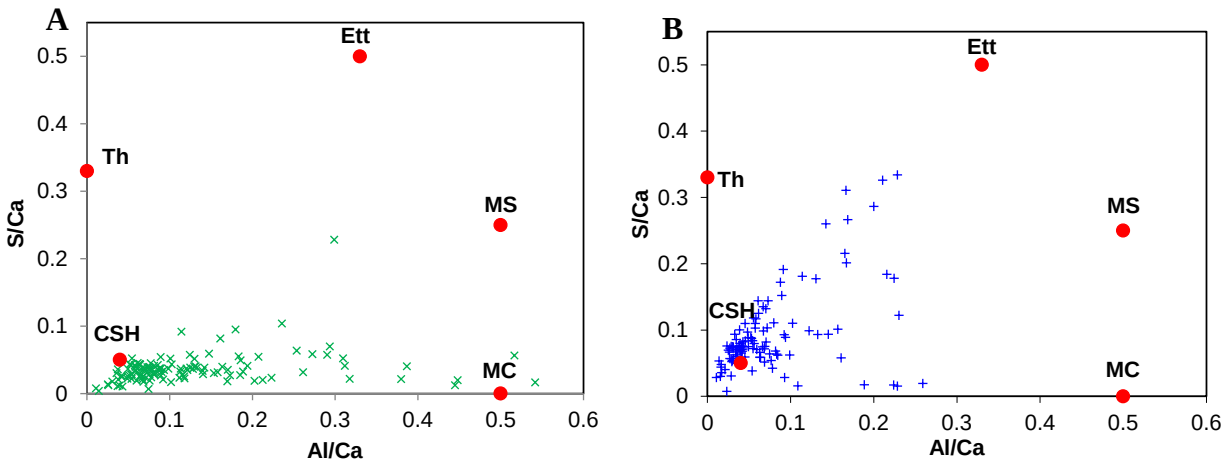

Figure 3.42: S/Ca versus Al/Ca-ratio in the cement paste of a dam (A) showing frequent formation of ettringite in air voids and in the cement paste of a concrete in a tunnel (B) exposed to external sulfate attack. The average sulfur content of the cement paste of the dam concrete is 1.1 mol-%, while in the cement paste of the tunnel concrete it is 5.3 mol-% (Ett = ettringite, Th = thaumasite, CSH = calcium-silicate-hydrate, MC = monocarbonate, MS = monosulfate).

In the literature, several cases of iron sulfide oxidation in concrete are reported [e.g. Thomas et al., 1989; Casanova et al., 1997; Ayora et al., 1998; Tagnit-Hamou et al., 2005; Lee et al., 2005]. Some of them concern dams, where this reaction takes place in the presence of AAR [Fernandes et al., 2004; Schmidt et al., 2011]. In the latter case, it is difficult to assess whether the iron sulfide oxidation is responsible for an expansion and if this is the case, how much of the expansion can be attributed to it. Oxidation products around iron sulfides in aggregates only show that an oxidation took place, but it possibly occurred before the aggregate was used in the concrete. Therefore, it has to be shown that cracks running from the aggregates into the paste are directly related to the oxidation of iron sulfides. When it has been shown that both iron sulfide oxidation and AAR lead to cracking, a qualitative assessment on the contribution of both processes to the expansion has to be based on the number and width of cracks related to each of the phenomena. Moreover, a substantial iron sulfide oxidation should lead to an internal sulfate attack by secondary ettringite formation, additionally contributing to expansion.

In a Swiss dam showing iron sulfide oxidation and AAR, oxidation products can be present within AAR products (Figure 3.43). Figure 3.44 shows an AAR-induced crack in an aggregate partly filled with AAR product next to iron sulfide with oxidation products but with no relation to a crack.

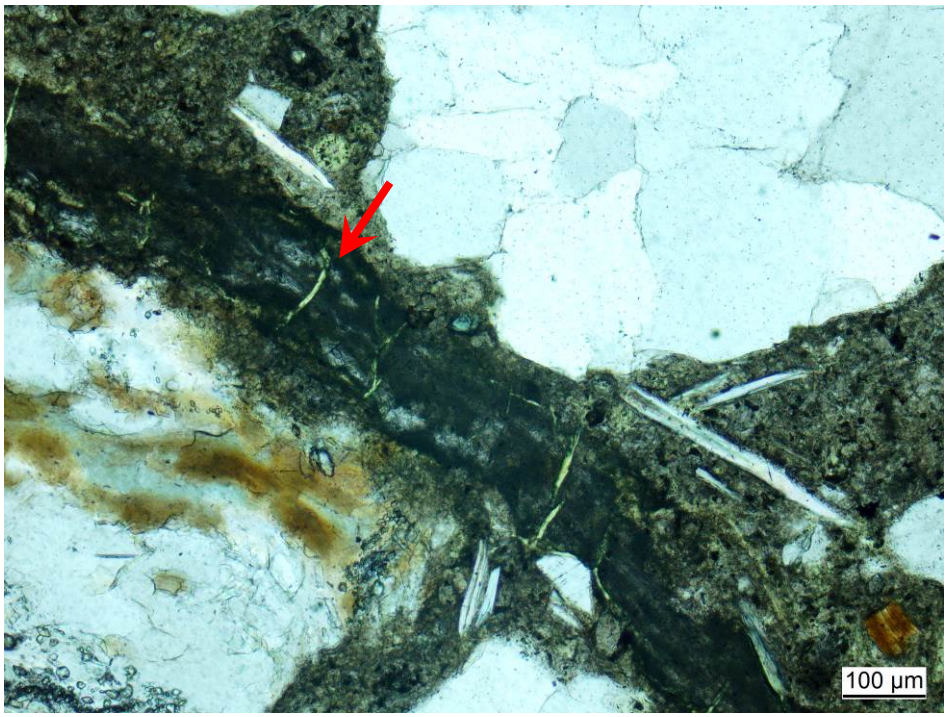

Figure 3.43: Concrete with AAR and iron sulfide oxidation showing black iron oxidation products in the AAR product (arrow) filling a crack in the cement paste. Concrete from a dam. Polarized light.

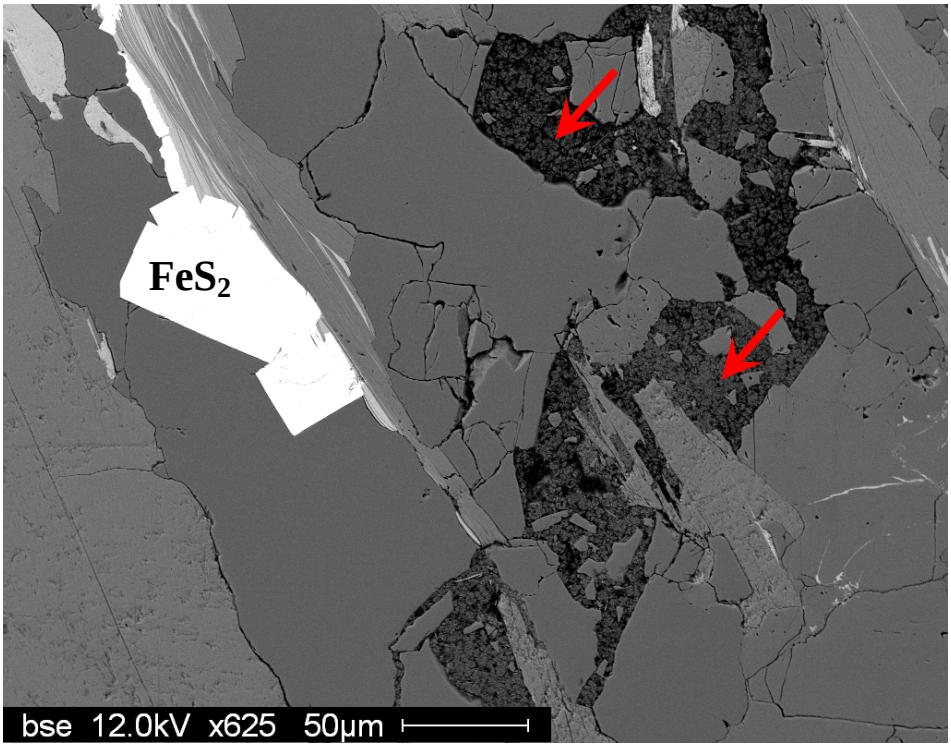

Figure 3.44: Iron sulfide (pyrite) and crack partly filled with AAR product (arrows). Concrete from a dam.

3.7 Conclusions and outlook

Cracks on the surface of concrete structures showing specific characteristics can already point towards AAR with high probability.

If there is AAR of any significance for the structure, polarized light microscopy permits to identify and diagnose it.

The combination between high resolution and chemical analysis of SEM with EDX gives further insight into AAR that is not provided by optical microscopy.

It is especially recommended to use a combination of polarized light microscopy and SEM with EDX for dams at the initial state of AAR or with weakly developed AAR.

The mentioned tools are sufficient to fulfill the task of diagnosing AAR in dams.

4. Methods for assessing the extent of AAR

4.1 Introduction

When the presence of AAR is established, the question arises about its severity. Several approaches can be used to assess the extent of AAR using macroscopic measurements, microscopic techniques, mechanical testing or non-destructive testing.

4.2 Macroscopic measurements

An indication about the expansion of the concrete can be derived from the crack-index [LCPC, 1997]. The crack-index is determined by measuring the crack width along pre-drawn lines (Figure 4.1) and is expressed as crack-width per measured length. However, it has to be kept in mind that the formation of the cracks may not be attributable solely to AAR.

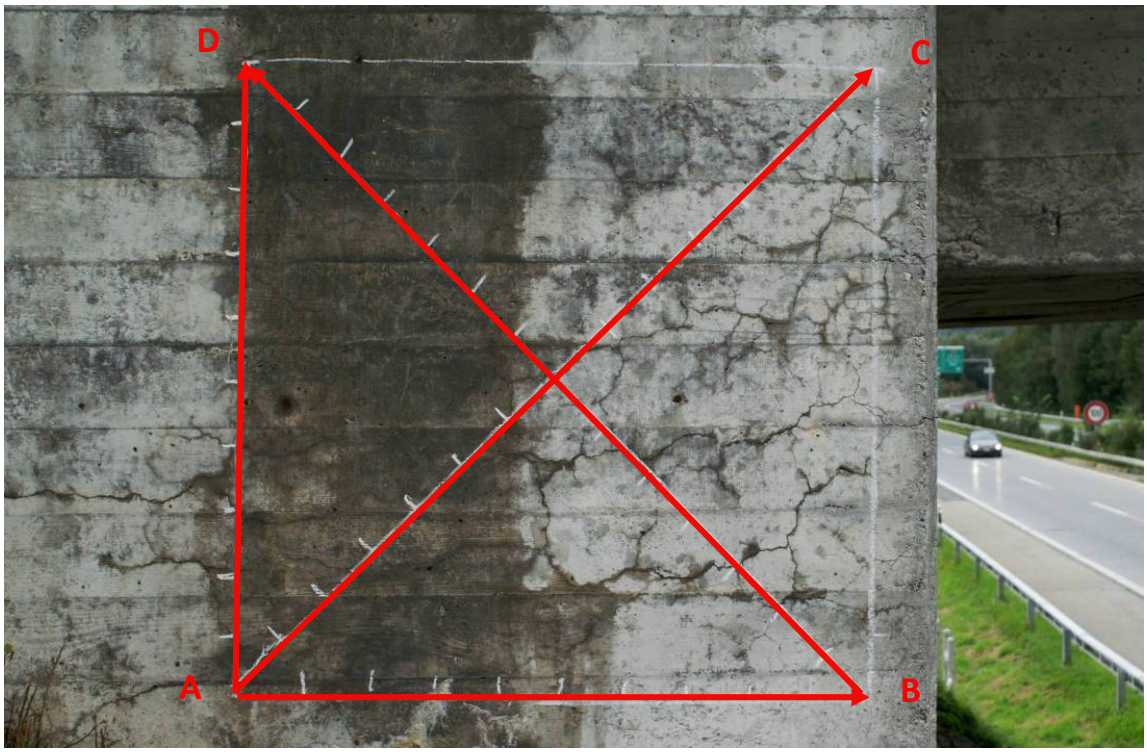

Figure 4.1: Determination of the crack-index along the lines A-B, A-C, A-D and B-C. Side of the square = 1 m.

4.3 Microscopy

The damage rating index (DRI) is used in North America to assess the extent of AAR. It was originally developed to assess AAR-related damage in dams and later extended as a tool for AAR-affected structures in general [Grant-Bellow, 1992; Dunbar & Grant-Bellow, 1995]. It is based on the identification of features related to AAR multiplied by a weighing factor. The DRI is conducted on polished concrete samples without impregnation at a magnification of 16×. This starting point has its problems, because polishing without impregnation can obscure or even destroy signs of AAR. Moreover, the low magnification used in these tests is not sufficient to reliably detect microcracks in concrete at an initial stage of AAR. There are some additional problems that are best pointed out by citing the Federal Highway Administration Report [Fournier et al., 2010]:

"The DRI method is a useful tool for the quantitative assessment, based on petrography, of internal damage in concrete due to ASR[1] or other mechanisms. However, as the results are very much related to the experience of the petrographer and since there is currently no standard test procedure available, the method is fairly subjective and the results can be quite variable from one operator to another. Consequently, it is highly recommended that the method be carried out by the same petrographer, at least on the sets of cores from the same structure."

Due to the problems related to sample preparation without impregnation, it seems mandatory to work with impregnated samples. As thin sections are an important tool for diagnosing AAR, it is obvious to use them for assessing the extent of the reaction as well. In Leemann & Merz [2013] the number of reacted aggregates has been used to compare the extent of AAR in the concrete performance test and in concrete from structures. Recently, this approach has been extended by adding the determination of a crack index to the analysis (unpublished reports). The determination of the crack-index on the concrete surface of

[1] In this report equivalent to AAR.

damaged structures is well known (see paragraph 4.2). It can be applied in a similar way on thin sections. The thin section is moved at a magnification of 50× or 100× in the fluorescent light mode along the lines shown in Figure 4.2. The width of the AAR-induced cracks intersecting with these lines is measured. The crack index can be calculated as crack width per measured length of the lines. The results of a combined determination of number of reacted aggregates and the crack width are shown in Table 4.1. This approach permits assessing the extent of AAR and comparing different parts of an investigated structure or different structures with each other. The disadvantage, like in any other method relying on operator judgment, is the comparability between different operators.

A determination of the petrography of the aggregates in the thin section gives additional information about AAR. First, it shows which type of aggregate is susceptible to AAR. Secondly, the number of aggregates having a specific petrography that have already reacted can be compared to the number of unreacted particles of the same petrography. This may help to assess to which stage AAR has presently already progressed. The determination of the volume of aggregates in general and of a specific lithology in particular may be quantified with point counting, to provide some additional information. It has to be taken into account that often aggregates with relatively large maximal grain size are used in dam concrete. Therefore, more thin sections have to be analyzed to obtain representative results.

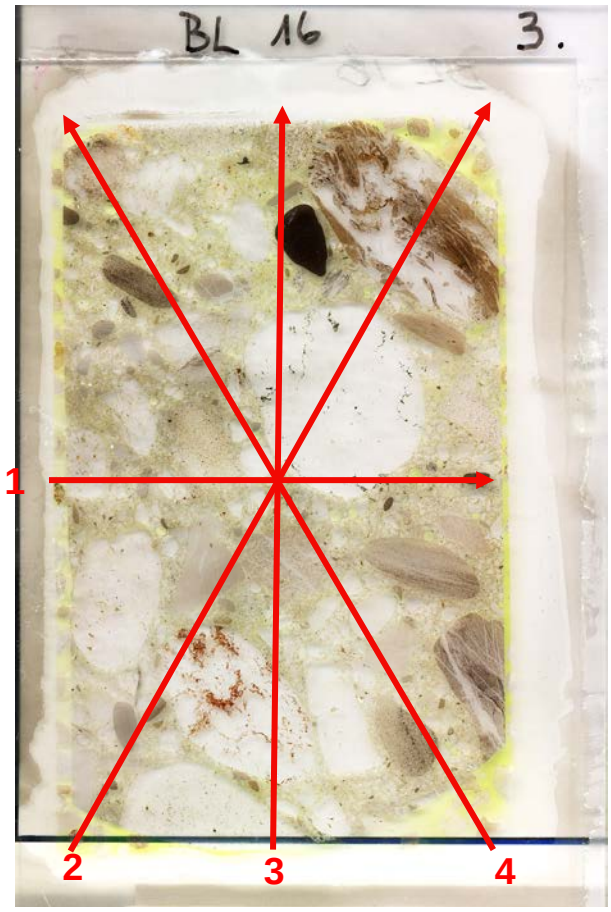

Figure 4.2: Thin section (52 × 85 mm^2) with lines along which the crack index is determined.

Table 4.1: Number of reacted aggregates and crack-index of thin sections from a several-meters long core in the foot area of a dam.

Thin section	Depth [m]	Orientation in relation to coring [-]	Number of reacted aggregates [number-%]	Crack-Index [mm/m]
D1	0.0-0.1	parallel	8	0.12
D2	0.1	perpendicular	6	0.04
D3	0.3-0.4	parallel	8	0.17
D4	0.4	perpendicular	6	0.00
D5	2.3-2.4	parallel	18	0.38
D6	3.1-3.2	parallel	24	0.35
D7	3.7	45°	0	0.00

In several studies, the extent of AAR was determined applying image analysis on SEM-images taken in the backscattering mode [Ben Haha et al., 2007; Leemann et al., 2008; Leemann & Merz, 2013]. However, the analyzed samples were always subjected to accelerated test conditions, resulting in a very high degree of quartz dissolution and expansion. In the case of accelerated microbar and mortar bar test, the determination of the extent of AAR is based on the amount of dissolved minerals in the aggregates. As the gaps left by the dissolved minerals are filled with epoxy, they can easily be analyzed due to the low backscattering contrast. In samples of the concrete performance test, the amount of dissolved minerals is minor. The gaps present in the aggregates are dominated by cracks. Here, the degree of reaction is more representative of a crack-index in area percentages.

Applying this method on concrete from structures has a major drawback. The extent of the reaction in such concrete is lower than in the lab samples. Consequently, the investigated area has to be increased considerably to get representative results. This makes the already work-intense method impossible to apply.

The impregnation of larger polished concrete specimens can provide information about the extent of AAR (Figure 4.3). In Lindgård et al. [2012], the surface of cut concrete prisms (70 × 280 mm^2) were impregnated with epoxy resin containing a fluorescent dye and photographed in UV-light. Crack segmentation was done with a commercial program. A good relation between expansion in the concrete prism test (0.04-0.43 %) and the crack area was established. No information is present in the paper about the achieved resolution. An open question is whether this method can be used for concrete of dams, which often shows expansions below the range of the laboratory concrete tested.

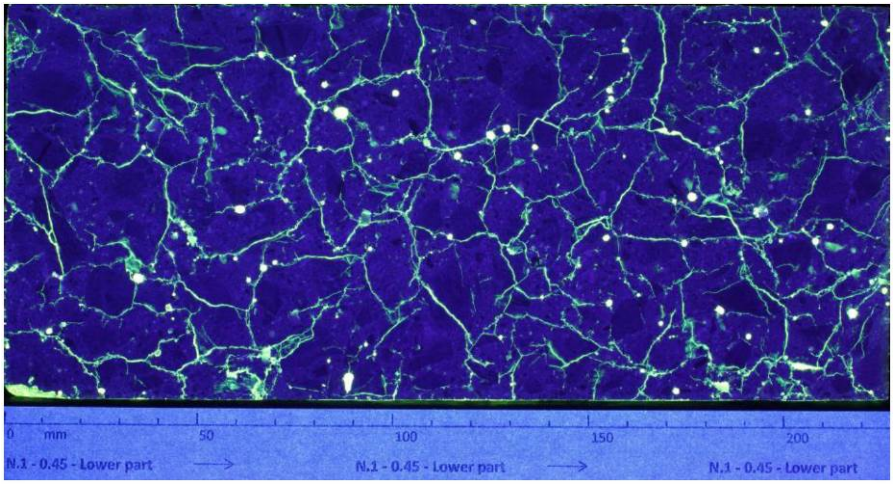

Figure 4.3: Cut prisms of a heavily cracked concrete (tested with the concrete performance test, recorded expansion: 0.43%) impregnated with epoxy resin containing a fluorescent dye activated by UV-light. From Lindgård et al. [2012].

4.4 Mechanical tests

Cracking caused by AAR influences the mechanical properties of the concrete. Typically, the compressive strength, the tensile strength, the splitting tensile strength and the E-modulus are determined on cores. However, it is difficult to assess how much the AAR has changed these parameters, because usually no independent reference values can be used for comparison. Therefore, such tests have to be performed on cores from different parts of a structure with different degrees of damage. Compressive strength is influenced relatively little by the cracks caused by AAR, while the effect on the E-modulus and especially the tensile strength is more pronounced. However, often cores fall apart along major cracks caused by AAR during coring or later during sample preparation. Consequently, the properties determined on the intact parts of a core often overestimate the quality of the concrete present in the structure.

One possibility to assess how much AAR has influenced the mechanical properties is a comparison between the different determined parameters. As an example, any of the mechanical parameters can be compared to the bulk density of the concrete. Variations of the water-to-cement ratio (w/c) cause a change of the mechanical properties. If some values do not follow the usual relationship between bulk density and mechanical properties in a concrete damaged by AAR, this may indicate different degrees of damage (Figure 4.4). E-modulus is more influenced by microcracks than compressive strength. The microcracks increase strain at the relatively low stress levels used to determine the E-modulus. On the other hand, they have an insignificant effect at the high stress level at which the concrete fails in the determination of compressive strength. Consequently, the comparison between these two parameters may indicate the level of damage (Figure 4.5). Using tensile strength or splitting tensile strength for such comparisons can be difficult, as these two parameters often have a large scatter.

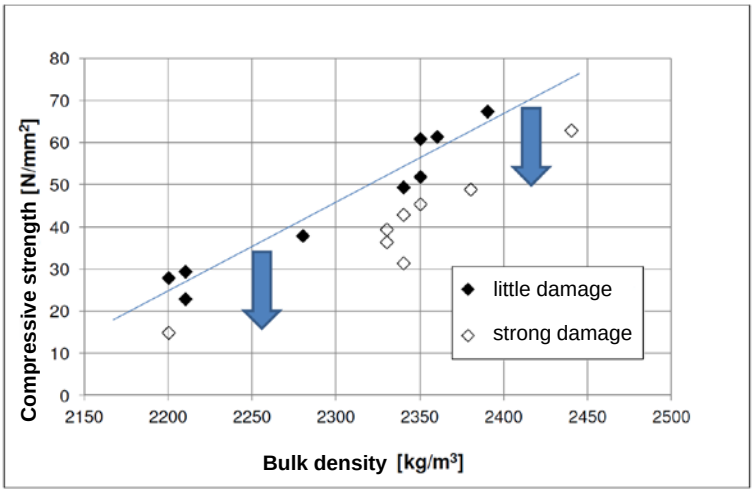

Figure 4.4: Relation between compressive strength and bulk density of concrete damaged by AAR. Concrete from a supporting wall [Merz & Leemann, 2012].

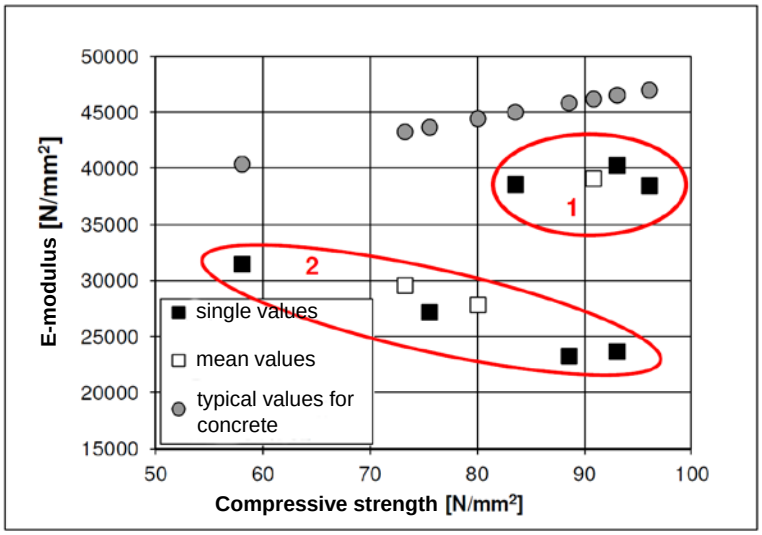

Figure 4.5: Relation between E-modulus and compressive strength for a little damaged part of a bridge (1) and a strongly damaged part of a bridge (2) [Merz & Leemann, 2012].

A different approach to assess the degree of damage with a mechanical test is the stiffness damage test. This test was developed for rocks [Walsh, 1965] but later applied to concrete as well [Crouch, 1987; Crisp et al., 1993]. The test is based on cyclic loading of concrete cores/cylinders. By testing concrete cylinders with different mix designs after exposing them to accelerating test conditions, a good correlation between the area of hysteresis between loading and unloading in the stress-strain-curve (first cycle), the plastic deformation during the first five loading cycles and the AAR-induced expansion was found [Smaoui et al., 2004a]. In Sanchez et al. [2012] it was shown that the change of average E-modulus between the second and third loading cycle can be used as additional criterion. However, Sanchez et al. [2012] pointed out that further research is needed to use the stiffness damage test for damage quantification.

4.5 Non-destructive evaluation (NDE)

Ideally, the assessment of the AAR damage extent and quality in any concrete structure or samples from it should be non-destructive in nature, for two main reasons: (a) avoid to introduce into the sample spurious sources of damage that are not related at all with AAR, e.g., additional cracks, but that may affect significantly the AAR damage assessment; (b) give the possibility to probe again the same region of the structure or sample in order to get a temporal evolution of the damage.

This report focuses mainly on the use of sound/ultrasounds-based NDE techniques as complementary tools to destructive techniques, e.g., optical microscopy of polished cross-sections or thin sections. A brief reference is made to X-ray Tomographic Microscopy, a fully 3D microscopy method that does not yet achieve the same spatial resolution of optical microscopy but is becoming closer to it. X-ray Tomographic Microscopy offers the possibility of inspecting samples in a completely non-destructive way and with almost no sample preparation. Main limitations are, however, the accessibility (due to the costs of the measurement setups) and the necessity of employing small samples to achieve the best spatial resolution allowed.

Section 4.5.1 is dedicated to one of the nowadays most used NDE technique based upon linear sound/ultrasound, the (ultrasound) pulse velocity (UPV) technique. This technique is relatively easy to implement, both at the laboratory scale and in the field, and has been the object of several standardizations. Despite its popularity, it is not an easy measure, if performed reliably, and has several limitations in terms of detectability of early and/or late damage development. New emerging methods and respective technologies based upon diffuse sound/ultrasounds are presented at the end of the section, to highlight their larger potential in detecting and characterizing damage with much larger sensitivity and resolution than the standard UPV technique.

Section 4.5.2 is dedicated to another category of sound/ultrasound NDE methods based upon nonlinear elasticity. These methods achieve much larger sensitivity and resolution in detecting damage, especially cracking, even at early age of its development. An overview is provided of the different techniques in this category and their limitations in terms of scalability from the laboratory to the field.

Finally, section 4.5.3 briefly introduces X-ray Tomographic Microscopy as a microscopy method complementary to the ones presented in the previous sections, bringing fully 3D information about the microstructure of a sample and requiring almost no sample preparation.

4.5.1 NDE with linear sound/ultrasounds

The UPV technique consists in two measurements: a length measurement on the sample (or structural member) along a specific direction, from point A to point B, usually on the surfaces of the sample/member, and the measurement of propagation time for a ultrasound pulse along the same direction, from A to B. The second measurement is also called a time-of-flight (TOF) measurement. The ratio between the length and the TOF provides an estimate of the bulk pulse propagation velocity.

The UPV is not generally mathematically related with the density and elastic moduli of the material, unless very specific geometrical conditions and elastic wave types are used, e.g., very long and thin rod-like samples and a purely longitudinal wave source. However, it has been shown for cement-based materials that the UPV can be a proxy of an actual mechanical parameter. For example, at least in early age concrete (up to 24 hours since casting), an exponential relation between UPV and compressive strength has been demonstrated [Swamy et al., 1984; Breysse, 2012].

Thanks to its (apparent) simplicity in implementation, the UPV technique has been widely used in NDE of concrete, both at the laboratory scale and for real concrete infrastructure. Several standards exist about its

implementation [ASTM C597-09; RILEM/NDT 1, 1971; DIN/ISO 8047]. However, its results are not easily and straightforwardly interpreted. Regarding the use of UPV as a proxy of a AAR damage metric, several studies have been published reporting different results strongly depending upon the conditioning protocol used for the AAR acceleration. With the progression of the AAR damage, a decrease in the UPV is expected, due to the nucleation and growth of cracks.

The UPV method is based upon the TOF measurement of the "ballistic" source pulse, i.e., the part of the injected pulse that travels from point A to point B only with relatively small forward scattering by the several material phase interfaces inside the concrete sample. The ballistic pulse is just one component of the propagating wave, the so-called "coherent component".

Crack nucleation and growth create new porosity and interfaces (crack boundaries) between media with different densities and elastic constants (the aggregate or cement paste and the inner region of the crack, i.e., the new porosity, filled in with either pore fluids or AAR products). The wave velocity in the new porosity is in general lower than in pure cement paste or in the aggregates because the material phases filling the cracks are either fluids or AAR products with low elastic moduli (between 7 and 9 GPa for the Young modulus [Leemann & Lura, 2013]). In addition, the cement paste or aggregate regions surrounding the cracks undergo a decrease in wave velocity as well, due to the disruption of their original structure. This is particularly significant for the crystalline phases in the aggregates. Thus, the larger the AAR damage degree, the larger the fraction of regions with lower wave velocities crossed by the ballistic pulse. Multiple scattering is also expected to increase with the damage degree.

The decrease in UPV with AAR damage progression has been documented in several laboratory studies involving AAR acceleration protocols. Saint-Pierre et al. [2007] measured the UPV of concrete cylinders (100 mm in diameter and 200 mm long) cast with both reactive (Spratt limestone, a fine-grained siliceous limestone with chalcedony inclusions) and non-reactive (Limeridge limestone, composed of calcite for 97%-by weight) aggregates. The samples followed the Canadian AAR acceleration protocol CSA A23.2-14A, consisting in submerging the samples in a 1M NaOH water-based solution kept at constant temperature of 38°C. At regular times, the authors removed the samples from the solution, measured the UPV and moved the samples back into the solution [Saint-Pierre et al., 2007]. Both the reactive samples and the non-reactive ones exhibited a continuous longitudinal expansion. In the reactive case, the expansion achieved the value of 0.20% at 52 weeks, while for the non-reactive one it remained below 0.02%. Standard petrographic analysis of similar samples confirmed AAR to be the source of the expansion and of the associated cracking. A monotonic decrease in the UPV was observed for the reactive samples mainly within the first 20 weeks. The non-reactive samples exhibited a slight increase in UPV till the 20^{th} week, followed by the achievement of a plateau level. At 52 weeks, the reactive samples' UPV was 8% lower than the one for the non-reactive samples. The observed continuous decrease in UPV might have been biased by a continuous uptake of the NaOH solution in the reactive samples, as evinced by the samples' mass time series. The mass steadily increased for the reactive samples while it increased up to 20 weeks only for the non-reactive samples, after which it achieved a plateau value. A continuous saturation of the AAR-related cracks still implies a contribution to the reduction of the macroscopic UPV. However, the decrease in UPV is lower when compared to empty cracks, ultimately resulting in a relatively small UPV difference between the reactive and non-reactive samples.

Even smaller differences in UPV values for samples with reactive *versus* non-reactive aggregates were observed by Sargolzahi et al. on concrete samples stored above water at 38°C, in sealed containers [Sargolzahi et al., 2010]. The types of reactive and non-reactive aggregates used in this study were the same as the ones used in the work by Saint-Pierre et al. [Saint-Pierre et al., 2007]. The UPV remained constant up to 10 weeks and approximately equal for both the reactive and the non-reactive samples. After that time, it decreased for both types of samples, with a slightly higher decrease rate for the reactive

samples. The authors reported a continuous mass increase for the reactive samples, along with the longitudinal expansion, suggesting that, as expected, the AAR progression was accompanied by a continuous, macroscopic uptake of water, driven by the formation of the hygroscopic AAR products and by the formation of the AAR cracks, which increased the samples' permeability. In addition to filling by the up-taken water or NaOH solution supplied during AAR acceleration protocols, crack filling by the AAR products themselves may slow down, stop or even reverse the UPV decrease with damage progression.

Swamy & Wan [1993]. performed a two-year long monitoring of longitudinal length, mass and UPV of concrete samples with aggregates having different degrees of AAR reactivity and different types of mineral admixtures, stored at 20°C and 96% RH [Swamy & Wan, 1993]. For all samples, they observed a similar qualitative temporal evolution for the UPV: an initial increase, during early age, followed by a decrease, whose onset corresponded to the appearance of the first cracks visible by eye on the surface; the achievement of a minimum, in correspondence of the achievement of a plateau level for the expansion; an increase, up to 2 years of measurements, without a complete recovery of the UPV values that had been measured at the end of the early age. The position in time of the achieved minimum and its value, relative to the end of early age value, as well as the final value at two years depended on the type of reactive aggregate, type of mineral admixture and amount of it. However, the pattern was the same. The authors of that work interpreted the recovery in UPV value, after the global minimum, in terms of crack filling by the AAR products accompanied by a slowing down or even a standstill in the formation of new cracks, since the expansion achieved a plateau level in correspondence of the UPV minimum.

A confirmation that crack growth and their filling, either by up-taken fluids or by AAR products or by both simultaneously, strongly affect the type of UPV temporal evolution was also obtained during an experimental campaign performed at Empa on mortar samples, with highly reactive aggregates containing alpine gneiss, subjected to the ASTM C 1260-94 AAR acceleration protocol. We performed expansion, mass and UPV measurements on identical samples, contrary to previous studies where different samples, produced with the same mixture, were used for the different types of measurements. In addition, we performed X-ray tomographic microscopy measurements, at different ages, on one of the six samples used. The samples continuously expanded during the four months of measurements (Figure 4.6a) with a continuous increase in the total crack volume, at least as determined from the quantitative analysis of the tomographic datasets for the scanned sample. However, the UPV decreased only up to 2 weeks. Then, it steadily increased, achieving values slightly smaller than the value at the beginning of the acceleration protocol (Figure 4.6b). The global minimum in UPV corresponded to a global maximum in mass (Figure 4.6c). After about 3 weeks, the mass steadily decreased. Therefore, the UPV recovery after the minimum at 2 weeks cannot be simply attributed to crack filling by the externally supplied 1M NaOH solution used in the acceleration protocol. Even though the X-ray tomographic microscopy measurements were performed only starting from 6 weeks, they allowed observing crack filling by solid material phases (likely AAR product).

Rivard et al. [2010] performed several hundreds of TOF measurements, each along a different path, on a dam located in eastern Canada, built 50 years ago and known since 20 years to be affected by AAR-damage. The source-receiver configurations were designed to cover a full vertical cross section of a region of the dam with ballistic propagation paths. The TOF datasets allowed to tomographically reconstruct the 2D spatial distribution of the PV on the cross section, a technique known as travel-time tomography [Bond et al., 2000 / Kepler et al., 2000]. The measurements were performed for 8 different vertical cross-sections. A region above the ceiling of a tunnel and extending up to the top of the dam exhibited very low PV values, in comparison to the rest of the structure.

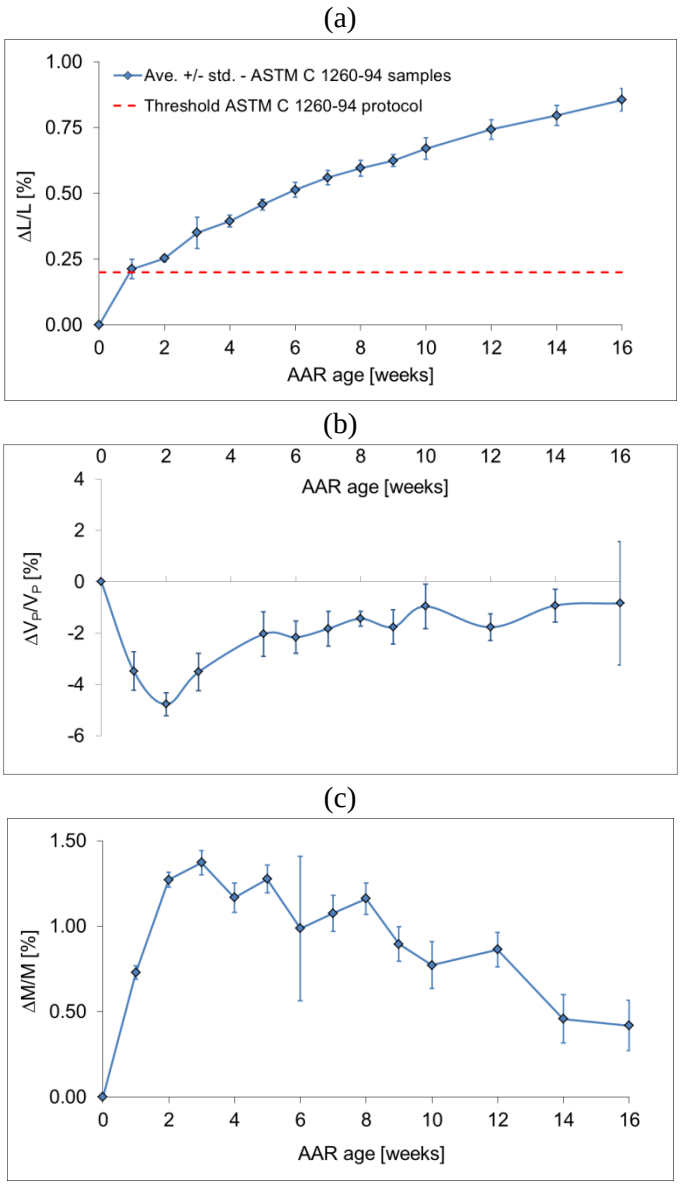

Figure 4.6: AAR acceleration by the ASTM C 1260-94 protocol for mortar samples (cylinders, 25 mm in diameter, 100 mm in length) with highly reactive aggregates, containing alpine gneiss. (a) Relative change in the longitudinal length (L). (b) Relative change in the UPV (V_P) for a longitudinally polarized ultrasound pulse at center frequency ν = 200 kHz. (c) Relative change in the sample mass. The markers indicate average values, each upper/lower error bar the standard deviation, both calculated over a population of six samples. The dashed red line in (a) indicates the minimum expansion threshold for classifying the aggregates as reactive, according to the standard.

Cores were drilled from the inner side of the inspection gallery in correspondence of the low PV region boundaries. The measurements were performed for 8 different vertical cross-sections. A region above the top of the inspection gallery and extending up to the top of the dam exhibited very low PV values, in comparison to the rest of the structure. Cores were drilled from the inner side of the tunnel in correspondence of the low PV region boundaries. Laboratory UPV measurements were performed on the cores and some of them were petrographically analyzed. The authors found extended evidence of features characteristic of AAR-induced cracking. This work represented a significant step forward in the application of the sound/ultrasound PV technique to the structural health monitoring of infrastructure

affected by AAR damage. However, the laboratory scale measurements proved that UPV values are (1) not extremely sensitive to AAR damage progression (the relative difference in UPV values for samples with reactive and non-reactive aggregates was never above 50%) and (2) they are strongly affected by a variety of factors other than just the cumulative amount of cracking, e.g., crack filling by fluids or AAR products. The latter feature makes the interpretation of UPV time series from cores or directly measured on the infrastructure very difficult.

Measurements based upon the incoherent part of a sound/ultrasound pulse have the potential of being much more sensitive to AAR-damage evolution than the UPV technique. The incoherent part of a propagated pulse consists of the segment of the waveform due to multiply-scattered parts of the source pulse, including back scattering. The multiply-scattered waves arrive at a recording point B after having extensively traveled across the sample, along very long paths. Thus, they have probed more extensively the medium. The larger the number of interfaces between different material phases are (e.g., due to cracks), the stronger is the multiple scattering. The level of multiple scattering depends not only upon the propagation medium structure but also on the source's frequency bandwith. Waves are strongly scattered only if the wavelength is of the same order of magnitude as the scatter size. In the case of concrete, this means that multiple scattering achieves enough strength when operating at a frequency above 100 kHz. In this frequency range, the multiply-scattered part of a propagated pulse appears as noise-like signals. The energy density associated with the multiply scattered pulse propagates in time and space according to a diffusion process, similar to a heat transfer process [Anugonda et al., 2001; Becker et al., 2003]. A diffusion-based analysis of diffusive waves allows indirectly measuring the ultrasound diffusivity and the intrinsic attenuation coefficient of a concrete sample.

Preliminary work on laboratory samples showed that AAR-damage progression can be monitored with high sensitivity by ultrasound diffusivity measurements [Deroo et al., 2010]. An increase in damage corresponds to a decrease in sound/ultrasound energy diffusivity, due to the increase in multiple scattering.

Saint-Pierre et al. performed ultrasonic attenuation measurements with the same type of pulse transmission measurements used in the UPV technique [Saint-Pierre et al., 2007]. They showed that the bulk, linear attenuation coefficient increased significantly with the sample age during an AAR acceleration protocol. The difference between reactive and non-reactive samples proved to be much larger than the difference in the corresponding UPV measurements. However, a bulk, linear attenuation coefficient measurement does not allow distinguishing between the intrinsic attenuation by the materials, due to their viscoelastic properties, and the contribution of multiple scattering to the bulk attenuation, the latter being more sensitive to cracking than the former.

Ultrasound diffusivity measurements lead to estimates of both the diffusivity and the intrinsic attenuation coefficient, thus they are considered as very promising sound/ultrasound-based AAR-damage detection methods for non-destructive evaluation of concrete.

It is also worth mentioning the Coda Wave Interferometry technique (also based upon diffuse waves), developed in geophysics and already applied in structural health monitoring [Stähler et al., 2011]. Coda Wave Interferometry allows calculating relative changes in wave velocities with (a) the highest sensitivity ever achieved nowadays in concrete [Larose & Hall, 2009] and (b) even in the absence of active sources, just using the environmental mechanical vibration noise in a concrete member due to surrounding perturbations [Snieder & Şafek, 2006]. The latter feature makes the technique potentially of extreme interest for the time-lapse monitoring of large infrastructures like dams.

4.5.2 NDE with nonlinear sound/ultrasounds

NDE measurements based upon nonlinear elastic waves exploit a manifold of physical phenomena occurring in every material in correspondence of finite amplitude strains. There is no unique definition of finite amplitude strain, the range for it varying upon the type of material and its type and level of damage. Indicatively, for both natural (rocks, soils) and human-made (ceramics, concrete) consolidated and unconsolidated granular materials, nonlinear elastic phenomena start to occur at strains larger than $10^{-7} \div 10^{-6}$. The nonlinear elastic phenomena are due to both the anharmonicity of crystal lattice vibrations (atomic-scale nonlinear elasticity) and more complicated processes involving frictional phenomena at interfaces (mesoscopic-scale nonlinear elasticity). The first type of nonlinear elasticity is fully described by the classical theory of elasticity for finite amplitude strains [Born & Huang, 1962; Landau & Lifschitz, 1975]. The second type has been cast in the framework of a nonlinear mesoscopic elasticity theory [Guyer & Johnson, 1999; Ostrowsky & Johnson, 2001; Guyer & Johnson, 2009].

Most of the nonlinear elastic phenomena are directly related with defects and damage in the respective, ideally damage-free materials: dislocations in crystalline and polycrystalline materials lead to larger lattice anharmonicity; cracks and debonding at grain boundaries lead to stronger nonlinear mesoscopic elastic effects. The types of nonlinear elastic phenomena that are more strongly related with cracks are those of mesoscopic origins, i.e., arising from frictional processes at tens/hundreds of microns scale interfaces. Several nonlinear elastic phenomena exploited for NDE purposes are related to the frequency response of a sample and include: (a) the generation of harmonics and sub-harmonics when a sample is excited with a purely harmonic vibration, (b) the generation of new frequency content by the nonlinear mixing of excitation waves and (c) the change of the resonance frequencies with the excitation amplitude. For a review of such phenomena we refer to the work of Guyer & Johnson [1999; 2009] and Ostrowsky & Johnson [2001]. Several NDE techniques exploiting such phenomena have been developed and applied in the last two decades. They fall under the common umbrella name of **nonlinear elastic wave spectroscopy** (NEWS) techniques.

One of the most commonly used NEWS techniques is called **single mode nonlinear resonant ultrasound spectroscopy** (SIMONRUS). It consists in exciting one specific vibration *eigen*mode (and in measuring the correspondent resonance frequency) at successive and increasing excitation amplitudes. The nonlinear mesoscopic elastic phenomenon observed in such a measurement consists in a decrease of the resonance frequency, corresponding to the decrease in the effective elastic moduli ("softening"), with the increase of the excitation amplitude. A 1D nonlinear and hysteretic[2] stress-strain constitutive law, proposed by Van Den Abeele et al., leads to the prediction of a quadratic polynomial relationship between the relative change in the resonance frequency and the strain wave amplitude at the point of detection [Van Den Abeele et al., 1997; Guyer et al., 1998]. The coefficients of the quadratic polynomial function are related to the hysteretic nonlinear elastic modulus and the classical cubic nonlinear elastic modulus, respectively for the linear and quadratic powers[3]. At strains of the order of $10^{-7} \div 10^{-6}$, the linear term is much larger than the quadratic one. The result, confirmed by most of the experiments, is a linear scaling between the relative change in the resonance frequency and the strain wave amplitude at the point of detection [Van Den Abeele et al., 2000; Bentahar et al., 2006]. The slope of the linear scaling, related to the hysteretic nonlinear elastic modulus, is a parameter having a very large sensitivity to the level of damage in the sample. This parameter has been used as a "damage index". The 1D nonlinear stress-strain constitutive law

[2] Hysteresis in the quasi-static stress-strain relationship is a typical nonlinear elastic effect that characterizes consolidated and unconsolidated granular material, as concrete, and that cannot be explained using the classical nonlinear elasticity theory based upon the theory of anharmonic lattice vibrations. Its origin has been described in the context of the phenomenological theory of nonlinear mesoscopic elasticity.

is valid only for samples with very large aspect ratios, e.g., for cylinders or beams with a large length compared with the linear size of the cross section. The analytical model proposed originally suggested the implementation of the corresponding measurement technique for samples with that geometrical feature.

A typical SIMONRUS implementation thus consists in exciting either a longitudinal or flexural vibration *eigen*mode for a very long and thin sample (aspect ratio of at least 3) via a piezoelectric transducer attached to one end. The vibration associated with the standing waves is then measured at a specific point on the sample surface, via an accelerometer (contact mode) or via a laser vibrometer (non-contact mode). The excitation consists in a pure sinusoidal oscillation. At a given excitation amplitude, the measurement is repeated for multiple frequencies. The result is a plot of the maximum amplitude of vibration at the detection point as a function of frequency[4]. The entire set of measurements is then repeated by increasing step-wise the excitation amplitude. SIMONRUS is a very powerful technique in that (1) it leads to the estimate of a physical parameter (a nonlinear elastic modulus) which is highly sensitive to damage (cracking, delamination) and (2) it has been proven to be very successful in detecting very early damage and in tracking down its temporal evolution with high resolution. Its implementation has been automatized by the Los Alamos National Laboratory [Payan et al, 2012].

The main disadvantage of SIMONRUS is that its standard implementation, described above, limits its application mainly to laboratory tests, where it is possible to produce (by casting or by coring) samples with geometry and shape satisfying as much as possible the large aspect ratio constraint. It is also possible to perform SIMONRUS measurements for samples with geometry not satisfying the constraint. However, in that case, the implementation requires first of all the identification of the exact vibration *eigen*mode that is going to be excited, for example by finite element method analysis, and the choice of the location on the sample surface where to record the output vibration signal. A corresponding stress-strain constitutive equation needs then to be formulated such that it contains a hysteretic term as introduced in the 1D case. The equation needs to lead, for that *eigen*mode of vibration, to the prediction of a resonance frequency shift proportional to the strain amplitude at the point of detection. See the work of Payan et al. for an example of SIMONRUS implementation for a parallelepiped sample without large aspect ratio [Payan et al., 2012].

SIMONRUS has been used, till nowadays, only for characterizing the evolution of AAR damage in samples following laboratory acceleration protocols. In almost all the cases, the samples fulfilled the requirement of a large aspect ratio. Two different implementations have been used. Sargolzahi *et al.* implemented the SIMONRUS technique in its most traditional version, based upon the excitation of a longitudinal *eigen*mode of vibration, usually the 1st one [Sargolzahi et al., 2010]. The measurements were performed on concrete samples cast in the laboratory with two different types of aggregates (“highly” reactive and “non-reactive”). The samples were subjected to the CSA A23.2-14A [1994] concrete prism test, similar to the ASTM C 1293 [2008] acceleration protocol. The SIMONRUS measurements were performed only 3 times within an overall time interval of 24 months, thus limiting the possibility of establishing a reliable correlation with longitudinal expansion, mass and linear elastic modulus. However, these preliminary results indicated a monotonic increase for the hysteretic nonlinear elastic modulus, in the range of hundreds %, compared with a maximum increase of the linear elastic modulus of 40%.

Chen et al. introduced a version of a 1D SIMONRUS method exploiting the excitation of a flexural vibration *eigen*mode [Chen et al., 2010; Chen et al., 2011]. The proposed method is called nonlinear

[3] The quadratic polynomial function does not have any zeroth-power term, thus it is characterized only by two coefficients.
[4] If the output signal is a velocity measured by a laser vibrometer, it is converted into acceleration by numerical differentiation. Then, the acceleration signal is converted into a strain signal by renormalization with the square of the angular frequency.

impact resonance acoustic spectroscopy (NIRAS). It differs from the traditional implementation of SIMONRUS in that the excitation of the *eigen*mode is obtained by impact with a calibrated hammer on a specific point of the sample surface, depending on the type of flexural vibration *eigen*mode that one wants to excite. The impact leads to a very wideband source pulse, allowing exciting also the wanted *eigen*mode. The resonance frequency is identified by Fourier analysis of the output signal. For the NIRAS theory, see the work of Chen et al. [2011]. The main advantage of the NIRAS method consists in a faster execution compared with the traditional SIMONRUS version, since a single impact is used as a source instead of a series of sinusoidal excitations at different frequencies. The main disadvantage consists in the simultaneous excitation of several vibration *eigen*modes for samples with not so large aspect ratio, with consequent difficulty in identifying the exact *eigen*mode excited. Chen et al. have applied the NIRAS technique to mortar samples following the AASHTO T 303 acceleration protocol, differing from ASTM C 1260-94 only for the prescribed water-to-cement ratio (0.50 instead of 0.47). The samples were clamped at one end (fixed boundary condition) and stress-free on all other lateral surfaces (cantilever beam flexural vibration) [Chen et al., 2010; Chen et al., 2011]. The authors used the temporal evolution of the hysteretic nonlinear elastic modulus for classifying the degree of reactivity of different aggregate types. They found out that such parameter is more sensitive than the longitudinal expansion to the AAR damage evolution in the very early stages of the acceleration protocol. In fact, the hysteretic nonlinear elastic modulus increases up to a maximum value, then decreases. The temporal location of the maximum and the increase rate depends upon the reactivity degree: the most reactive aggregates lead to a faster increase. The decrease following the global maximum value is attributed to the widening of the cracks beyond a critical size, such that the standing waves excited at successively increasing amplitudes may not be able to trigger enough nonlinear elastic response of the material.

Lésnicki et al. implemented a different version of NIRAS, consisting in exciting another type of flexural vibration *eigen*mode: the samples satisfied stress-free boundary conditions for all the lateral surfaces and the impact was imparted in the center of one lateral surface [Lésnicki et al., 2011; Lésnicki et al., 2012]. The technique was applied to concrete samples subjected to the concrete prism test ASTM C 1293 [2007]. The samples were either cast in the laboratory, using aggregates with different reactivity degrees and different mix designs, including also supplementary cementitious materials [Lésnicki et al., 2012], or obtained from cores coming from infrastructures known to be affected by AAR damage since a few decades. No dams were included in the tested infrastructure. The temporal evolution pattern for the hysteretic nonlinear elasticity modulus observed for the laboratory mortar samples was confirmed also for the concrete samples: the samples with the most reactive aggregates exhibited a fast increase in the nonlinear modulus up to a certain age, followed by a slow decrease. The temporal location of the maximum was also dependent upon the aggregate type and the reactivity degree: the larger the reactivity degree, the sooner the maximum.

Even though the source of decrease in the nonlinear elastic modulus is not yet completely understood, the results published till nowadays suggest a limited range of applicability for the NIRAS method: it is more sensitive than any other technique to the early damage development but cannot be used for the time-lapsed assessment of the damage evolution at later stages, when cracks are already too wide (thickness larger than a few hundreds of microns). This conclusion can be extended to the overall SIMONRUS method.

Another NEWS technique has been exploited for tracking the temporal evolution of AAR damage in laboratory mortar samples cast with aggregates of different reactivity. This technique is called **nonlinear wave modulation spectroscopy** (NWMS) and is based upon the generation of new frequency content for a low amplitude, high frequency f_2 harmonic “probing” (or modulated) wave by a high amplitude, low frequency $f_1 << f_2$ “pump” wave. The modulated wave shows not only its original, input frequency f_2 but also additional linear combination frequencies, e.g., $f_2 \pm f_1$, called side-band frequencies. The classical

nonlinear elasticity theory predicts that the amplitude of the modulated wave at any of the side-band frequency should scale linearly with the amplitude of the pump wave and with the amplitude of the probe wave, being the proportionality constant related with the quadratic nonlinear elastic modulus. Thus, a NWMS measurement usually consists in repeating the modulation measurement at increasing pump wave amplitudes, in order to determine the linear scaling coefficient, thus the nonlinear elastic modulus.

Chen et al. have shown for mortar samples that the linear relationship is valid not only for the amplitude of the signals but also for their power spectral densities, integrated over the frequency range of the side-bands and of the pump wave frequency bandwidth [Chen et al., 2008; Chen et al., 2009]. This result does not allow relating the proportionality coefficient directly to the quadratic nonlinear elastic modulus of the materials. However, that coefficient can still be used as a phenomenological damage index. For mortar samples following the AASHTO T 303 [2012] AAR acceleration protocol, Chen et al. have shown that the empirical damage index increases with AAR age up to a maximum global value, followed by a decrease. As for the results obtained with similar samples and similar acceleration protocol but with SIMONRUS measurements, the temporal location of the maximum and the increase rate depends upon the aggregate reactivity degree: the larger the degree, the faster and sooner the maximum is achieved. In addition, the empirical damage index in those measurements achieved significantly different values for the different aggregates already within the first two days since the start of the acceleration protocol, while the expansion measurements failed to clearly show a difference between the samples. This latter result confirms the usefulness of nonlinear ultrasonics NDE measurements for the early age detection of AAR damage and the differentiation between different types of aggregates.

While the SIMONRUS technique is not useful for damage detection and characterization in actual concrete infrastructure, due to the impossibility of exciting a single vibration *eigen*mode in the field, the NWMS technique could in principle be implemented in the field, since it is based upon transmission measurements. One of the difficulties in achieving such goal consists in the need to define a precise volume of the structure where the pump and probe waves would overlap with each other and interact. The second major limitation consists in the small amount of energy associated with the nonlinearly modulated side-band signals, especially for materials with high attenuation as concrete and for long distance of propagation compared with the wavelength. The latter problem affects in general every NEWS technique: the nonlinear generated frequency content is usually very small in terms of mechanical wave energy.

An alternative to the NEWS techniques is the **scaling subtraction method** (SSM), which has been proven to be successful in detecting damage evolution in concrete for different types of damage mechanisms. The SSM consists in performing simple transmission measurements with a burst through a concrete sample or structure member, at increasing excitation amplitudes, starting with a very small amplitude (called reference excitation amplitude) in correspondence of which the nonlinear elastic response is almost negligible. For each excitation amplitude, a digital signal, called SSM signal, can be synthesized from the transmission signal at the reference amplitude and from the signal at the current excitation amplitude. The SSM signal is defined as the difference between the current transmission signal and the signal that would be obtained in correspondence of that excitation amplitude if the propagation medium was completely linear elastic. This ideal signal can be defined as the reference transmission signal scaled up of the same scaling factor existing between the current excitation signal and the reference one, being the two identical in shape and timing but differing only for the amplitude. The SSM signal contains in itself information about the nonlinear elastic response of the material. Its maximum amplitude or root mean squared value (in time) is related to the corresponding value for the transmission signal according to a power law, whose parameters can be used as damage indicators (damage intensity and damage type, respectively for the coefficient multiplying the power law and the power law exponent) [Bruno et al., 2009]. The SSM method has the disadvantage of being based upon damage parameters that, at the time of this report, have not yet

being related to physical parameters as nonlinear elastic moduli. Among its advantages, there is a higher sensitiveness in detecting the evolution of cracking compared with NEWS techniques [Bentahar et al., 2013] and its proved, successful application to a variety of damage processes in concrete, including damage due to mechanical [Antonaci et al., 2010a; Antonaci et al., 2010b] and thermal loading [Scalerandi et al., 2013].

Figure 4.7 shows the temporal evolution of the relative change of one SSM damage index, the coefficient multiplying the power law, estimating the "strength" of the nonlinear elastic response. That parameter was calculated out of SSM measurements performed at Empa every week on two sets of mortar samples following the accelerated mortar bar test (AMBT) protocol ASTM C 1260-94 (see Section 3.2.1 and Figure 4.6 for more information about the experimental campaign). The relative change was calculated in respect to the initial value of the parameter, before the start of the immersion into the 1 M NaOH solution kept at constant temperature equal to 80°C. Each sample set included six samples. One set was for samples following the AAR acceleration protocol, the other for reference samples, cast at the same time and according to the same mix design as for the other samples but not following the acceleration protocol. These reference samples were kept instead in a climatic chamber at 90% RH and 21°C. Each point in the plot in Figure 4.7 is an average value of the SSM damage index over the set of respective samples, while the error bar was calculated as the standard deviation. Figure 4.7 shows that the SSM damage index increased monotonically up to 14 weeks in the samples following the acceleration protocol. The relative increase was very large, of the order of several hundred %, much larger than the relative change in the UPV (compare with Figure 4.6b). The monotonic increase in the damage index accompanied the continuous longitudinal expansion of the samples (see Figure 4.6a). On the contrary, no significant variation was observed for the SSM index in the case of the reference samples. The error bars in Figure 4.7, for the AAR-accelerated samples, increased significantly at later AAR ages, very likely due to different degrees of crack progression and crack filling in different samples. However, a clear trend was obtained for the average value. The significant drop after 14 weeks of acceleration protocol could be attributed to crack filling, as evinced from the X-ray tomographic microscopy measurements on one sample among those following the protocol. However, this remains a hypothesis, since only one sample out of six was scanned. The results reported in Figure 4.7 suggest that the SSM damage index may be adopted as a very sensitive indicator for tracking the progression of the AAR damage.

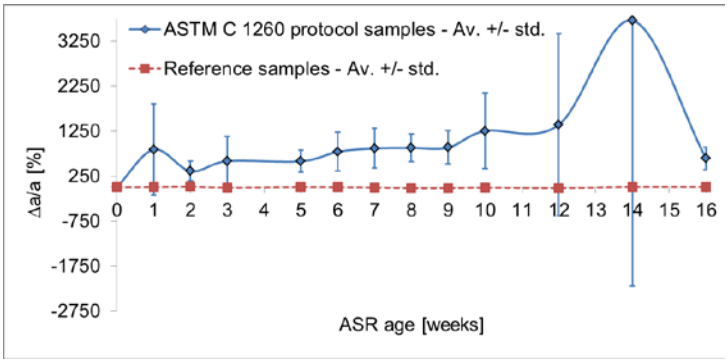

Figure 4.7: relative change for the SSM damage index indicating the strength of the overall nonlinear elastic response of mortar samples. The relative change is calculated in respect of the AAR age = 0 week, corresponding to the time before the start of the AAR acceleration. The plots refer to two sets of mortar samples cast at the same time according to the same mix design. Six samples followed the ASTM C 1260-94 AAR acceleration protocol (blue line), while other six samples remained in a climatic chamber at 90% RH and 22°C (red line, reference sample). Each point is the average value over the sample set, while the error bar was calculated as the standard deviation. Experimental campaign performed at the Concrete and Construction Chemistry Laboratory and Metrology/Electronics/Reliability Laboratory, Empa.

4.5.3 NDE with X-ray tomographic microscopy

Among the NDE methods for AAR damage detection and characterization, X-ray tomographic microscopy (XTM) has started to be used as a technique complementary to the optical microscopy techniques described in Section 3.2. At the laboratory scale, XTM consists in the use of a cone-beam, micro-focus X-ray setup for tomographic imaging. The divergent, cone-beam geometry of the X-ray radiation allows selecting different magnification factors, so that different spatial resolutions can be achieved. The maximum achievable spatial resolution is of the order of a few microns. The maximum sample size could be of the order of ten cm, with a corresponding spatial resolution of the order of 50 microns. XTM can be performed also exploiting synchrotron radiation, achieving in that case higher spatial resolution, thanks to an X-ray beam with parallel geometry and highly collimation, together with a high resolution X-ray detector. The spatial resolution for samples a few mm thick in the beam direction can be of the order of 500 nm.

XTM cannot substitute the optical microscopy techniques, in that it does not achieve the same spatial resolution and it does not allow achieving the same contrast as obtained with cross polarized light. However, it offers other advantages, first of all the possibility of acquiring 3D images of the sample in a completely non-destructive way, without the need of any labor-intensive and invasive sample preparation procedure. The average scan time for a sample of a few cm in thickness along the beam direction goes from 1 hour to 10 minutes. Figure 4.8 shows a digital cross-sectional slice from 3D tomographic datasets of a mortar sample affected by AAR damage, accelerated via the ASTM C 1260-94 protocol. The sample was cylindrical, 25 mm in diameter. The three insets refer approximately to the same vertical cross-section along the vertical position of the sample, extracted from three different datasets acquired at different AAR ages. The region of interest (ROI) highlighted in the red box and magnified in the sub-insets shows an aggregate affected by a temporally evolving crack. The crack first got wider between 6 and 9 weeks (insets (a) and (b)), then it disappeared, very likely by filling in with AAR products. The measurements were performed at Empa with a micro-focus X-ray source set at 140 kV and 70 μA.

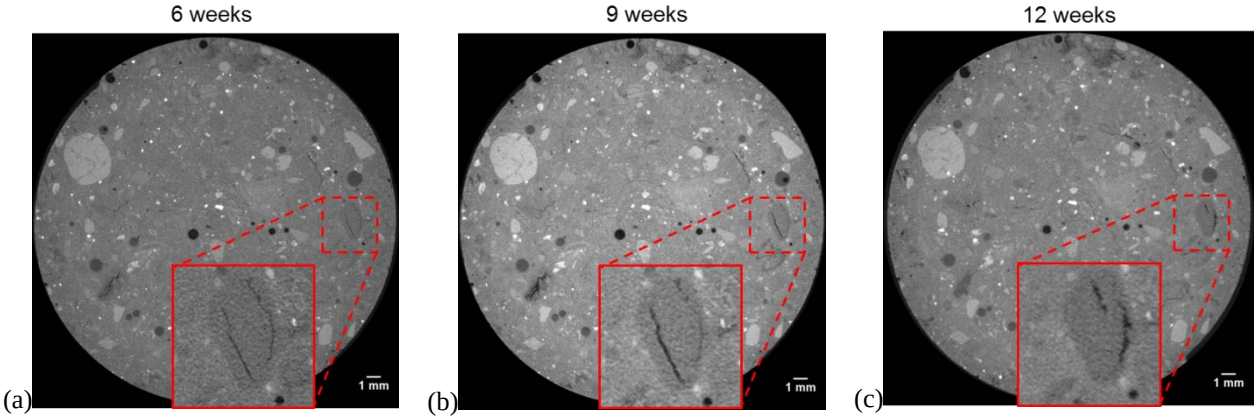

Figure 4.8: digital cross-sectional slices from 3D X-ray tomographic microscopy datasets of the same mortar sample at three different times during the ASTM C 1260-94 AAR acceleration protocol. Inset (a): 6 weeks. Inset (b): 9 weeks. Inset (c): 12 weeks. The sample was cast with highly reactive aggregates containing Swiss alpine gneiss. The measurements were performed at Empa with a micro-focus X-ray source set at 140 keV and 70 μA. The voxel lateral size was about 27 μm and the actual spatial resolution was of the order of 40 μm. The red, dashed boxes highlight a region of interest including an aggregate exhibiting cracks evolving in time, first growing in width, then almost disappearing, likely due to filling by AAR products.

Figure 4.9 shows a cross-sectional slice from a 3D X-ray tomographic microscopy dataset of a 7 mm-diameter mortar sample that followed the ASTM C 1260-94 AMBT till the age of 8 weeks. The sample was cast with highly reactive aggregates containing Swiss alpine gneiss. The measurement was performed

with hard X-rays at 30 keV energy produced at the Swiss Light Source (SLS) synchrotron radiation facility, Paul Scherrer Institute, via the XTM setup available at the TOMCAT beamline. A special wide field-of-view developed at TOMCAT was adopted to be able to fit the sample within the detector's field-of-view without the need of reducing the spatial resolution. The voxel lateral size was 1.85 μm, corresponding to about 5 μm of effective spatial resolution. With such high spatial resolution, it is possible to resolve the boundaries of most of the largest micro-cracks produced by the AAR. The advantage of a XTM dataset as that shown in Figure 4.9 consists in the availability of 3D information about the damage patterns, obtained on the sample with a complete non-destructive procedure. The only possibility of adding damage to the sample could come from the radiation dose imparted. However, the scanning time at 3rd generation synchrotron radiation facilities is nowadays of the order of minutes (2 minutes in the case of our scanning), reducing the total dose to minimum levels not affecting the samples. With such 3D datasets, detailed statistical properties about the cracking mechanisms can be obtained by 3D image analysis [Marinoni et al., 2009; Voltolini et al., 2011] and used both as input and as validation dataset of AAR damage computational models.

Given the limited and expensive access to synchrotron radiation facilities, XTM performed with synchrotron radiation can be mainly exploited for basic research purposes. However, laboratory scale XTM setups are becoming widespread in industrial contexts, including for petrophysical characterization of geomaterials of interest for oil/gas field developments. Their application to AAR damage detection and characterization has the potential of becoming more widespread as well, providing information that can complement that obtained by 2D optical microscopy [Weise et al., 2013].

4.6 Conclusions and outlook

The general problem of analysis dependent on imaging is the choice between size and resolution. With increasing resolution the analysed size, and with it the representativeness, decreases. Therefore, SEM is no suitable methods to assess the extent of damage in dams. The resolution and size provided by thin sections make them the most reasonable tool available. The applicability of impregnating and photographing larger concrete specimens with subsequent image analysis needs further investigation. However, it seems to be an excellent method for assessing the extent of damage with relatively little expense of work, at least for concrete with severe AAR.

The determination of the mechanical properties of concrete is a common procedure in any investigation of a concrete structure. The assessment of how much AAR has altered the mechanical properties of the concrete in a dam is difficult due to the variations in concrete quality in these large structures and the lack of comparative standard properties.

Non-destructive methods have a great potential to assess variations in concrete quality in general and variations in degree of damage in particular, but their applicability on dams has still to be explored.

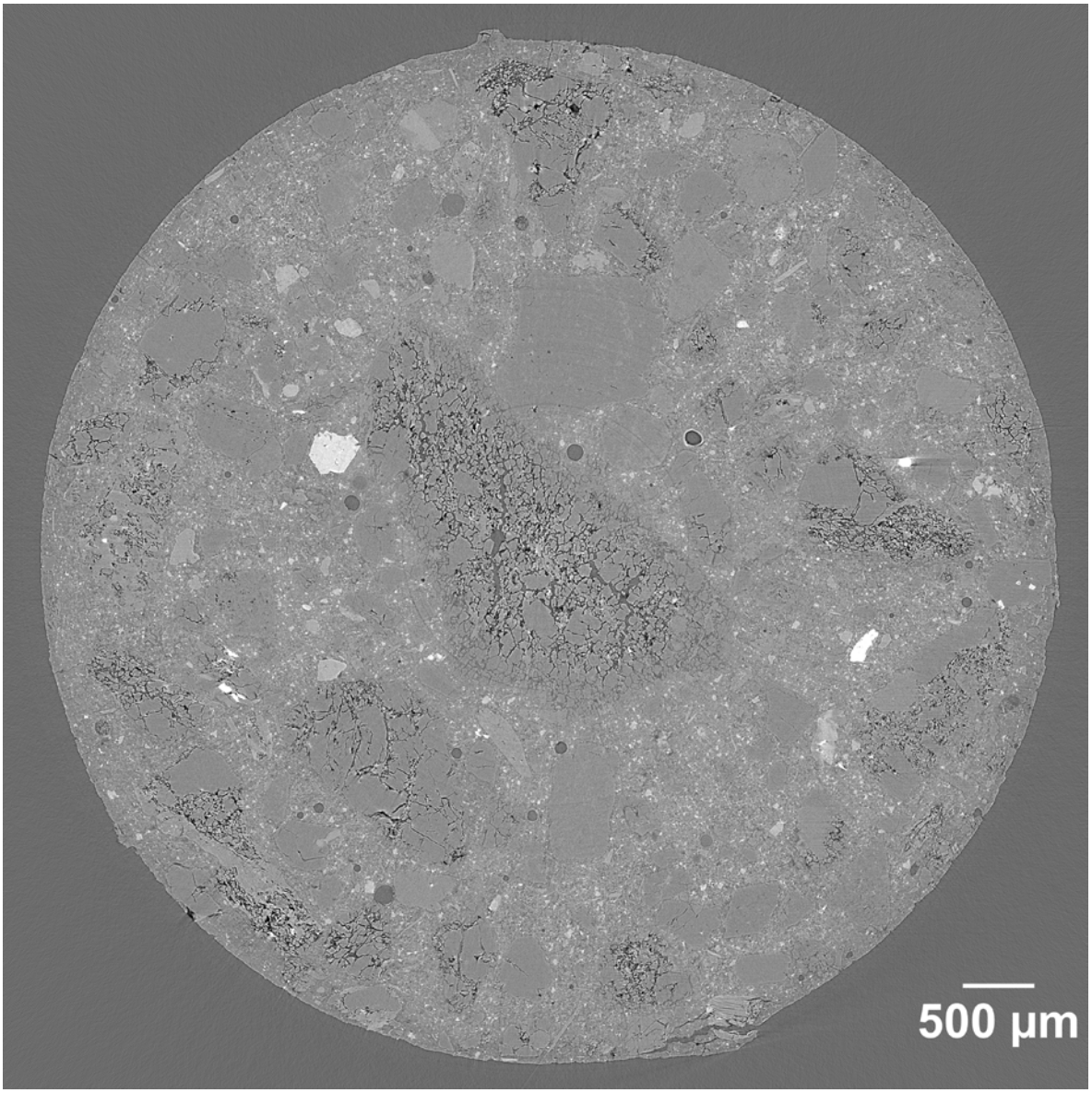

Figure 4.9: digital cross-sectional slice from a 3D X-ray tomographic microscopy dataset of a mortar sample affected by AAR damage due to AAR acceleration by the ASTM C 1260-94 protocol, followed for 8 weeks. The measurement was performed at the synchrotron radiation TOMCAT beamline of the Swiss Light Source (SLS), Paul Scherrer Institute (PSI), ETH Domain, within the framework of the project n°20120164 funded by the SLS. The tomographic scanning was performed with beam energy of 30 keV and with sample-to-detector distance of 40 mm, to achieve edge-enhancement effects for better highlighting the crack boundaries. A single tomographic scan lasted about 2 minutes, following a wide field-of-view protocol consisting in a 360° total rotation angle for the sample, avoiding the need of having the sample completely fitted within the field-of-view of the detector. The lateral voxel size was 1.85 µm.

5. Prognosis

The determination of the residual expansion potential can be useful to assess the future behaviour of a concrete structure affected by AAR [e.g., Larive, 1998; Bérubé et al., 2000b; Carles-Giberges & Cyr, 2002; Godart et al., 2004; Wood, 2004]. It permits a relatively fast assessment of the concrete's expansion potential compared to on-site monitoring. The results may be used for modelling [Multon & Toutlemonde, 2006a], when combined with data about temperature and moisture conditions of the structure. Furthermore, they may help to plan maintenance and costs involved.

As already described, cores have to be sealed in plastic bags immediately after coring. It is recommended to produce thin sections in the immediate vicinity of the core sections selected for the residual expansion test. Additionally, the alkali content (water and/or acid soluble) of the concrete should be determined to get an indication about the amount of alkalis available for reaction [Godart et al., 2013]. It has to be pointed out that aggregates can be source of alkalis in addition to the cement [Bérubé et al., 2002; Constantiner & Diamond, 2003; Leemann & Holzer, 2005]. When the acid-soluble alkali content is determined, some alkalis can be dissolved from minerals in the aggregates.

Usually, the residual expansion test is conducted at 38 °C and in saturated air [LCPC, 1997]. However, immersion in water or NaOH solutions can be used as well [Bérubé et al., 2004; Smaoui et al., 2004b; Multon, 2004; Multon et al., 2008]. There are different opinions about data interpretation during the assessment of the results. In the residual expansion test performed in saturated air, different phases of expansion can be distinguished (Figure 5.1):

- phase 1: expansion during conditioning;
- phase 2: expansion at elevated temperature and in saturated air;
- phase 3: shrinkage, during drying, up to the initial weight at the beginning of phase 1 (irreversible expansion)

The initial expansion recorded in the test is mainly caused by moisture uptake of the sample during phase 1. However, some expansion during phase 1 can possibly be attributed to AAR. On the other hand, some of the expansion recorded during phase 2 may be attributable to moisture uptake, as the cores usually still gain some weight. The determination of the alkali content in the water at the bottom of the storage containers holding the cores can provide information about alkali leaching. By drying the cores at the end of the test until they reach the weight at the start of phase 1, the irreversible expansion is determined.

In regard to this type of test, there are several uncertainties that have an effect on the resulting expansion and data analysis [Merz & Leemann, 2013]:

- coring direction in relation to casting direction;
- size of the cores;
- duration of the test (typically one to two years);
- decision between the substantially different diametral and longitudinal expansion values for assessing the actual, characteristic expansion value;
- decision on the characteristic expansion for the residual expansion potential (phase 2 non-linear, phase 2 linear, irreversible expansion);
- effect of leaching on the resulting expansion as function of test duration and specimen size.

It has to be kept in mind that the expansion potential uncovered in the test may not be activated in the structure. Additionally, the stress state of the concrete in the structure [Multon & Toutlemonde, 2006b], the relation between core diameter and maximum aggregate size [Gao et al., 2011] and the orientation of the cores in regard to the casting direction [Larive, 1998; Smaoui et al, 2004b] all have an effect on the measured expansion These issues clearly demonstrate that care is advisable when expansion values are transferred to a structure or used for modelling. At the current state of knowledge the residual expansion potential can be used to qualitatively compare different structures or different components of the same structure [Merz & Leemann, 2013]. Additional information, like the expansion rate derived from the crack index on the structure and the age of the structure, may help to better assess the results of the residual expansion test. If the situation allows it, longtime monitoring is recommended [Vézina & Bouchard, 2008;

Sellier et al., 2009]. In dams, such data are often available from the regular surveys of the structure. However, it is obvious that further research on the topic is needed.

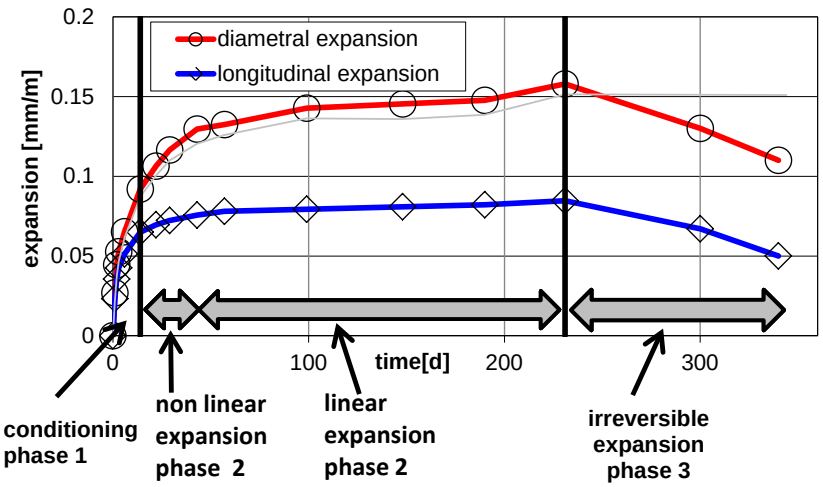

Figure 5.1: Different phases of expansion during the residual expansion measurements in longitudinal and diametral direction of cores.

6. Relation between diagnosis and modeling

Significant efforts have been dedicated to the development of computational models of AAR-induced damage in concrete. The “spectrum” of models is very broad. It may actually be more appropriate to speak of “spectra” of models, depending upon the specific features that the models try to describe and simulate. Souma and Xi have provided a possible classification of “spectra”, or categories, of computational models in their literature review about AAR damage in concrete dams [Souma & Xi, 2004].

They distinguish between models of the basic physical-chemical processes leading to the formation of AAR products and the respective swelling due to water uptake [Suwito et al., 2002] and models of the mechanical response of concrete to that swelling, coupling the concrete mechanics with the physico-chemical processes [Bournazel & Moranville, 1997; Capra & Bournazel, 1998; Ulm et al., 2000; Lemarchand et al., 2002; Pignatelli et al., 2013].

Another classification is based upon the spatial scale of the processes addressed by the models. The range goes from the aggregate scale [Dunant & Scrivener, 2010], to be considered as the microscopic scale, to the scale of a full concrete structure [Léger et al., 1996; Saouma & Perotti, 2006; Fairbairn et al., 2006; Grimal et al., 2010], the macroscopic scale, passing through intermediate scales, e.g., by considering features as the aggregate size distribution and the cement paste porosity, or by adopting a poro-mechanics approach [Pesavento et al., 2012].

Finally, another classification is based upon the approach used in modeling, e.g., by the development of constitutive laws based upon basic thermodynamic and mechanical principles [Li & Coussy, 2002] or by microscopic scale Finite Element Method simulations [Dunant & Scrivener, 2010].

Beyond its fundamental role in complementing and/or expanding the knowledge about the AAR itself and the correspondent damage in concrete, computational modeling can play a fundamental and unique role in the diagnosis and prognosis of AAR damage for concrete structures.

The work of Li and Coussy is adopted here as one possible example of computational modeling work developed with the purpose of supporting the diagnosis of an actual concrete structure, starting from a

limited number of experimental data available about its AAR damage evolution [Li & Coussy, 2002]. Several other examples can be found in the literature (e.g. [Saouma & Perotti, 2006]). The work of Li and Coussy focuses not only on the chosen approach and the details of the modeling but also on the methodological issues related with the development of computational models to be used for diagnosis and prognosis of AAR damage in concrete structures. According to Li and Coussy, any computational model of AAR damage aiming at the assessment of a structure requires two fundamental components: (1) a model of the AAR product swelling, according to correct kinetics and (2) a model of the response of the material (concrete) to the swelling. The model usage workflow should consists in three main steps: (a) collection of data about the structure, (b) calibration of the model's parameters against the collected data and (c) execution of time-space scaled simulations to assess "in-silico" the current state of the structure (diagnosis) and to forecast its future development (prognosis).

The specific model proposed by Li and Coussy is based upon the development of two sets of chemo-mechanical constitutive equations for AAR-affected concrete. The approach is thus a macroscopic scale one, based upon thermodynamic principles. The first set of equations does not account for plastic strains, thus it is limited to the description of structures affected by early age damage, e.g., in the absence of surface cracks, or to free swelling concrete, e.g., cores obtained from an actual structure and used for residual expansion measurements. The second set of constitutive equations takes into account plastic strains due to the restraining (and other types of) boundary conditions a structure is subject to. These equations can be used for the simulation of the behavior of an actual damaged structure. A third set of constitutive equations is also proposed, where plastic strains directly created by the AAR product swelling itself are taken into account. The latter set of equations is more limited, due to higher difficulties in experimentally constraining the values of some of their parameters.

The first two types of constitutive equations can be adopted in finite element method (FEM) computational codes. This was done by the authors for assessing the current damage stage of an AAR-affected concrete pier, used as support for a steel truss bridge in Africa. The reason for using both types of equations consists in the fact that they share some basic unknown parameters. The optimal estimation of those parameters came from the calibration of both model types against two different types of experimental data, residual expansion strains of a core from the structure and strains from certain locations on the structure itself. The cross-calibration allowed for the identification of all the unknown parameters, after which the FEM model based upon the second set of constitutive equations could be used for calculating the spatial distribution of plastic strains in the structure. This result led to the design and "in-silico" testing of a retro-fitting design.

7. Summary

Established methods and tools to diagnose AAR in concrete structures exist. Diagnosing AAR starts at the macroscopic level and proceeds to the microscopic level. It relies on the identification of specific crack patterns and specific reaction products. The reaction products can be identified based both on morphology and on chemical composition.

As dams start having problems at already relatively low expansion levels, the challenge in such structures is to diagnose AAR that may still be at an early stage. Here the combination of SEM with EDX becomes an indispensable and effective tool for diagnosis.

In addition to the diagnosis of AAR, the assessment of its degree and extent poses new challenges:

- The disadvantage of optical microscopy methods is that the analyzable volume decreases with increasing resolution. Large thin sections offer a good compromise between analyzed volume and resolution. The use of large polished sections (up to several decimeters in linear dimension) with

epoxy impregnation, imaging and subsequent analysis needs to be explored for the application in dams. The use of mechanical tests to assess the degree of damage is problematic due to lack of direct reference values. In addition, for concrete with a low degree of damage they may not be sensitive enough. This assessment includes the stiffness damage test.

- The number of coring sites and number of cores taken from a structure depends on the level of accuracy required and the funding available. The use of NDE methods may have a potential to go beyond the possibilities of the classical approach of taking cores. However, the application of the different NDE methods on dams is still in its infancy and consequently needs further research.

A fundamental question about dams affected by AAR is the future development of AAR and the consequences for the structures. The determination of the residual expansion potential seems to be an appropriate tool for prognosis. However, several questions about the test protocol and data analysis, on one hand, and the relatively small database, on the other hand, leave some uncertainties on the transferability of the results to the structures and the use in models.

Computational models could become in the future very useful tools in the diagnosis and prognosis of AAR damage in a concrete structure, e.g., a dam. However, they are only complementary and synergistically dependent upon experimental characterizations of the damage itself. All the models require a parameter calibration step that is highly dependent upon the amount, type and quality of data available about the damage type, extent and about the structure response to the damage itself.

8. References

AASHTO T 299-93, Standard method of test for rapid identification of alkali-silica reaction products in concrete, 2004.

AASHTO T 303-00, Standard method of test for accelerated detection of potentially deleterious expansion of mortar bars due to alkali-silica reaction, 2012.

Antonaci P., Bruno C.L.E., Bocca P.G., Scalerandi M., Gliozzi A.S., Nonlinear ultrasonic evaluation of load effects on discontinuities in concrete, Cem. Concr. Res. 40 (2010b), 340-346.

Antonaci P., Bruno C.L.E., Gliozzi A.S., Scalerandi M., Monitoring evolution of compressive damage in concrete with linear and nonlinear ultrasonic methods, Cem. Concr. Res. 40 (2010a) 1106-1113.

Anugonda P., Wien J.S., Turner J.A., Diffusion of ultrasound in concrete, Ultrasonics 39 (2001) 429-435.

ASTM C597-09, Standard test method for pulse velocity through concrete, ASTM International, 2010.

ASTM C1260-07, Standard test method for potential alkali reactivity of aggregates (mortar-bar method), ASTM International, 2007.

ASTM C 1293, Standard test method for determination of length change of concrete due to alkali-silica reaction, ASTM International, 2008.

Ayora C., Chinchón S., Aguado A., Guirado F., Weathering of iron sulfides and concrete alteration: thermodynamic model and observation in dams from central Pyrenees, Spain, Cem. Concr. Res. 28 (1998) 591-603.

Becker J., Jacobs L.J., Qu J., Characterization of cement-based materials using diffuse ultrasound, J. of Eng. Mech. 129 (2003) 1478-1484.

Ben Haha M., Gallucci E., Guidoum A., Scrivener K.L., Relation of expansion due to alkali silica reaction to the degree of reaction measured by SEM image analysis, Cem. Concr. Res. 37 (2007) 1206-1214.

Bentahar M., El Aqra H., El Guerjouma R., Griffa M., Scalerandi M., Hysteretic elasticity in damaged concrete: Quantitative analysis of slow and fast dynamics, Phys. Rev. B 73 (2006), 014116/1-10.

Bentahar M., El Guerjouma R., Idijmarene S., Scalerandi M., Influence of noise on the threshold for detection of elastic nonlinearity, J. Appl. Phys. 113 (2013) 043516/1-11.

Bérubé M.A., Duchesne J., Does silica fume merely postpone expansion due to alkali-aggregate reactivity?, Constr. Build. Mat. 7 (1993) 137-143.

Bérubé M.A., Duchesne J., Dorion J.F., Rivest M., Laboratory assessment of alkali contribution by aggregates to concrete and application to concrete structures affected by alkali-silica reactivity, Cem. Concr. Res. 32 (2002) 1215-1227.

Bérubé M.A., Fournier B., Durand B. (eds.), Alkali-Aggregate Reaction in Concrete. Proceedings of the 11th International Conference on Alkali–Aggregate Reaction in Concrete, CRIB, Sainte Foy, Québec City, Canada, 2000.

Bérubé M.A., Frenette J., Pedneault A., Rivest M., Laboratory assessment of the potential rate of ASR expansion of field concrete, in: Bérubé M.A., Fournier B., Durand B. (eds.), Proceedings of the 11th ICAAR, Québec, Canada, Québec, Canada, 2000, 821-830.

Bérubé M.A., Smaoui N., Côté T., Expansion tests on cores from ASR-affected structures, in: Tang M., Deng M. (eds.), Proceedings of the 12th ICAAR, Bejing, China, 2004, 821-832.

Bond L.J., Kepler W.F., Frangopol D.M., Improved assessment of mass concrete dams using acoustic travel time tomography. Part I-theory, Construction and Building Materials 14 (2000), 133-146.

Born M., Huang K., Dynamical theory of crystal lattices. London (UK): Oxfor University Press, 1962.

Bournazel J.-P., Moranville M., Durability of concrete: the crossroad between chemistry and mechanics, Cem. Concr. Res., 27 (1997) 1543–1552.

Breysse D., Nondestructive evaluation of concrete strength: An historical review and new perspectives combining NDT methods, Construction and Building Materials 33 (2012) 139-163.

Broekmans M.A.T.M. (ed), Alkali-Aggregate Reaction in Concrete. Proceedings of the 13th International Conference on Alkali–Aggregate Reaction in Concrete, Trondheim, Norway, 2008.

Bruno C., Gliozzi A., Scalerandi M., Antonaci P., Analysis of elastic nonlinearity using the scaling subtraction method, Phys. Rev. B 79 (2009) 064108/1-13.

Capra B., Bournazel J.-P., Modeling of induced mechanical effects of alkali-aggregate reactions, Cem. Concr. Res. 28 (1998) 251–260.

Carles-Giberges A., Cyr M., Interpretation of expansion curves of concrete subjected to accelerated alkali-aggregate reaction (AAR) tests, Cem. Concr. Res. 32 (2002) 691-700.

Casanova I., Aguada A., Agullo L., Aggregate expansivity due to sulfide oxidation II. Physio-chemical modeling of sulfate attack, Cem. Concr. Res. 27 (1997) 1627-1632.

Charlwood R., Lecture at AAR Workshop, EPFL, Lausanne, 2013.

Chen J., Jayapalan A.R., Kim J.-Y., Kurtis K.E., Jacobs L.J., Nonlinear wave modulation spectroscopy method for ultra-accelerated alkali-silica reaction assessment, ACI Mat. J. 106 (2009) 340–348.

Chen J., Jayapalan A.R., Kim J.-Y., Kurtis K.E., Jacobs L.J., Rapid evaluation of alkali–silica reactivity of aggregates using a nonlinear resonance spectroscopy technique, Cem. Concr. Res. 40 (2010) 914–923.

Chen J., Kim J.-Y., Kurtis K.E., Jacobs L.J., Theoretical and experimental study of the nonlinear resonance vibration of cementitious materials with an application to damage characterization, J. Acoust. Soc. Amer. 130 (2011) 2728–2737.

Chen X.J., Kim J.-Y., Kurtis K.E., Qu J., Shen C.W., Jacobs L.J., Characterization of progressive microcracking in Portland cement mortar using nonlinear ultrasonics, NDT & E Int. 41 (2008) 112–118.

Cole W.F., Lancucki C.J., Products formed in an aged concrete the occurrence of okenite, Cem Concr Res 13 (1983) 611-618.

Cole W.F., Lancucki C.J., Sandy M.J., Products formed in an aged concrete, Cem. Concr. Res. 11 (1981) 443-454.

Collins C.L., Ideker J.H, Willis G.S., Kurtis K.E., Examination of the effects of LiOH, LiCl, and LiNO3 on alkali–silica reaction, Cem. Conc. Res. 34 (2004) 1403-14015.

Constantiner D., Diamond S., Alkali release from feldspars into pore solutions, Cem. Concr. Res. 33 (2003) 549-554.

Crisp T.M., Waldron, P., Wood, J.G.M., Development of a non-destructive test to quantity damage in deteriorated concrete, Mag. Concr. Res. 45 (1993) 247-256.

Crouch, R.S., Specification for the determination of stiffness damage parameters from the low cyclic uniaxial compression of plain concrete cores. Revision A, Mott, Hay & Anderson, Special services division, Internal technical note, 1987.

CSA A23.2-14A, Potential expansivity of aggregates (procedure for length change due to AAR in concrete prisms. CSA A23.2-94 - Methods of Test for Concrete. Canadian Standards Association, Rexdale, Ontario, Canada., 1994, 205-214.

Davies G., Oberholster R.E., Alkali-silica reaction products and their development, Cem. Concr. Res. 18 (1988) 621-635.

De Ceukelaire L., The determination of the most common crystalline alkali-silica reaction product, Mater. Struct. 24 (1991) 169-171.

Deroo F., Kim J.-Y., Qu J., Sabra K., Jacobs L.J., Detection of damage in concrete using diffuse ultrasound, The Journal of the Acoustical Society of America 127 (2010) 3315-3318.

DIN/ISO 8047, Hardened Concrete-Determination of Ultrasonic Pulse Velocity, DIN (19??).

Duchesne J., Bérubé M.A., Long-term effectiveness of supplementary cementing materials against alkali–silica reaction, Cem. Concr. Res. 31 (2001) 1057-1063.

Dunant C.F., Scrivener K.L., Micro-mechanical modelling of alkali–silica-reaction-induced degradation using the AMIE framework, Cem. Concr. Res. 40 (2010) 517–525.

Dunbar. P.A., Grattan-Bellew, P.E., Results of Damage Rating Evaluation of Condition of Concrete from a Number of Structures Affected by AAR, Proceedings of CANMET/ACI International Workshop on AAR in Concrete, Dartmouth, Nova Scotia, CANMET, Department of Natural Resources Canada, 1995, pp. 257-265.

Fairbairn E.M.R., Ribeiro F.L.B., Lopes L.E., Toledo-Filho R.D., Silvoso M.M., Modelling the structural behaviour of a dam affected by alkali-silica reaction, Comm. Num. Met. Eng. 22 (2006) 1–12.

Fernandes I., Noronha F., Teles M., Examination of the concrete from an old Portuguese dam: Texture and composition of alkali–silica gel, Mat. Charact. 58 (2007) 1160-1170.

Fernandes I., Noronhaa F., Teles M., Microscopic analysis of alkali–aggregate reaction products in a 50-year-old concrete, Mat. Charact. 53 (2004) 295-306.

Fernandes I., Silva A.S., Gomes J.P., de Castro A.T., Noronha F., Characterization of AAR in Fagilde dam, in: Broekmans M.A.T.M., Wigum B.J. (eds), Proceedings 13th ICAAR, Trondheim, Norway, 2008.

Fournier B., Bérubé M.A., Folliard K.J., Thomas M., Report on the diagnosis, prognosis, and mitigation of alkali-silica reaction (ASR) in transportation structures, FHWA-HIF-09-004, 2010.

Gao X.X., Multon S., Cyr M., Sellier A., Optimising an expansion test for the assessment of alkali–silica reaction in concrete structures, Mater. Struct. 44 (2011) 1641-1653.

Godart B., de Rooij M., Wood J.G.M. Guide to the diagnosis and appraisal of AAR damage to concrete in structures, part 1 diagnosis (AAR 6.1). RILEM State-of-the-Art Reports, Springer, 2013.

Godart B., Mahut B., Fasseu P., Michel M., The guide for aiding to the management of structures damaged by concrete expansion in France, in: Tang, M. Deng M. (eds.), Proceedings of the 12th ICAAR, Bejing, China, 2004, 1219-1228.

Grattan-Bellew, P.E., Comparison of laboratory and field evaluation of alkali-silica reaction in large dams, Proceedings of the First International Conference on Concrete Alkali-Aggregate Reactions in Hydroelectric Plants and Dams, Fredericton, NB, Canada, 23 p., September-October 1992.

Grimal E., Sellier A., Multon S., Le Pape Y., Bourdarot E., Concrete modelling for expertise of structures affected by alkali aggregate reaction, Cem. Concr. Res. 40 (2010) 502-507.

Guyer R.A., Johnson P.A., Nonlinear Mesoscopic Elasticity. The complex behavior of rocks, soil and concrete. Weinheim (Germany): Wiley-VCH, 2009.

Guyer R.A., Johnson P.A., Nonlinear Mesoscopic Elasticity: Evidence for a new class of materials, Physics Today 52 (1999) 30–36.

Guyer R.A., McCall K.R., Van Den Abeele K.E.-A., Slow elastic dynamics in a resonant bar of rock, Geophys. Res. Lett. 25 (1998) 1585–1588.

Jakobsen U.H., Laugesen P., Thaulow N., Determination of water-cement ratio in hardened concrete by optical fluorescence microscopy, ACI Special Publication 191 (1999) 27-42.

Jakobsen U.H., Thaulow N., Johansen V., Analyses of sodium- and potassium-rich droplets observed on the surface of alkali-silica reactive aggregates and on gel in polished thin sections, Cem. Conc. Res. 22 (1992) 1148-1160.

Katayama T., ASR gel in concrete subject to freeze – thaw cycles – comparison between laboratory and field concretes from Newfoundland, Canada, in: Broekmans M.A.T.M., Wigum B.J. (eds), Proceedings of the 13th ICAAR, Trondheim, Norway, 2008.

Katayama T., Petrographic study of the alkali-aggregate reactions in concrete. Doctoral thesis (Science), Department of Earth and Planetary Science, Graduate School of Science, University of Tokyo, 2012.

Katayama T., Petrography of the Kingston experimental sidewalk at age of 22 years - ASR as the cause of deleteriously expansive, so-called alkali-carbonate reaction. Proceedings of the 14th ICAAR, Austin/TX, 2012.

Katayama T., The so-called alkali-carbonate reaction (ACR) - Its mineralogical and geochemical details, with special reference to ASR, Cem. Concr. Res. 40 (2010) 643-675.

Kawamura, M. Takemoto K., Correlation between pore solution composition and alkali silica expansion in mortars containing various fly ashes and blastfurnace slags, Int. J. Cem. Compos. Lightweight Concr. 10 (1988) 215-223.

Kepler W.F., Bond L.J., Frangopol D.M., Improved assessment of mass concrete dams using acoustic travel time tomography. Part II-application, Construction and Building Materials 14 (2000), 147-1156.

Kjellsen K.O., Monsøy A., Isachsen K., Detwiler R.J., Preparation of flat-polished specimens for SEM-backscattered electron imaging and X-ray microanalysis - importance of epoxy impregnation, Cem. Concr. Res. 33 (2003) 611-616.

Knudson T., Taulow N., Quantitative microanalyses of alkali–silica gel in concrete, Cem Concr Res 5 (1975) 443-454.

Landau L.D., Lifshitz E.M., Theory of elasticity. Course of Theoretical Physics, vol. 7. Bristol (UK): Pergamon Press, 1975.

Lane D.S., Ozyildirim C., Preventive measures for alkali-silica reactions (binary and ternary systems), Cem. Conc. Res. 29 (1999) 1281-1288.

Larive C., Apports combinés de l'expérimentation et de la modélisation à la comprehension de l'alcali-réaction et de ses effets mécaniques. PhD Thesis ENPC, published by LCPC, Paris, OA 28, 1998.

Larose E., Hall S., Monitoring stress related velocity variation in concrete with a 2×10−5 relative resolution using diffuse ultrasound, The Journal of the Acoustical Society of America 125 (2009) 1853-1856.

LCPC, Alcali-réaction du béton: Essais d'expansion résiduelle sur béton durci, Méthode d'essai 44, 1997.

LCPC, Détermination de l'indice de fissuration d'un parement de béton, Méthode d'essai LPC 47, 1997.

Lee H., Cody R.D., Cody A.M., Spry P.G., The formation and role of ettringite in Iowa highway concrete deterioration, Cem. Concr. Res. 35 (2005) 332–343.

Leemann A., Holzer L., Alkali-aggregate reaction - identifying reactive silicates in complex aggregates by ESEM observation of dissolution features, Cem. Concr. Compos. 27 (2005) 796-801.

Leemann A., Lothenbach B., The influence of potassium–sodium ratio in cement on concrete expansion due to alkali-aggregate reaction, Cem. Concr. Res. 38 (2008) 1162-1168.

Leemann A., Lura P., E-modulus of the alkali–silica-reaction product determined by micro-indentation, Construction and Building Materials 44 (2013) 221-227.

Leemann A., Merz C., An attempt to validate the ultra-accelerated microbar and the concrete performance test with the degree of AAR-induced damage observed in concrete structures, Cem. Concr. Res. 49 (2013) 29-37.

Léger P., Coté P., Tinawi R., Finite Element Analysis of Concrete Swelling due to Alkali-Aggregate Reactions in Dams, Comp. Struct. 60 (1996) 601–611.

Lemarchand E., Dormieux L., Ulm F.-J., Elements of micromechanics of ASR-induced swelling in concrete structures, Concr. Sci. Eng. 4 (2002)12–22.

Leśnicki K.J., Kim J.-Y., Kurtis K.E., Jacobs L.J., Characterization of ASR damage in concrete using nonlinear impact resonance acoustic spectroscopy technique, NDT & E Int. 44 (2011), 721–727.

Leśnicki K.J., Kim J.-Y.,. Kurtis K.E, Jacobs L.J., Assessment of alkali–silica reaction damage through quantification of concrete nonlinearity, Mat. Struct. 46 (2012) 497–509.

Li K, Coussy O., Concrete ASR degradation: from material modeling to structure assessment, Concr. Sci. Eng. 4 (2002) 35–46.

Lindgård J., Haugen M., Castro N., Thomas M.D.A., Advantages of using plane polished section analysis as part of the microstructural analysis to describe internal cracking due to alkali-silica reaction. Proceedings of the 14th ICAAR, Austin/TX, 2012.

Lindgård J., Sellevold E.J., Thomas M.D.A., Pedersen B., Justnes H., Rønning T.F., Alkali–silica reaction (ASR) - performance testing: Influence of specimen pre-treatment, exposure conditions and prism size on concrete porosity, moisture state and transport, Cem. Concr. Res. 53 (2013) 145-167.

Lindgård J., Thomas M.D.A., Sellevold E.J., Pedersen B., Andiç-Çakır Ö., Justnes H., Rønning T.F., Alkali–silica reaction (ASR) - performance testing: Influence of specimen pre-treatment, exposure conditions and prism size on alkali leaching and prism expansion, Cem. Concr. Res. 53 (2013) 68-90.

Marfil S.A., Maiza P.J., Deteriorated pavements due to the alkali–silica reaction: a petrographic study of three cases in Argentina. Cem. Concr. Res. 31 (2001) 1017-1021.

Marinoni N., Voltolini M., Mancini L., Vignola P., Pagani A., Pavese A., An investigation of mortars affected by alkali-silica reaction by X-ray synchrotron microtomography: a preliminary study, J. Mat. Sci. 44 (2009) 5815-5823.

Merz C., Leemann A., Assessment of the residual expansion potential of concrete fromstructures damaged by AAR, Cem. Concr. Res. 52 (2013) 182-189.

Merz C., Leemann A., Validierung der AAR-Prüfungen für Neubau und Instandsetzung, ASTRA-Bericht. AGB 2005/023 und AGB 2006/003, Bern, 2012.

Mullick A.K., Distress in a concrete gravity dam due to alkali silica reaction, Int. J. Cem. Compos. Lightweight Concr. 10 (1988) 225-232.

Mullick A.K., Samuel G., Sinha S.K., Wason R.C., Assessment of residual expansion potential in concrete structures due to alkali-silica reaction. Proceedings IV International Conference on Durability of Building Materials and Components. Singapore, Vol. 11, 1987, 793-800.

Multon S., Evaluation expérimentale et théorique des effets mécaniques de l'alcali-réaction sur structures modèles, (PhD Thesis) 46LCPC, Paris, OA, 2004.

Multon S., Barin J-X., Godart B., Toutlemonde F., Estimation of the residual expansion of concrete affected by alkali silica reaction, ASCE, J. Mat. Civ. Eng. 20 (2008) 54-62.

Multon S., Evaluation expérimentale et théorique des effets mécaniques de l'alcali-réaction sur structures modèles, PhD Thesis, published by LCPC, Paris, OA 46, 2004.

Multon S., Seignol J.F., Toutlemonde F., Chemomechanical assessment of beams damaged by alkali-silica reaction, J. Mat. Civ. Eng. 18 (2006a) 500-509.

Multon S., Toutlemonde F., Effect of applied stresses on alkali–silica reaction induced expansions, Cem. Concr. Res. 36 (2006b) 912–920.

Natesaiyer K.C., Hover K.C., Further study of an in-situ identification method for alkali-silica reaction products in concrete, Cem. Conc. Res. 19 (1989) 770-778.

Ostrovsky L.A., Johnson P.A., Dynamic nonlinear elasticity in geomaterials, Riv. Nuov. Cimento 24 (2001) 1–46.

Payan C., Ulrich T.J., Le Bas P.-Y., Guimaraes M., Quantitative linear and nonlinear resonant inspection techniques for characterizing thermal damage in concrete, Acoustics 2012 Nantes, 2012.

Pesavento F., Gawin D., Wyrzykowski M., Schrefler B.A., Simoni L., Modeling alkali–silica reaction in non-isothermal, partially saturated cement based materials, Comp. Met. Appl. Mech. *Eng.* 225–228 (2012) 95–115.

Peterson K., Gress D., van Dam T., Sutter L., Crystallized alkali–silica gel in concrete from the late 1890s, Cem Concr Res 36 (2006) 1523-1532.

Pignatelli R., Comi C., Monteiro P.J.M., A coupled mechanical and chemical damage model for concrete affected by alkali–silica reaction, Cem. Concr. Res. 53 (2013) 196–210.

Regamey, J.M., Hammerschlag, J.G., Barrage d'Illsee - assaintment. Research and Development in the Field of Dams, Proceedings of the ICOLD-Symposium (Crans-Montana, Switzerland), 1995.

Richardson I.G., Electron microscopy of cements. In: Bensted J., Barnes P. (editors). Structure and Performance of Cements (2nd ed.), Spon Press, London (2002), pp. 500-556.

RILEM/NDT 1, Testing of Concrete by the Ultrasonic Pulse Method, RILEM (1971).

Rivard P., Ballivy G., Gravel C., Saint-Pierre F., Monitoring of a hydraulic structure affected by ASR: A case study, Cement and Concrete Research 40 (2010) 676–680.

Saint-Pierre F., Rivard P., Ballivy G., Measurement of alkali–silica reaction progression by ultrasonic waves attenuation, Cement and Concrete Research 37 (2007) 948-956.

Saouma V., Perotti L., Constitutive model for alkali-aggregate reactions, ACI Mat. J. 103 (2006) 194-202.

Sanchez, L., Fournier, B., Jolin, M., Critical parameters of the stiffness damage test for assessing concrete damage due to alkali-silica reaction. Proceedings of the 13th International Conference on Alkali–Aggregate Reaction in Concrete, Austin, Texas, 2012.

Sargolzahi M., Kodjo S.A., Rivard P., Rhazi J., Effectiveness of nondestructive testing for the evaluation of alkali–silica reaction in concrete, Construction and Building Materials 24 (2010) 1398-1403.

Scalerandi M., Griffa M., Antonaci P., Wyrzykowski M., Lura P., Nonlinear elastic response of thermally damaged consolidated granular media, J. Appl. Phys. 113 (2013) 154902/1-9.

Schmidt T., Leemann A., Gallucci E., Scrivener K., Physical and microstructural aspects of iron sulfide degradation in concrete, Cem. Concr. Res. 41 (2011) 263-269.

Scrivener K.L., Backscattered electron imaging of cementitious microstructures: understanding and quantification, Cem. Concr. Compos. 26 (2004) 935-945.

Sellier A., Bourdarot E., Multon S., Cyr M., Grimal E., Combination of structural monitoring and laboratory tests for assessment of alkali-aggregate reaction swelling: application to gate structure dam, ACI Mater. J. 106 (2009) 281–290.

Shayan A., Alkali aggregate reaction in a 60-year old dam in Australia. Int. J. Cem. Compos. Lightweight Concr. 10 (1988) 259-266.

Shayan A., Quick M., Microstructure and composition of AAR products in conventional standard and new accelerated testing, in: Okada K., Nishibayashi S., Kawamura M. (eds.), Proceedings of the 8th ICAAR, Kyoto, Japan, 1989, 475-482.

Smaoui N., Bérubé M.A., Fournier B., Bissonnette B., Durand B., Evaluation of expansion attained to date by ASR-affected concrete, in: Tang, M. Deng M. (eds.), Proceedings of the 12th ICAAR, Bejing, China, 2004a, 1005-1015.

Smaoui N., Bérubé M.A., Fournier B., Bissonnette B., Influence of specimen geometry, orientation of casting plane and mode of concrete consolidation on expansion due to ASR,. Cem. Concr. Agg. 26 (2004) 58-70.

Snieder R., Şafak E., Extracting the building response using seismic interferometry: theory and application to the Millikan library in Pasadena, California, Bulletin of the Seismological Society of America 96 (2006) 586-598.

Souma V., Xi Y., Literature Review of Alkali Aggregate Reactions in Concrete Dams, Report n° CU/SA-XI-2004/001, Structural Engineering and Structural Mechanics Research Series, Dept. of Civil, Env. and Arch. Eng., Univ. of Colorado (2004).

St. John D.A., Poole A.W., Sims I., Concrete petrography - a handbook of investigative techniques. Arnold, London, 1998.

Stähler S.C., Sens-Schönfelder C., Niederleithinger E., Monitoring stress changes in a concrete bridge with coda wave interferometry, The Journal of the Acoustical Society of America 129 (2011) 1945-1952.

Stark D., De Puy G.W., Alkali-silica reaction in five dams in Southwestern United States, ACI Special Publication, 100 (1987) 1759-1786.

Suwito A., Jin W., Xi Y., Meyer C., A mathematical model for the pessimum size effect of ASR in concrete, Concr. Sci. Eng. 4 (2002), 23-34.

Swamy R.N., Al-Hamed A.H., The Use of pulse velocity measurements to estimate strength of air-dried cubes and hence in situ strength of concrete, In Situ/Nondestructive Testing of Concrete, ACI Publication SP-82, ACI, Detroit (MI) (1984) 247-276.

Swamy R.N., Wan R.W.M., Use of dynamic nondestructive test methods to monitor concrete deterioration due to alkali-silica reaction. Cement, Concrete and Aggregates 15 (1993) 32-49.

Tagnit-Hamou A., Saric-Coric M., Rivard P., Internal deterioration of concrete by the oxidation of pyrrhotitic aggregates, Cem. Concr. Res. 35 (2005) 99-107.

Tang M., Deng M. (eds.), Alkali-Aggregate Reaction in Concrete, Proceedings of the 12th International Conference on Alkali–Aggregate Reaction in Concrete. International Academic Publishers, World Publishing Corporation, Beijing, China, 2004.

Thaulow N., Jakobson U.H., Clark B., Composition of alkali silica gel and ettringite in concrete railroad ties: SEM–EDX and X-ray diffraction analysis, Cem. Concr. Res. 26 (1996) 309-318.

Thomas M., Kwilosz J. (eds), Alkali-aggregate reaction in concrete. Proceedings of the 14th International Conference on Alkali–Aggregate Reaction in Concrete, Austin, Texas, 2012.

Thomas M.D.A., 'The role of calcium hydroxide in alkali recycling in concrete, in: Skalny J. (ed), Proceedings of the Workshop on the Role of Calcium Hydroxide in Concrete, Materials Science of Concrete, American Ceramic Society, Westerville, OH, 2001, 225-236.

Thomas M.D.A, Kettle R.J., Morton J.A., Expansion of cement-stabilized minestone due to the oxidation of pyrite, Geotechnical Engineering, Transportation Research Record 1219, 1989, 113-120.

Thomas M.D.A., Shehata M.H., Shashiprakash S.G., Hopkins D.S., Cail K., Use of ternary cementitious systems containing silica fume and fly ash in concrete, Cem Concr. Res. 29 (1999) 1207-1214.

Thomas M., Fournier B., Folliard K., Ideker J., Shehatad M., Test methods for evaluating preventive measures for controlling expansion due to alkali–silica reaction in concrete, Cem Concr. Res. 36 (2006) 1842-1856.

Ulm F-J., Coussy O., Kefei L., Larive C., Thermo-chemo-mechanics of ASR expansion in concrete structures, J. Eng. Mech. 126 (2000) 233–242.

Van Den Abeele K.E., Johnson P.A., Guyer R.A., McCall K.R., On the quasi-analytic treatment of hysteretic nonlinear response in elastic wave propagation, J. Acoust. Soc. Amer. 101 (1997) 1885.

Van Den Abeele K.E.-A., Carmeliet J., Ten Cate J.A., Johnson P.A., Nonlinear elastic wave spectroscopy (NEWS) techniques to discern material damage, part II: single-mode nonlinear resonance acoustic spectroscopy, Res. Nondestr. Eval. 12 (2000) 31–42.

Vézina D., Bouchard D., Concrete highway structures showing signs of ASR distress: monitoring program at the Ministère des Transports du Québec, in: Fournier B. (ed.), Marc-André Bérubé Symposium on Alkali-Aggregate Reactivity in Concrete, Montréal, Canada, 2006, 413-422.

Voltolini M., Marinoni N., Mancini L., Synchrotron X-ray computed microtomography investigation of a mortar affected by alkali–silica reaction: a quantitative characterization of its microstructural features, J. Mat. Sci. 46 (2011) 6633-6641.

Walsh J.B., The effects of cracks on the uniaxial elastic compression of rocks, J. Geophys. Res. 70 (1965) 339 -411.

Weise F., Voland K., Pirskawetz S., Meinel D., Innovative measurement techniques for characterising internal damage processes in concrete due to ASR, Proceed. 14th Int. Conf. on Alkali-Aggregate Reactions, Austin, Texas (USA), 2012, 021811.

Wood J.G.M., When does AAR stop: in the laboratory and in the field? in: Tang, M. Deng M. (eds.), Proceedings of the 12th ICAAR, Bejing, China, 2004, 1016-1024.

Appendix: List of Abbreviations

AAR: alkali-aggregate reaction
ACR: alkali-carbonate reaction
AMBT: accelerated mortar bar test
ASR: alkali-silica reaction
CSH: calcium-silicate-hydrate
DRI: damage rating index
EDX: energy dispersive X-ray spectroscopy
EPMA: electron probe micro analyzer
ETH: Swiss Federal Institutes of Technology
FEM: finite element method
IR: infrared
LCPC: laboratoire centrale des ponts et Chaussées
NDE: non-destructive evaluation
NEWS: nonlinear elastic wave spectroscopy
NIRAS: nonlinear impact resonance acoustic spectroscopy
NWMS: nonlinear wave modulation spectroscopy
PSI: Paul Scherrer Institute
PV: pulse velocity
SEM: secondary electron microscopy
SIMONRUS: single mode nonlinear resonant ultrasound spectroscopy
SLS: Swiss Light Source
SSM: scaling subtraction method
TOF: time-of-flight
UPV: ultrasound pulse velocity
WDS: wavelength-dispersive X-ray spectroscopy
XRD: X-Ray diffraction
XTM: X-ray tomographic microscopy
3D: three dimensional